VOLUME XLIII

GEMS & GEMOLOGY

SPRING 2007

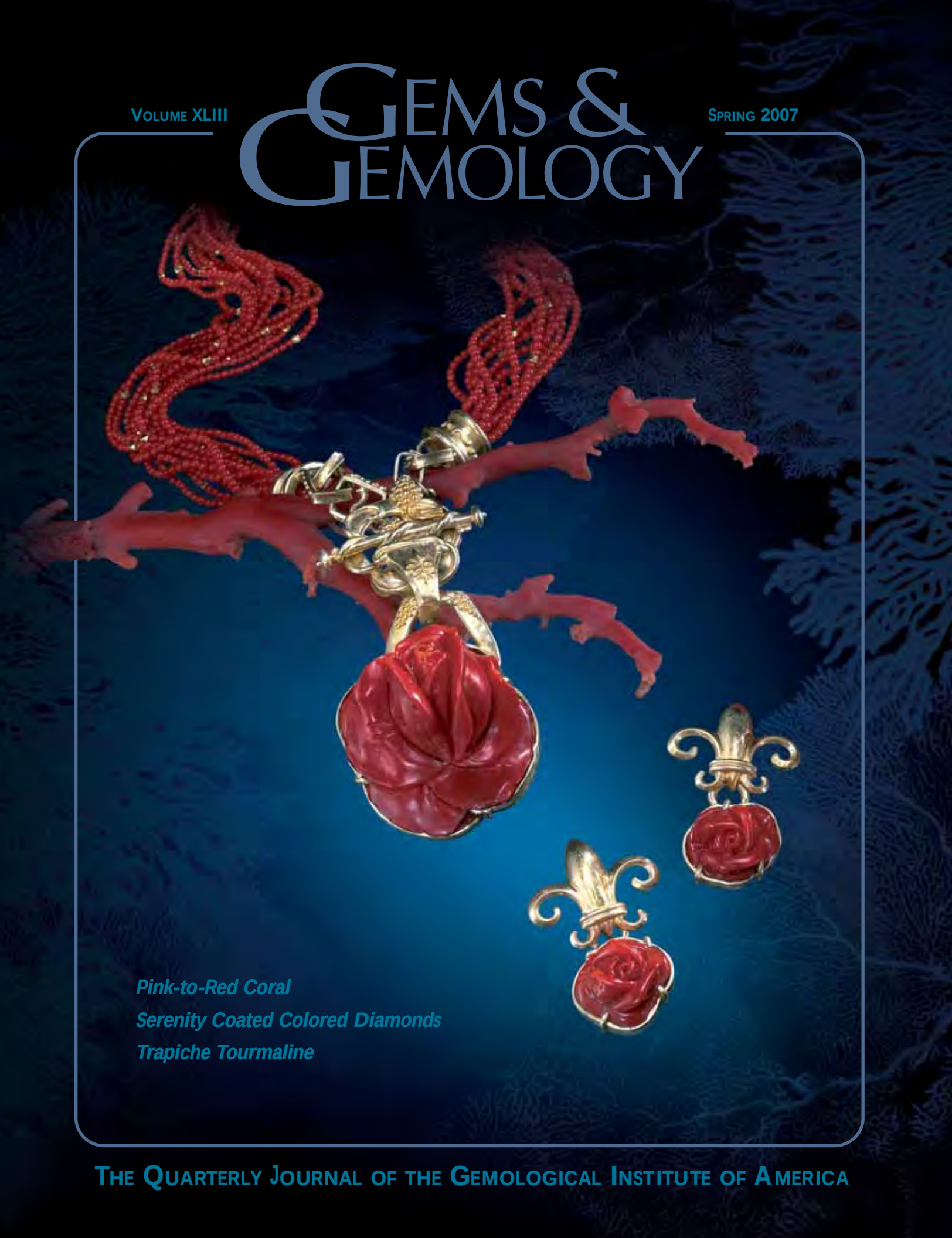

Pink-to-Red Coral

Serenity Coated Colored Diamonds

Trapiche Tourmaline

THE QUARTERLY JOURNAL OF THE GEMOLOGICAL INSTITUTE OF AMERICA

GEMS & GEMOLOGY®

Spring 2007 Volume 43, No. 1

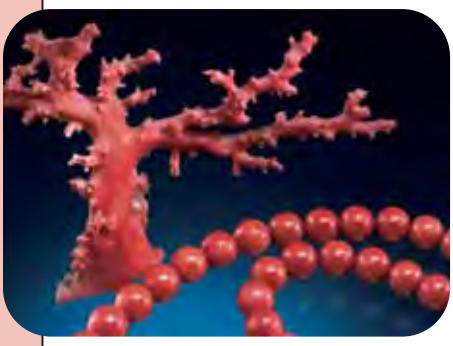

pg. 5

pg. 18

EDITORIAL

FEATURE ARTICLES

REGULAR FEATURES

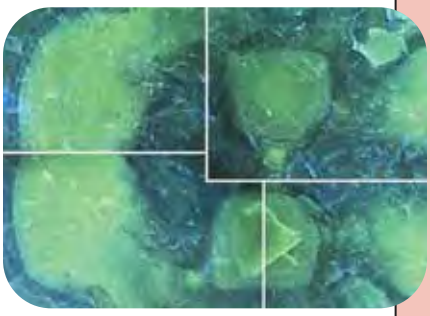

pg. 51

pg. 60

GEMS & GEMOLOGY

SUBSCRIPTIONS

Subscriptions to addresses in the U.S. are priced as follows: **$74.95** for one year (4 issues), **$194.95** for three years (12 issues). Subscriptions sent elsewhere are **$85.00** for one year, **$225.00** for three years. Canadian subscribers should add GST.

Special rates are available for GIA alumni and current GIA students. One year: **$64.95** to addresses in the U.S., **$75.00** elsewhere; three years: **$179.95** to addresses in the U.S., **$210.00** elsewhere. Please have your student or Alumni number ready when ordering. Go to www.gia.edu or contact the Circulation Coordinator.

Single copies of this issue may be purchased for **$19.00** in the U.S., **$22.00** elsewhere. Discounts are given for bulk orders of 10 or more of any one issue. A limited number of back issues are also available for purchase. Please address all inquiries regarding subscriptions and single copy or back issue purchases to the Circulation Coordinator (see above) or visit www.gia.edu.

To obtain a Japanese translation of *Gems & Gemology*, contact GIA Japan, Okachimachi Cy Bldg., 5-15-14 Ueno, Taitoku, Tokyo 110, Japan. Our Canadian goods and service registration number is 126142892RT.

MANUSCRIPT SUBMISSIONS

Gems & Gemology welcomes the submission of articles on all aspects of the field. Please see the Guidelines for Authors on our Website, or contact the Managing Editor. Letters on articles published in *Gems & Gemology* are also welcome.

Gems & Gemology is published quarterly by the Gemological Institute of America, a nonprofit educational organization for the gem and jewelry industry, The Robert Mouawad Campus, 5345 Armada Drive, Carlsbad, CA 92008.

Postmaster: Return undeliverable copies of *Gems & Gemology* to The Robert Mouawad Campus, 5345 Armada Drive, Carlsbad, CA 92008.

ABOUT THE COVER

Pink-to-red coral has been valued as a gem material for thousands of years, but a variety of developments—climate change, overharvesting, and legal restrictions—have conspired to dramatically reduce the availability of gem-quality material. As more dyed coral has entered the market to fill this void, accurate determination of the cause of color is increasingly important. The lead article in this issue, by Christopher Smith and coauthors, reviews the current status of this material and how treated-color coral can be properly identified.

Shown here is a dramatic necklace and earring suite of carved natural-color red coral set in 18K gold. Courtesy of Castelnuovo d'Aiassa Designs, Mount Hamilton, California; photo by Harold & Erica Van Pelt.

Color separations for Gems & Gemology *are by Pacific-plus, Carlsbad, California.*
Printing is by Allen Press, Lawrence, Kansas.

 ISSN 0016-626X

The Dr. Edward J. Gübelin Most Valuable Article Award

Congratulations
to Margrethe Gram-Jensen
of Overijse, Belgium,
whose ballot was drawn from the many entries to win a three-year subscription to Gems & Gemology, and copies of the two Gems & Gemology in Review volumes, Colored Diamonds and Synthetic Diamonds.

Gems & Gemology is pleased to announce the winners of the **Dr. Edward J. Gübelin Most Valuable Article Award** for 2006, as voted by the journal's readers. We extend our sincerest thanks to all the subscribers who participated in the voting.

The first-place article was "The Impact of Internal Whitish and Reflective Graining on the Clarity Grading of D-to-Z Color Diamonds at the GIA Laboratory" (Winter 2006), which reviewed the elusive nature of this type of graining in diamonds and the methodology that GIA graders use to determine its impact on diamond clarity grades. Receiving second place was "Identification and Durability of Lead Glass–Filled Rubies" (Spring 2006), a study of this new corundum treatment and techniques to identify it. Third place was awarded to "'Paraíba'-type Copper-bearing Tourmaline from Brazil, Nigeria, and Mozambique: Chemical Fingerprinting by LA-ICP-MS" (Spring 2006), which described how this analytical technique can separate—on the basis of chemical composition—bright blue-to-green copper-bearing tourmaline from the localities in which it has been found.

The authors of these three articles will share cash prizes of $2,000, $1,000, and $500, respectively. Following are brief biographies of the winning authors.

John M. King

Thomas M. Moses

Wuyi Wang

FIRST PLACE

The Impact of Internal Whitish and Reflective Graining on the Clarity Grading of D-to-Z Color Diamonds at the GIA Laboratory

John M. King, Thomas M. Moses, and Wuyi Wang

John M. King is technical director of the GIA Laboratory in New York and the editor of *Gems & Gemology in Review: Colored Diamonds*. Mr. King, who is also a noted artist, received his Master of Fine Arts degree from Hunter College, City University of New York. **Thomas M. Moses** is senior vice president, GIA Laboratory and Research, New York. **Wuyi Wang** is manager, Research Projects, GIA Laboratory, New York. Dr. Wang holds a Ph.D. in geology from the University of Tsukuba in Japan, and has considerable research experience in diamond geochemistry and diamond treatment.

SECOND PLACE

Identification and Durability of Lead Glass–Filled Rubies

Shane F. McClure, Christopher P. Smith, Wuyi Wang, and Matthew Hall


Shane F. McClure


Christopher P. Smith


Matthew Hall

Shane F. McClure is director of Identification Services at the GIA Laboratory in Carlsbad, California. A popular lecturer, Mr. McClure is also well known for his articles on gem identification and is coeditor of *G&G*'s Lab Notes section. **Christopher P. Smith** is vice president and chief gemologist at American Gemological Laboratories, New York City; at the time the article was written, he was director of Identification Services at the GIA Laboratory in New York. Mr. Smith has written numerous articles for *G&G* and other publications, and is a member of the *G&G* Editorial Review Board. **Wuyi Wang** was profiled in the first-place entry. **Matthew Hall** is manager of Identification Services at the GIA Laboratory in New York. Mr. Hall has a bachelor's degree in geology from Franklin and Marshall College and a master's in geology and geochemistry from the University of Maryland.

THIRD PLACE

"Paraíba"-type Copper-bearing Tourmaline from Brazil, Nigeria, and Mozambique: Chemical Fingerprinting by LA-ICP-MS

Ahmadjan Abduriyim, Hiroshi Kitawaki, Masashi Furuya, and Dietmar Schwarz


Ahmadjan Abduriyim


Hiroshi Kitawaki


Masashi Furuya


Dietmar Schwarz

Ahmadjan Abduriyim is manager of the Research Laboratory at the Gemmological Association of All Japan (GAAJ) in Tokyo. Dr. Abduriyim has a B.Sc. in geochemistry, petrology, and mineralogy from Beijing University, and M.Sc. and Ph.D. degrees in mineralogy from Kyoto University. **Hiroshi Kitawaki** is director of the Research Laboratory at GAAJ. Mr. Kitawaki has a B.Sc. degree in geology from Niigata University, Tokyo, and more than 15 years of experience in diamond and colored stone research and education. **Masashi Furuya** is director of the Japan Germany Gemmological Laboratory in Kofu, Japan. Mr. Furuya has multiple degrees in German from Reitaku University, Kashiwa, Japan, and over 30 years of experience in the jewelry industry. **Dietmar Schwarz** is research manager at the Gübelin Gem Lab in Lucerne, Switzerland. Dr. Schwarz is a former scientific lecturer at the German Academic Exchange Service and professor of mineralogy and gemology at Ouro Preto Federal University, Minas Gerais, Brazil.

Letters

MORE ON SYNTHETIC CORUNDUM "GEM ROUGH"

The report on synthetic corundum "gem rough" in Tanzania (Winter 2006 Gem News International, p. 282) is both interesting and helpful, and Mr. Farooq Hashmi is kind to alert the industry and provide these samples for analysis. However, I would add that although laser ablation–inductively coupled plasma–mass spectrometry (LA-ICP-MS) is wonderful when it is accessible, simple pocket instruments such as rare-earth magnets can instantly provide useful information for those dealing with gems in remote locations.

By applying the magnetic separation approach that I presented at last summer's Gemological Research Conference in San Diego (see the Fall 2006 *Gems & Gemology*, p. 124) to distinguish between spessartine rough and orange sapphire rough, gem dealers might avert this potentially costly misrepresentation. Mn-rich spessartine generally can be characterized by a relatively strong magnetic response, using the direct or pendulum method. Though not diagnostic, the lack of such a response (as with sapphire) could quickly flag this material as something other than spessartine.

Your readers may find the magnetic separation table in the *G&G* Data Depository (http://lgdl.gia.edu/pdfs/gumpesberger-table.pdf) helpful; there is also a related article in the Winter 2006 issue of *Canadian Gemmologist* (S. Gumpesberger, "Magnetic separation of gemstones," Vol. 27, No. 4, pp. 120–124).

Sylvia Gumpesberger
Canadian Gemmological Association
Toronto, Ontario

FALL 2006 ISSUE REQUIRED READING

Unaccustomed as I am to writing letters of this kind—especially to *G&G*—scientific integrity compels me to acknowledge and commend your Fall 2006 issue.

As one unable to attend, I found your coverage of the 4th International Gemological Symposium extremely interesting.

On the other hand, your 2006 GIA Gemological Research Conference was simply outstanding. The information imparted both by the speakers and through the poster presentations should be required reading for all who would call themselves gemologists.

Keep up the good work.

Dr. W. Wm. Hanneman
Poulsbo, Washington

IN MEMORIAM: DAVID HARGETT (1953–2007)

Gemologist and author David Hargett passed away recently in New York, the city he called his home for most of his adult life. He was 53. Dave worked for the GIA Laboratory in New York for 16 years as a colleague of current GIA Laboratory senior vice president Tom Moses and their gemological mentor, G. Robert Crowningshield. Dave began his career with GIA in January 1977 after obtaining his Graduate Gemologist (G.G.) diploma in Santa Monica, California, followed later by a bachelor's degree from New York University.

At the East Coast GIA Laboratory, Dave served for several years as manager of the Gem Identification Department, where he was instrumental in developing many of the techniques still used today to recognize synthetic and treated colored stones, as well as cultured pearls and enhanced diamonds. The author or co-author of many *Gems & Gemology* Lab Notes on unusual gem materials, in 1989 he also co-authored the award-winning Koivula et al. article on "The Characterization and Identification of Filled Diamonds." Dave was very fond of gemologically related travel, and he particularly enjoyed exploring the gem mining areas of Mexico and Central America. In its Summer 1990 issue, *G&G* published Dave's definitive paper on the jadeite deposits of Guatemala. Dave left GIA in 1992 and started his own consulting business, which allowed him to focus on areas of gemology he had come to enjoy.

Those who were fortunate enough to know Dave Hargett as a friend remember him as a kind and generous person with an amazing sense of humor. Those who worked with him remember him as an excellent gemologist with a keen and curious mind. Through his dedicated gemological research and an overall strong work ethic, he gained the respect and admiration of gemologists all over the world. He will be missed by many, both within and outside the gemological community.

PINK-TO-RED CORAL: A GUIDE TO DETERMINING ORIGIN OF COLOR

Christopher P. Smith, Shane F. McClure, Sally Eaton-Magaña, and David M. Kondo

Pink-to-red coral has a long history as an ornamental gem material in jewelry, carvings, and sculptures. However, due to a variety of environmental and legal factors, the supply of high-quality, natural-color coral in this color range has dramatically decreased in recent years—and the quantity of dyed coral on the market has increased. From a study of more than 1,000 natural- and treated-color samples, this article summarizes the procedures that are useful to identify the color origin of pink-to-red coral. A variety of techniques—including magnification, exposure to acetone, and Raman analysis—can determine if the color of a piece of such coral is dyed. Although there are limitations to the use of magnification and acetone, Raman analysis can establish conclusively that the color is natural.

Coral is an organic gem material that has been used for ornamental purposes (figure 1) for several thousand years (see, e.g., Walton, 1959). Amulets of red coral dating back to 8000 BC were uncovered in Neolithic graves in Switzerland, coral jewelry was made in Sumeria and Egypt around 3000 BC, and Chinese cultures have valued coral highly since about 1000 BC (Liverino, 1989). The material also is mentioned in the ancient writings of both Theophrastus (Greece, 4th century BC) and Pliny (Italy, 1st century AD; Caley and Richards, 1956). Due to its distinctive natural form, coral has been used not only for jewelry, but also for dramatic carvings and sculptures that highlight the natural form of the coral branch (figure 2). The region centered around Torre del Greco near Naples, Italy, has a long tradition as an important fashioning center for coral (Bauer, 1969; Pizzolato, 2005). This is largely because the Mediterranean Sea has been a major source of the world's pink-to-red ornamental coral. Today, commercial quantities of pink-to-red coral also are found off the coasts of Japan and China (Henn, 2006).

Fine specimens of attractive pink-to-red coral are the most desirable yet among the least available. This limitation has led to the practice of dyeing pale-colored and white coral into the more highly valued shades of pink to red. Commonly, the coral is bleached prior to the dyeing process so that better penetration and more homogeneous coloration may be achieved (figure 3). Additionally, polymer impregnation—with or without a coloring agent—may be used to enhance the appearance of coral and give it a smoother surface, which makes it more comfortable to wear (see, e.g., Pederson, 2004).

The present article looks at the current status of this ornamental material—its formation, supply, and the potential impact of environmental considerations—as well as the techniques used to distinguish between natural-color and dyed corals. In particular, this article will outline some of the procedures typically used by gemologists and gemological laboratories to determine the origin of color for pink-to-red coral.

See end of article for About the Authors and Acknowledgments.
GEMS & GEMOLOGY, Vol. 43, No. 1, pp. 4–15.

Figure 1. For thousands of years, coral like the branch shown here has been fashioned for use as carvings and in jewelry. Although the harvesting of gem-quality pink-to-red coral has decreased steadily in recent years because of environmental and other problems, leading to a proliferation of dyed material, fine pieces such as these beads (13–17 mm) and cabochons (24 mm) continue to enter the marketplace. Courtesy of R. H. & Co., Glendale, California; photo by Harold & Erica Van Pelt.

GENERAL BACKGROUND

Formation/Biology. Because it shows aspects of the mineral, animal, and plant kingdoms, coral was not properly classified until the 17th century (Liverino, 1989). A branch of coral is the skeletal remains of a colony of tiny animals called coral polyps (figure 4). The term *coral* can refer to both the marine animal and the material produced from its skeletal remains. Polyps are simple organisms with a mouth surrounded by tentacles and gastrovascular function. A polyp colony consists of three different parts: the sclerax, the coenosarc, and the polyps themselves. The sclerax is the hard skeleton left behind by the coral polyps, and it is this material that can be worked as a gem material. The coenosarc is the tissue that binds the polyps to the skeleton. In addition to organic macromolecules such as proteins, polysaccharides, and lipids, the coral skeleton also contains biogenic (i.e., biologically generated) carbonates ($CaCO_3$). The two major polymorphs are calcite and aragonite (see, e.g., Rolandi et al., 2005; Bocchio et al., 2006). The polyps precipitate the major components of most coral branches from sea water (Liverino, 1989): calcium carbonate (82–87%) and magnesium carbonate (~7%).

A new coral colony is originally created through sexual reproduction, but it continues to grow through gemmation, whereby a polyp separates off a portion of itself to create a new polyp. Coral requires a sturdy foundation such as rocks, other coral, or debris (e.g., a shipwreck), and it has a growth rate of a

Figure 2. Coral lends itself to extraordinary carvings, such as this Asian-inspired piece (28.6 cm tall × 30.5 cm wide) that conforms to the natural form of the coral branch. Photo © Harold & Erica Van Pelt.

few millimeters up to 1–2 cm per year (Liverino, 1989; Chadwick, 1999).

Pink-to-red coral in the Mediterranean Sea can grow at depths of 5–300 m. The red coral harvested from the waters near Japan and China is often recovered from depths down to 400 m (Liverino, 1989; O'Donoghue, 2006), but it has been discovered near Hawaii at depths down to 1,000 m (O'Donoghue, 2006). According to Rolandi et al. (2005), there are two classes of coral that have skeletons tough enough to be used as gem materials and for carvings: Hydrozoa and Anthozoa. Within these classes, there are again two orders that produce a majority of the species of pink-to-red corals used for ornamental purposes: Stylasterina and Coralliidae, respectively. However, various species of pink-to-red coral typically have not been differentiated within the jewelry industry (Pederson, 2004).

Present Coral Supply and Environmental Considerations. By some estimates, coral reefs cover about 0.25% of the oceans' subsurface area and support approximately 25% of all known ocean species (Chadwick, 1999). However, beds of coral species that are large enough to support harvesting are becoming increasingly scarce. The annual harvest of red coral in the Mediterranean Sea decreased from about 100 tonnes in 1976 to about 25 tonnes in 2000 (Tsounis, 2005). To reach such coral forests, divers must now go to greater depths than in the past. As an example, along Costa Brava in the northwest Mediterranean Sea, only 10% of the dives to retrieve coral are to depths of less than 30 m, while 70% are to depths of 30–50 m (Tsounis, 2005).

A wide range of factors are responsible for depleting the world's total coral supply, including global warming, industrial pollution, oil spills, thermal stress caused by heated discharge from power plants, destructive fishing through the use of cyanide and dynamite, human overpopulation in coastal areas, and, finally, overharvesting of the coral itself. Given the depths at which most of the pink-to-red coral beds are principally found, overharvesting has had the greatest impact. Japan and other countries, such as the U.S. (Hawaiian islands), that wish to preserve a sustainable supply of coral have established strict limits on the quantities and types of coral that may be harvested (Laurs, 2000; Prost, 2001). These restrictions also limit the available areas and depths at which harvesting is permissible.

Note that the chemical bleaching performed on some harvested coral prior to dyeing is very different from the "bleaching" that other species of coral (usually not considered gem material) have experienced over the last few years. This latter bleaching, which has been the subject of much media attention (e.g., Fountain, 2004; Bierman, 2005; Doney, 2006),

is the natural response of a living coral ecosystem to environmental changes such as increases in water temperatures and differences in the acidity and salinity of the water (Chadwick, 1999). Typically, many shallow-water corals coexist in a symbiotic relationship with various colored algae, which indirectly provide the polyps' primary source of food. Environmental stressors may cause the algae to leave the coral's surface, exposing the white skeleton. The previously vibrant corals then appear quite bleak. Deprived of their major food source, they have difficulty surviving (Doney, 2006).

The reduction in supply of high-quality, natural-color coral has led to a greater amount of dyed-color, lower-quality coral in the most highly valued shades of pink to red. Some U.S. dealers report that a large portion, as high as 90–95%, of the new coral entering the market is color-enhanced (Prost, 2001).

Origin of Color. In the 1980s, carotene was established as the cause of color in pink-to-red coral (Merlin and Delé, 1983; Merlin, 1985). Carotene is one of more than 600 related natural pigments that are collectively grouped as carotenoids and are produced primarily in phytoplankton, algae, and plants (Rolandi et al., 2005). Carotenoids are responsible for a broad range of colors in both plants and animals, depending on the complex formed and its incorporation into the host. For example, carrots are a vibrant orange due to alpha- and beta-carotene, tomatoes are red due to lycopene, and flamingos are pink due to the presence of astaxanthin in their diet; all of these colorants are carotenoids. In coral skeletons, various carotenoids are also responsible for yellow, orange, brown, and blue-to-violet hues. The specific color is influenced by the carotenoid's incorporation into the skeleton (Rolandi et al., 2005). In addition, carotenoids form complexes with other materials—most notably proteins—that may significantly influence the color exhibited.

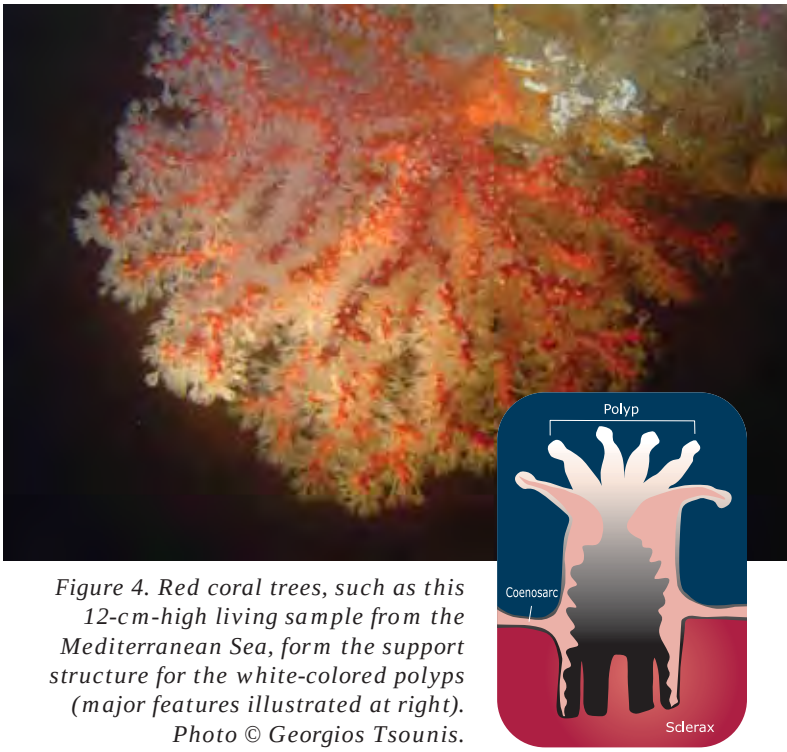

Figure 4. Red coral trees, such as this 12-cm-high living sample from the Mediterranean Sea, form the support structure for the white-colored polyps (major features illustrated at right). Photo © Georgios Tsounis.

Figure 3. The coral branch on the left (67 mm) has been bleached, which is commonly performed prior to dyeing to improve the penetration of the dye and allow for a more homogeneous coloration after dyeing. The branch on the right has been dyed red. Also clearly evident in these two samples of Corallium rubrum *are striations parallel to the length of the branches. The grooves are canals that the coral polyps used to transport nutrients and are one of the most distinguishing characteristics of the coral structure. Photo by Jessica Arditi.*

Gemological Properties. The identification of coral is made through a variety of properties. GIA's *Gem Identification Lab Manual* (2005) indicates that key tests include: refractive index (1.486–1.658), birefringence (0.172—accompanied by a birefringence blink), and magnification. The ribbed, pitted, and scalloped structures of natural coral (refer to the "Microscopic Examination and General Observations" section below) provide a readily available means of separating coral from its most commonly encountered imitators, including shell and plastic, with magnification. Reconstituted coral is produced from low-quality coral that has been pulverized, mixed with an

Figure 5. Natural-color coral can span a wide range of hues, including these examples (2.5–11.8 mm) of the most valuable shades of pink to red. These strands of coral belong to the following species: (1) Melithaea ochracaea, *(2)* Corallium elatius, *(3)* Corallium rubrum, *(4)* Corallium elatius, *(5)* Corallium *species*, *(6)* Corallium secundum, *and (7)* Corallium rubrum. *Photo by Jessica Arditi.*

epoxy, reformed into blocks, dyed, and then used to make jewelry (Weldon, 2003). It does not show a surface pattern or a ribbed structure.

A careful R.I. reading, S.G. determination, and infrared spectroscopy—combined with observation of specific growth-structures—may provide clues to the particular species of the coral. Such tests may also help determine if the coral species is predominantly composed of calcite or aragonite (Kaczorowska et al., 2003; Pederson, 2004; Rolandi et al., 2005); however, these topics are outside the scope of this article. Because so little has been published in the recent gemological literature on the identification of dye in coral, especially given the analytical techniques that are now available, we conducted numerous tests—standard gemological exams and more sophisticated spectroscopic analyses—on known treated and untreated samples to determine which methods were most effective.

MATERIALS AND METHODS

One of the authors (CPS) acquired seven strands of coral beads covering four species of the Coralliidae order—*Corallium elatius*, *Corallium rubrum*, *Corallium secundum*, and *Melithaea ochracaea*—as well as samples of unknown species (figure 5), all of which were represented as natural color. They ranged from pinkish orange to pink and red. In addition, 11 strands of coral—all represented as dyed—were obtained (see, e.g., figure 6). Most of these belonged to the *Corallium rubrum* species, with the dyed colors ranging from pink-orange and various shades of light pink to red. Included in this group were two strands of *Melithaea ochracaea* that had been treated with a colored polymer. We also analyzed 10 known natural-color and dyed coral specimens from the GIA reference collection and 24 dyed samples from the collection of one of the authors (SFM). In all, well over 1,000 pieces of natural-color and dyed coral were included in this study.

All of the samples were examined using a standard GIA Gemolite binocular microscope with

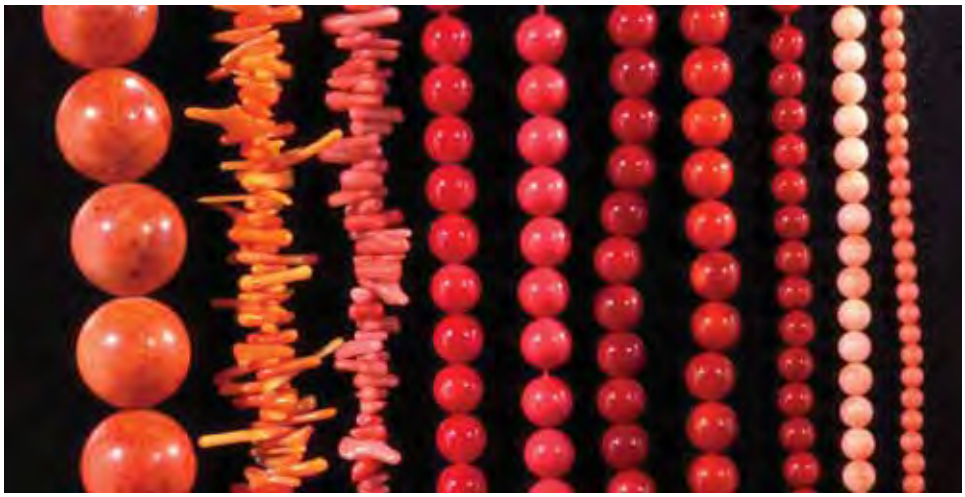

Figure 6. Coral (here, 3.5–18.0 mm) can be dyed almost any color, but it is seen most commonly in the gem trade as pink to red. Photo by Jessica Arditi.

fiber-optic illumination. Acetone and a cotton swab, such as a Q-tip, were used to test inconspicuous areas of the coral on a random sample of approximately 50 pieces of each group (natural-color and treated) for the presence of dye.

A Renishaw System 1000 Raman micro-spectrometer with an argon-ion laser (514 nm excitation) was used to analyze 40 natural-color and 40 dyed samples (including approximately 10 with a colored polymer), covering the complete color range. For the Raman analysis, we used a variety of magnifying lenses, from 5× to 50×. The integration times varied from 3 to 20 seconds per grating sequence. The spectra were taken over two different ranges. The first extended from 2000 to 100 cm^{-1} and covered the standard range used to identify the key Raman bands of a material. The second extended from 517 to 1000 nm, with the intent of measuring Raman bands outside of the previous range as well as any photoluminescence bands that might be present (refer to Raman Spectroscopy below).

Reflectance spectra of 10 natural-color and 14 dyed coral samples that varied from pink to red were acquired for the 200–850 nm range with a Perkin Elmer Lambda 950 ultraviolet/visible/near-infrared (UV-Vis-NIR) spectrometer utilizing an integrating sphere, with a 1.0 nm scan interval and 141 nm per minute scan speed. Although reflectance spectra are typically shown as % reflectance (%R), the authors have elected to portray the spectra in absorbance, as the negative log of %R divided by 100 (i.e., $-\log[\frac{\%R}{100}]$), since most spectra in gemological publications are shown using absorbance. To confirm the validity of this approach, we performed absorption spectroscopy on thin slices made from seven of the samples (four pink-to-red natural-color and three dyed) using the same spectrometer and measuring conditions. The two types of spectra, reflectance (converted to absorbance) and absorbance, were virtually identical.

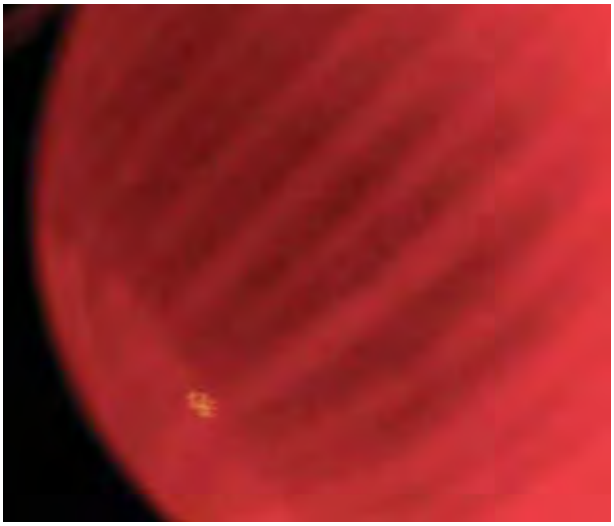

Figure 7. The parallel striations that are obvious in "rough" coral are also clearly evident after the material has been fashioned, so they readily separate coral from its simulants. Note, however, that this structure is visible in both natural-color and dyed coral. Photomicrograph by C. P. Smith; fiber-optic illumination, magnified 18×.

RESULTS AND DISCUSSION

Microscopic Examination and General Observations. The structures of the most common ornamental corals—*Corallium elatius*, *Corallium rubrum*, and *Corallium secundum*—typically consist of two patterns. The first is a ribbed or striated pattern that extends roughly parallel to the length of the coral branch (figure 7). The other is a concentric, scalloped structure (figure 8). Natural features

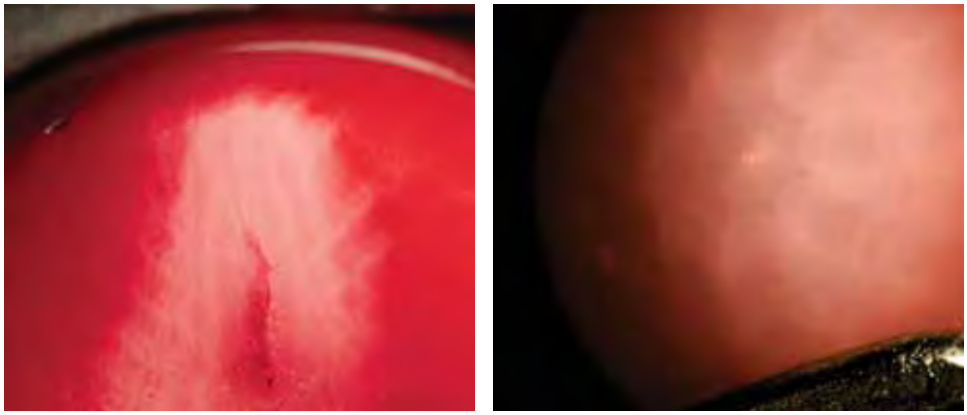

Figure 8. A concentric scalloped pattern is also characteristic of natural coral and will readily distinguish it from its most common imitators shell and plastic. Photomicrographs by C. P. Smith; fiber-optic illumination, magnified 15× (left, dyed coral) and 25× (right, natural-color coral).

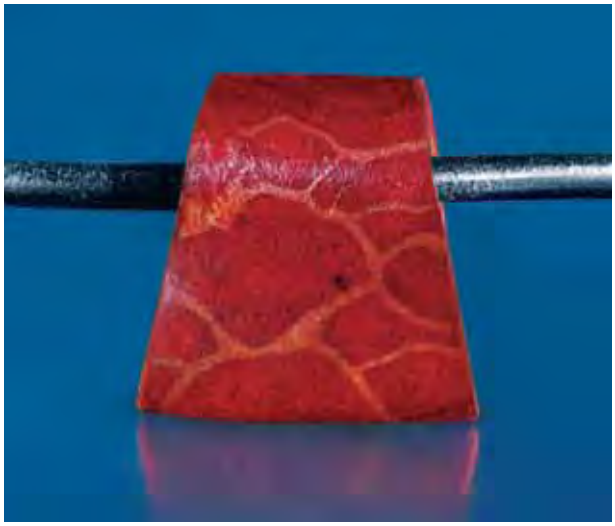

Figure 9. The red coral species Melithaea ochracaea *(sometimes referred to as "red king coral") is notable for its distinctive patterning. This piece measures 2.8 cm at the base. Courtesy of Holly Smith; photo by Elizabeth Schrader.*

dotting the coral surface, which may be described as pits and pock marks, also are common and characteristic of many *Corallium* species. The unusual patterns (figure 9) and the open and porous structure (figure 10) of the red coral species *Melithaea ochracaea* are particularly distinctive. Such features were observed in all the coral beads examined in this study, both natural-color and dyed, depending on their species.

Coral occurs naturally in a broad range of attractive pinkish orange to pink and red colors (again, see figure 5). Similarly, coral may be dyed to virtually any color; however, only results for coral that has been dyed pale pink to deep red and pink-orange are reported in this study (again, see figure 6). In some instances, the colors achieved by dyeing appear very similar to those seen in natural-color coral. Commonly, though, the dyed coral is very different in appearance from its natural-color counterpart (see, e.g., figure 11). Therefore, visual observation of color may provide an important clue to the presence of dye. In addition, the surface pits and cavities common to coral readily act as receptacles for dye concentrations (figure 12), as do fractures or separations in the concentric growth pattern. In such instances—where visual observation is insufficient—the use of acetone and a cotton swab may be effective to identify the presence of dye (figure 13). This reaction was observed in many of the dyed samples we tested; however, it was very faint in several samples and not evident at all in a few. A piece of coral may also be immersed in acetone to see if any dye leaves the coral structure and turns the acetone pink (although we did not conduct this test on our samples). However, both of these techniques are somewhat destructive, as a positive test removes some of the color imparted by the dye. For this reason—and because, as our testing with a cotton swab showed, the results are not always conclusive—we also investigated two nondestructive analytical techniques.

Figure 10. The characteristic "open" structure of Melithaea ochracaea *is evident whether the coral is fashioned with the channels open (left, magnified 15×) or if it has been impregnated with a polymer (right, magnified 25×). Today it is common to treat this species of coral with a polymer to reduce its rough texture and allow it to take a better polish. The polymer has a yellow-orange color, as may be seen in the open pores of the treated sample. Photomicrographs by C. P. Smith.*

Figure 11. Often the dyes used to treat coral will impart a vivid red hue, as in this 14 mm bead, that is not found in nature. Photo by Jessica Arditi.

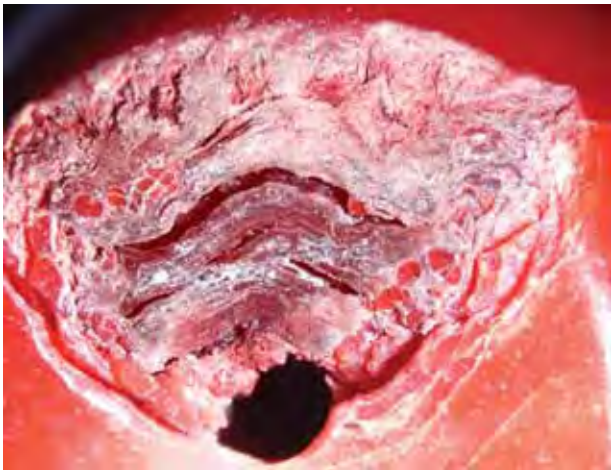

Figure 12. Coral can be a brittle material, as well as somewhat porous. Breaks or cavities at the surface commonly contain concentrated remnants of the dye that was used to color it. The very dark red masses obvious near the drill hole in this sample readily identified this bead as dyed, even without magnification. Photomicrograph by C. P. Smith; magnified 13×.

Raman and Photoluminescence Spectroscopy. The Raman spectra of these four species of coral typically exhibit a combination of bands associated with both the coral matrix ($CaCO_3$) and the compounds responsible for the color (figure 14). A distinct band positioned at approximately 1087 cm^{-1}, with subordinate peaks at approximately 714 and 283 cm^{-1}, is indicative of the calcium carbonate phase forming the skeleton of the coral. All of the samples we tested with Raman spectroscopy, both natural-color and dyed, showed this feature.

Figure 13. Acetone has traditionally been used to confirm the presence of dye in coral. Commonly this test involves dipping a cotton swab in acetone and then rubbing the cotton on an inconspicuous area of the sample to see if any of the color rubs off. Occasionally, the item is immersed in acetone to see if the liquid will discolor slightly. In both cases, this test may be destructive to the color of the sample. Photo by Jessica Arditi.

Natural color in pink-to-red coral may be readily identified by the presence of certain organic pigments incorporated into the coral skeleton. A pair of distinct Raman peaks positioned at approximately 1520 and 1123 cm^{-1}, with subordinate peaks at approximately 1297 and 1020 cm^{-1}, identify carotene

Figure 14. The Raman spectrum of coral identifies the biogenic calcium carbonate phase of the skeleton ($CaCO_3$), with peaks positioned at approximately 1087, 714, and 283 cm^{-1}. The Raman spectrum of natural-color coral typically reveals additional peaks related to organic pigments, such as those positioned here at 1520, 1123, and 1020 cm^{-1}.

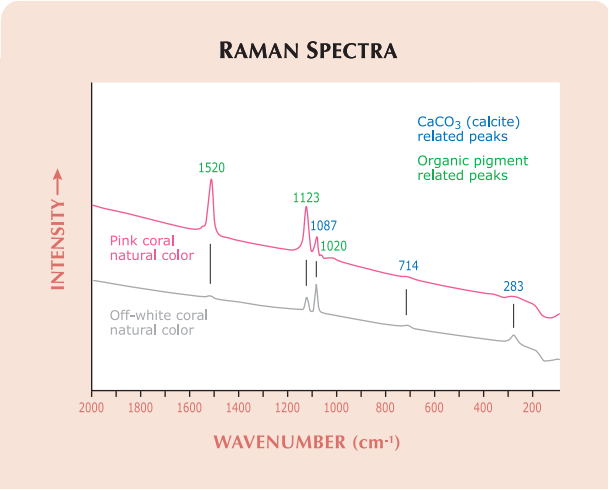

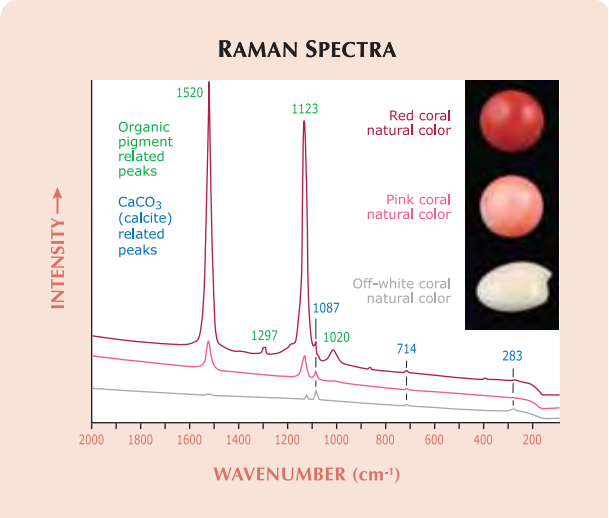

Figure 15. Carotene is the organic pigment responsible for the pink-to-red shades of natural-color coral. In the Raman spectra of these three natural-color corals, the intensity of the carotene peaks (with two dominant peaks at approximately 1520 and 1123 cm^{-1} and minor peaks at approximately 1297 and 1020 cm^{-1}) correlates directly with the saturation of color. The bands marked in blue, with the main peak positioned at ~1087 cm^{-1}, identify the calcium carbonate phase ($CaCO_3$) of the coral.

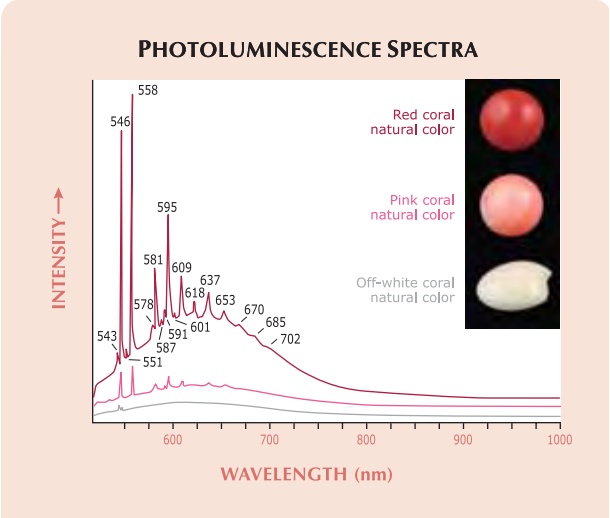

Figure 16. By scanning the full Raman spectral range capable with a 514 nm excitation Ar-ion laser (517–1000 nm), carotene pigments are seen to be responsible for a range of peaks in the same samples as illustrated in figure 15.

(Urmos et al., 1991; Kaczorowska et al., 2003; Rolandi et al., 2005). In our experience, the intensity of these carotene peaks directly correlates to the saturation of the pink-to-red color, as was the case with the natural-color samples we tested (figure 15).

Using the full spectral range of the 514 nm Ar-ion laser (517–1000 nm; figure 16), we observed a series of peaks positioned at approximately 543 (1020 cm^{-1}), 546 (1123 cm^{-1}), 551 (1297 cm^{-1}), 558 (1520 cm^{-1}), 578, 581, 587, 591, 595, 601, 607, 609, 618, 637, 653, 670, 685, and 702 nm, as well as other subordinate peaks, all of which are due to carotene pigments. In contrast, the dyed pink-to-red coral samples did not exhibit the Raman spectrum associated with carotene. Instead, they typically showed an increase in underlying photoluminescence in the standard Raman spectral range of 2000–100 cm^{-1}, in addition to a series of very weak peaks positioned at approximately 1608, 1492, 1482, 1455, 1378, 1353, 1327, 1290, 1032, 906, 817, and 701 cm^{-1} (figure 17; details of many of these peaks cannot be observed at the scale shown). With the extended spectral range (517–1000 nm), we observed that the dominant photoluminescence of the dye was centered between approximately 630 and 665 nm, the asymmetry of this photoluminescence structure indicating that it likely consists of multiple bands (figure 18). In the *Melithaea ochracaea* samples that had been treated with a colored polymer, we noted a compound spectrum of carotene peaks and a dominant broad luminescence band.

Since the dye or colored polymer may be incor-

Figure 17. The Raman spectra of dyed pink-to-red coral are identified by the increasing photoluminescence extending beyond 2000 cm^{-1}, as well as the absence of peaks associated with carotene. Often a series of very weak peaks attributed to dye may also be evident, such as the structure seen here between 1700 and 1300 cm^{-1} in the green spectrum. The red spectrum illustrates a common occurrence, where the luminescence of the dye is so strong that no other structure or Raman peaks are evident.

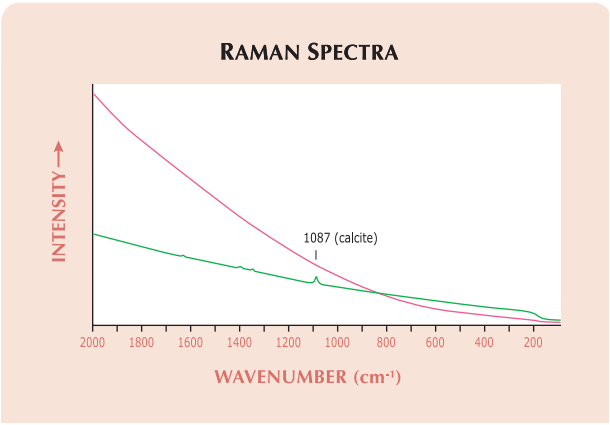

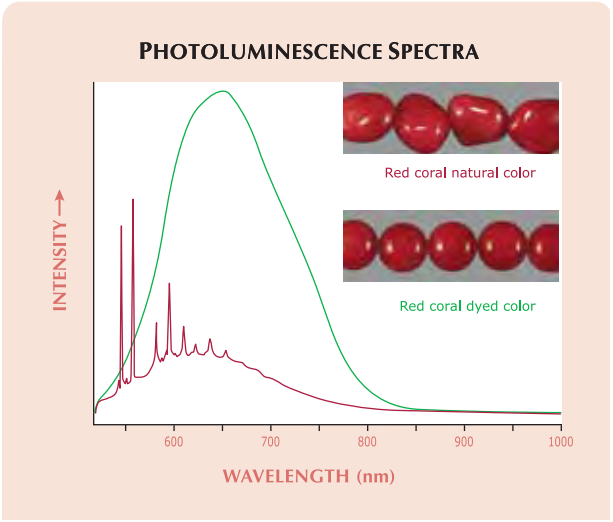

Figure 18. Photoluminescence in the 517–1000 nm spectral range clearly illustrates the differences between the series of very strong carotene peaks in the area of ~540–700 nm in natural-color coral and the dominant photoluminescence band structure centered at ~630–665 nm in dyed red coral.

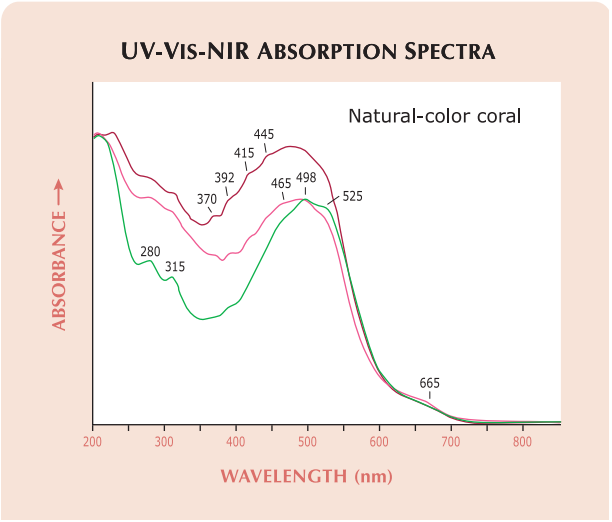

Figure 19. As these three representative spectra indicate, natural-color pink-to-red coral has a series of broad absorption bands in the UV-Vis-NIR region. The predominant absorption consists of a multiple-band structure with individual positions located at ~465, 498, and 525 nm. The same general combination of absorptions was recorded in all the natural-color coral tested during this study.

porated unevenly, our samples also confirmed the wisdom of analyzing several areas on the piece in question. In some areas with a partial natural coloration, we noted a combination of spectral features: the presence of carotene-related peaks indicating natural color, together with the significantly increased broad luminescence indicating dyed color. In such instances, the intensity of the carotene-related peaks was not consistent with the saturation of color in the area analyzed.

Reflectance Spectroscopy. The UV-Vis-NIR spectra of the pink-to-red coral samples were dominated by a series of broad absorption bands. In the natural-color samples, the primary absorption responsible for the color consisted of a multiple-band structure composed of at least three independent bands located at approximately 465, 498, and 525 nm (figure 19). At the tail of this absorption on the high-wavelength side, most of the natural-color samples showed another broad absorption feature positioned at ~665 nm. Also seen in most of the samples were absorptions positioned at approximately 370, 392, 415, and 445 nm, as well as other broad bands deeper in the UV region at approximately 280 and 315 nm.

In the dyed samples, the spectra were dominated by an absorption feature that saturated the detector in the spectral range between approximately 400 and 550 nm (figure 20). The 465, 498, and 525 nm bands noted in the natural-color corals were not evident. We also did not record the weak broad bands at approximately 315, 370, 392, 415, and 445 nm that are present in natural-color coral. However, the

Figure 20. The absorption spectra of these three samples of dyed coral have a predominant absorption in the 400–550 nm range, similar to that seen in the natural-color coral shown in figure 19. However, several of the associated, subordinate broad absorption bands present in natural-color coral are not seen. In addition, there is a slightly modified absorption trend in the deep UV region.

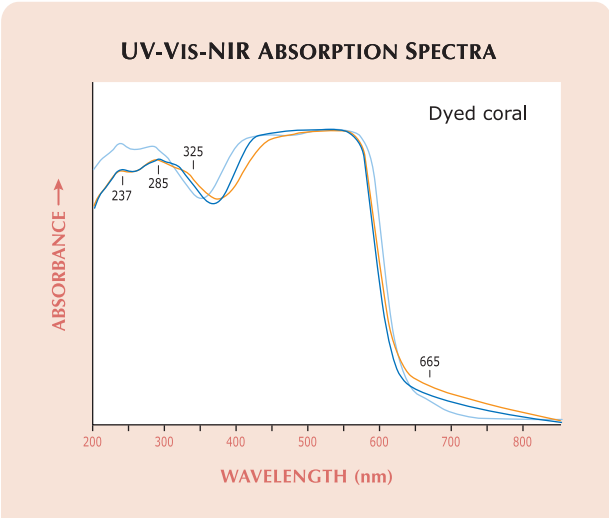

Figure 21. Pink-to-red coral, with its natural variations in color, can be carved to create unique pieces of jewelry such as this image of a woman's face (56 mm high). Courtesy of Castelnuovo d'Aiassa Designs, Mount Hamilton, California; photo by Harold & Erica Van Pelt.

broad feature at 665 nm was weakly present in a few of the dyed specimens. In addition, we also noted three weak bands in the UV region of the spectrum positioned at approximately 237, 285, and 325 nm.

IDENTIFICATION

Once it has been established that an item is coral, several tests may be conducted to determine if its pink-to-red color is natural or dyed. The visual appearance of the coral may provide an indication of the origin of color, but such observations should not be considered conclusive. Additionally, although microscopic examination alone can prove the presence of dye in color-treated coral (through concentrations of color in surface pits, cavities, or fractures), the lack of such features is insufficient to prove that the color of a specimen is natural. Historically, gemologists have used acetone to confirm the presence of dye, but as our experiments showed, not all dyed coral will respond to acetone. In those cases where acetone is inconclusive or the use of this potentially destructive test is not advisable, the coloring agent may be conclusively and nondestructively identified with Raman spectroscopy. By establishing the presence of carotene in the Raman spectrum—with its two dominant peaks located at approximately 1520 and 1123 cm^{-1}—and correlating it to the intensity of color, it is possible to confirm the natural color of pink-to-red coral. In contrast, dyed pink-to-red coral is characterized by a dominant underlying photoluminescence band centered between approximately 630 and 665 nm, usually without specific carotene-related peaks (again, see figure 18). Because dye may be unevenly distributed, it is important to analyze several areas on the sample. In areas that contain a partial natural coloration, the spectra will show a combination of carotene-related peaks (that will not correspond to the intensity of color, as would be the case with untreated pink-to-red coral) and significantly increased broad photoluminescence centered at approximately 630–665 nm.

The study revealed some potentially interesting trends in the UV-Vis-NIR spectra of the natural-color and dyed samples. However, more testing is needed to establish the consistency of these findings and their usefulness in making this distinction.

SUMMARY AND CONCLUSION

Coral has been used in jewelry and *objets d'art* for thousands of years, and it continues to be very popular in many markets today (figure 21). Attractive

shades of pink to red are typically considered the most valuable. Unfortunately, the global supply of gem-quality coral is diminishing, as overharvesting and other factors have had a detrimental effect on existing coral beds. This has led to an increased use of dyes to expand the availability of the most sought-after colors. In some cases, microscopy or testing with acetone is sufficient to identify the presence of a dye. However, the use of acetone to remove color may be somewhat destructive, and the results are not always conclusive. UV-Vis-NIR reflectance spectroscopy may provide clues to the natural or dyed condition of a piece of coral, but further work is necessary to confirm the applicability of this testing procedure. However, Raman analysis is a nondestructive method that can conclusively determine the natural origin of such colors, as well as the presence of dye. Carotene, the natural coloring agent for pink-to-red coral, may be readily identified by its signature Raman spectrum.

ABOUT THE AUTHORS

Mr. Smith (chsmith@aglgemlab.com) is vice president and chief gemologist at American Gemological Laboratories (AGL), New York City; at the time the article was originally written, he was director of Identification Services at the GIA Laboratory in New York. Mr. McClure is director of Identification Services at the GIA Laboratory in Carlsbad, California. Dr. Eaton-Magaña is technical editor of Gems & Gemology*, and Mr. Kondo is a research technician at the GIA Laboratory, New York.*

ACKNOWLEDGMENTS

The authors thank Peter Rohm of Rohm GesmbH & Co. KG, Linz, Germany, for supplying both natural-color and dyed samples of known coral species. They also thank the following for helpful discussions on the origin of color in coral: Dr. Carolyn Van der Bogert, former research scientist at the GIA Laboratory, New York; Wendi Mayerson, former senior staff gemologist in the Identification Department, GIA Laboratory, New York; and Shane Elen, analytical equipment supervisor at GIA Research, Carlsbad.

REFERENCES

Bauer M. (1969) *Precious Stones*. Charles E. Tuttle & Co., Rutland, VT.

Bierman F. (2005) Coral reefs in peril, report says. *New York Times*, March 13, http://query.nytimes.com/gst/fullpage.html?sec=travel&res=9801E4D61E3DF930A25750C0A9639C8B63.

Bocchio R., Bracco S., Brajkovic A., Comotti A., Rolandi V. (2006) Gem corals: X-ray diffraction, solid state NMR, elemental analysis. *Australian Gemmologist*, Vol. 22, pp. 524–532.

Caley E.R., Richards J.C. (1956) *Theophrastus on Stones*. Ohio State University Press, Columbus, Ohio.

Chadwick D.H. (1999) Coral in peril. *National Geographic*, Vol. 195, No. 1, pp. 30–37.

Doney S.C. (2006) The dangers of ocean acidification. *Scientific American*, Vol. 294, No. 3, pp. 58–65.

Fountain H. (2004) When coral turns white. *New York Times*, June 15, http://www.nytimes.com/2004/06/15/science/15obse.html?ex=1402632000&en=a14415ae73ca3ef4&ei=5007&partner=USERLAND#.

Henn U. (2006) Corals in the gem and jewellery trade. *Gemmologie: Zeitschrift der Deutshen Gemmologischen Gesellschaft*, Vol. 55, No. 3/4, pp. 77–104 (in German with English abstract).

Gemological Institute of America (2005) *Gem Identification Lab Manual*, 5th ed. Gemological Institute of America, Carlsbad, CA.

Kaczorowska B., Hacura A., Kupka T., Wrzalik R., Talik E., Pasterny G., Matuszewska A. (2003) Spectroscopic characterization of natural corals. *Analytical and Bioanalytical Chemistry*, Vol. 377, No. 6, pp. 1032–1037.

Laurs B. (2000) Gem News: Coral exploration resumes in Hawaii. *Gems & Gemology*, Vol. 36, No. 3, pp. 263–264.

Liverino B. (1989) *Red Coral*. Transl. by J. H. Johnson, Analisi-Trend s.c.r.l., Bologna, Italy.

Merlin J.C. (1985) Resonance Raman spectroscopy of carotenoids and carotenoid-containing systems. *Pure and Applied Chemistry*, Vol. 57, pp. 758–792.

Merlin J.C., Delé M.L. (1983) Étude par spectroscopie Raman de résonance de la pigmentation des sequelettes calcaires de certains coreaux. *Bulletin de la Société Zoologique de France*, Vol. 108, pp. 289–301.

O'Donoghue M. (2006) *Gems: Their Sources, Descriptions and Identification*, 6th ed. Butterworth-Heinemann, Oxford, U.K.

Pederson M.C. (2004) *Gem and Ornamental Materials of Organic Origin*. Elsevier Butterworth-Heinemann, Oxford, U.K.

Pizzolato V. (2005) Coral and Torre del Greco. http://www.gimav.it/glassinstyle/giugno/coral.pdf.

Prost M.A. (2001) In the red. *Colored Stone*, Vol. 14, No. 4, pp. 32–33.

Rolandi V., Brajkovic A., Adamo I., Bocchio R., Landonio M. (2005) Gem corals: Classification and spectroscopic features. *Australian Gemmologist*, Vol. 22, No. 7, pp. 285–297.

Tsounis G. (2005) Demography, reproductive biology and trophic ecology of red coral (*Corallium rubrum* L.) at the Costa Brava (NW Mediterranean): Ecological data as a tool for management. Alfred Wegener Institute for Polar and Marine Research, Bremerhaven, Germany, http://web.awi.de/Publications/Tso2005d.pdf.

Urmos J., Sharma S.K., Mackenzie F.T. (1991) Characterization of some biogenic carbonates with Raman spectroscopy. *American Mineralogist*, Vol. 76, No. 3–4, pp. 641–646.

Walton J. (1959) Coral: Classification of species, method of formation and characteristics. *Gemmologist*, Vol. 28, No. 335, pp. 105–116.

Weldon R. (2003) The sea's vanishing gift. *Professional Jeweler*, Vol. 16, No. 8, pp. 35–36.

SERENITY COATED COLORED DIAMONDS: DETECTION AND DURABILITY

Andy H. Shen, Wuyi Wang, Matthew S. Hall, Steven Novak, Shane F. McClure, James E. Shigley, and Thomas M. Moses

Gemological, spectroscopic, and chemical properties of diamonds treated using the new Serenity Technologies coating technique for inducing various "fancy" colors are reported. This technique produces colors that include intense blue, green, yellow, and orange to pink to purple-pink. The presence of a coating can be identified with magnification by observation of an interference-related colored (often bronzy) film, scratches, and colorless and/or dark areas on the surface of the pavilion facets. UV-Vis absorption spectra and chemical analysis provide confirmation of the treatment. Chemical analysis also revealed that the coating is a SiO_2 film doped with Au and/or Ag for blue, pink, and yellow coloration, or with a surface Fe_2O_3 film for orange. No evidence was detected of either chemical diffusion or implantation of foreign elements into the diamond. While the colors produced by this treatment are stable to some standard jewelry repair and cleaning procedures, they are not considered permanent.

The importance of fancy-color diamonds in the marketplace, and the high price-per-carat values due to their rarity, have created a market niche for treated colored diamonds that are moderately priced and more readily available. In this article, we describe a new type of treated diamond that is surface-coated with a thin layer of foreign material to create the apparent color (figure 1). This treatment is carried out on a commercial basis by Serenity Technologies Inc. of Temecula, California. Serenity cooperated with GIA to treat several diamonds, which were documented both before and after the treatment process. GIA also examined more than 100 diamonds treated by this method that were obtained in the marketplace. Some features of this type of coated diamond were recently reported (see Epelboym et al., 2006; Wang et al., 2006a; Kitawaki, 2007; Moses et al., 2007). The present article expands our understanding of this material by detailing the gemological and spectroscopic features of the coated diamonds, the nature of the coatings used, and the durability of the coatings during standard conditions of jewelry repair, care, and wear.

BACKGROUND

For centuries, merchants have used various forms of coating, dyeing, or "painting" to add a thin layer of colored foreign material to part or all of a gemstone's surface with the intent of masking an underlying bodycolor or creating a more desirable color appearance. In 1950, Edward Gübelin discussed the physics related to several possible newer gemstone coatings, including CaF_2 and SiO_2 (Gübelin, 1950). One of the first reported examples of this treatment in modern history was a blue-coated diamond briefly described by Crowningshield (1959). Because of the apparent proliferation of coated diamonds at that time, several practical methods were developed to aid gemologists (Miles, 1962, 1964). In these articles, Eunice Miles described the detection of such coatings by careful examination with a binocular

See end of article for About the Authors and Acknowledgments.
GEMS & GEMOLOGY, Vol. 43, No. 1, pp. 16–34.

Figure 1. A variety of colors can be produced on polished diamonds by a new coating technique from Serenity Technologies, Inc. These color-treated diamonds are now being sold commercially in the jewelry market. The stones shown here range from 0.01 to 0.70 ct. Composite photo by Jessica Arditi and Jian Xin (Jae) Liao.

microscope. She used a combination of reflected and diffused transmitted light to examine the facets for iridescent colors, scratches, a spotty or blotchy appearance to the color, or areas where the color had been removed (e.g., along facet junctions). Coated diamonds continued to be reported periodically in the Lab Notes column of *Gems & Gemology* over the next several decades (see, e.g., Crowningshield, 1965; Liddicoat, 1966; Fryer, 1983; Hargett, 1989; Sheby, 2003).

The coating materials used in the past varied in adhesion, durability, and extent of coated area on the diamond's surface. Although we do not know for certain, we believe that a variety of coating materials were used. These older color-treatment processes may seem unsophisticated or outdated in comparison to permanent techniques such as irradiation and high-pressure, high-temperature (HPHT) annealing, which are most prevalent today. However, recent technological advances could have significant implications for the application of coatings onto diamonds with respect to their color, thickness, and durability. This "modernization" of coating materials and application technologies was evident in diamonds recently identified as having a thin coating of calcium fluoride (CaF_2) doped with gold to produce a pink color (Evans et al., 2005; Wang et al., 2006b).

The number of coated diamonds being submitted to the GIA Laboratory has increased dramatically in recent months. Most of these diamonds have CaF_2 coatings and appear pink and strongly saturated, but others are much lighter in tone (e.g., figure 2). These lighter coated diamonds have proved to be a challenge for even our most experienced gemologists, as the interference colors associated with the coating are very subdued and areas (such as facet junctions) where the film might have been polished off are not readily discernable. Therefore, the presence of the CaF_2 coating can be missed if careful examination protocols are not followed.

Figure 2. The light pink coloration of these diamonds (each about 1 ct) is created by a thin coating of calcium fluoride doped with gold. This gives a convincing resemblance to the color of some natural pink diamonds and creates a challenge in gem identification. Photo by C. D. Mengason.

Figure 3. These six diamonds (0.34–0.40 ct) were colorless or near-colorless before being subjected to a new coating process to create their gray-violet, yellow, purplish pink, and pink-to-orange color appearances. Additional information is provided in table 1. Composite photo by Jian Xin (Jae) Liao.

Consequently, when we learned that a new source was introducing large quantities of coated diamonds with various colors into the marketplace, we undertook the following investigation into the characterization and identification of this treated material. We also studied the durability of these coated diamonds to standard jewelry manufacturing, repair, and cleaning procedures, as well as to household products they might come into contact with during consumer wear.

MATERIALS AND METHODS

Materials. A total of 102 coated diamonds were obtained from dealers who had their diamonds treated by Serenity Technologies (see, e.g., figure 1). The hues of these diamonds included blue (16 samples), green (16), orange (16), pink (20), purple-pink (18), and yellow (16). The green and yellow diamonds were all round brilliant cuts with weights of 0.01–0.03 ct. No larger coated diamonds with these colors were available in the market during this study. The other colors ranged from 0.03 to 0.70 ct and were faceted into various styles. According to the treater, there is no limitation on the size of diamond that can be coated by this process (J. Neogi, pers. comm., 2007). In addition, Serenity Technologies agreed to treat six colorless to near-colorless natural diamonds that GIA supplied (0.34–0.40 ct; see figure 3 and table 1), which allowed us to examine their gemological and spectroscopic properties before and after treatment.

Gemological Examination. All samples were observed with a gemological microscope and various lighting conditions. Electrical conductivity of two blue-coated diamonds was tested using the method previously described by King et al. (1998). Reactions to UV radiation for all samples were checked in a darkened room with conventional four-watt long-wave (366 nm) and short-wave (254 nm) Ultraviolet Products lamps, and—for the six GIA before/after stones—with the DTC DiamondView deep-ultraviolet (<230 nm) imaging system (Welbourn et al., 1996). The colors of these treated diamonds were described in accordance with the GIA colored diamond grading system (King et al., 1994) to facilitate discussion of color changes during these experiments. Note that GIA does not issue grading reports on coated diamonds, so these color designations should be interpreted as *equivalent* colors only.

Spectroscopic Analysis. Absorption spectra were recorded for all six of the before/after samples and several randomly selected market samples (eight blue and 21 orange, purple-pink, or pink coated diamonds; the yellow and green samples were too small to analyze). They were recorded in the mid-infrared (6000–400 cm^{-1}, 1 cm^{-1} resolution) and near-infrared (up to 11,000 cm^{-1}, 4 cm^{-1} resolution) ranges at room temperature with a Thermo-Nicolet Nexus 670 Fourier-transform infrared (FTIR) spectrometer equipped with KBr and quartz beam splitters. A diffuse reflectance apparatus was used to focus the incident beam on the sample, and a total of 512 scans per spectrum were collected to improve the signal-to-noise ratio. Absorption spectra in the ultraviolet/visible/near-infrared (UV-Vis-NIR) range were recorded on two samples of each color except green with a Thermo-Spectronic Unicam UV500 spectrophotometer over 250–850 nm (sampling interval of 0.1 nm). The samples were mounted in a cryogenic cell and cooled to liquid nitrogen temperature (–196°C).

Raman and photoluminescence (PL) spectra were recorded on four (gray-violet, orange, purplish pink, and yellow) of the six diamonds treated for this study—both before and after treatment—using a Renishaw inVia Raman confocal microspectrometer with an Ar-ion laser operating at two excitation wavelengths, 488.0 and 514.5 nm. Raman spectra were collected at room temperature. Up to five scans were accumulated to achieve a better signal-to-noise ratio. For the PL analyses, the samples were cooled by direct immersion in liquid nitrogen. The lasers were carefully focused on the coated surfaces.

Chemical Analysis. We used several techniques to determine the chemical composition of the coating materials. Three coated diamonds (orange, pink, and blue; 0.30, 0.30, and 0.59 ct, respectively) were imaged and chemically analyzed using a high-resolution analytical scanning electron microscope (LEO 1550 VP FESEM) at the California Institute of Technology in Pasadena. This instrument was equipped with an Oxford INCA Energy 300 X-ray energy-dispersive spectrometer (EDS) system. The analysis was performed using an accelerating voltage of 20 kV and electron beam current of 10 nA; no additional coating (e.g., carbon) was applied.

Chemical analysis was also performed with a Thermo-Noran Spectrace QuanX energy-dispersive X-ray fluorescence (EDXRF) spectrometer on a few samples of each color from the market group as well as on the six GIA samples after treatment. A collimator of 3.5 mm diameter was used. Beam current was automatically controlled to maintain a 50% dead time in data collection. The live time for data accumulation was 100 seconds. All spectra were collected under vacuum at ~0.01 Pa.

Analysis of the pink, purple-pink, yellow (no. 79539; table 1), orange, and blue surface coatings was carried out by secondary ion mass spectroscopy (SIMS) sputter depth profiling by the Evans Analytical Group, East Windsor, New Jersey (Wilson et al., 1989). This technique measures elemental signals while a small cavity (80×80 µm) is slowly etched into the surface of the sample. Polished diamond facets provide ideal flat surfaces for this analysis so that profiles with high depth resolution can be acquired. Therefore, we could discern the chemical composition of any chemically distinct layer with a thickness of several nanometers within the coatings. This analysis was carried out using a Phi 6600 quadrupole-based SIMS instrument. Depth profiles were acquired at one location on each diamond using an oxygen ion beam focused to a diameter of approximately 10 µm. This beam was rastered over an area of 50–80 μm^2 with a sputtering rate of 0.2 nm/second depth. This low sputtering rate was necessary to adequately sample the very thin coatings on these diamonds. Mass spectra were acquired for each sample to detect the chemical elements present in the films, and then the most abundant signals were selected to be followed in the depth profiles. The depth scales were calibrated against a SiO_2 film of known thickness. Note that the green stones acquired from the market were too small to be tested by this method.

RESULTS

Gemological Features. These coated diamonds were remarkable for the large variety of natural-looking colors (again, see figure 1). All of the commercial samples except the yellow diamonds were strongly saturated, corresponding to the GIA grades of Fancy Intense to Fancy Vivid. Most of the yellow samples showed some degree of brown modifier, and only a few of the blue diamonds had a modifying hue. A yellow modifier was seen in many of the green and orange diamonds. The before/after experiments confirmed the production of yellow, orange, orangy pink, purplish pink, and pink colors by this new coating method (again, see figure 3; table 1 lists the corresponding color grades). It is interesting to note that a Fancy

TABLE 1. Characteristics of six diamonds before and after coating.[a]

Sample no.	Weight (ct)	Clarity	Color		Fluorescence to short-wave UV		Fluorescence to long-wave UV	
			Before	After	Before	After	Before	After
79538	0.36	VS_1	I	Fancy gray-violet	Inert	Inert	Weak blue	Weak blue
79539	0.37	VS_2	I	Fancy Light yellow	Weak yellow	Weak yellow	Strong blue	Strong blue
79540	0.38	VS_1	J	Fancy Intense orangy pink	Inert	Inert	Moderate blue	Moderate blue, chalky
79541	0.34	VVS_1	E	Fancy Vivid orange	Inert	Inert	Inert	Inert
79542	0.40	VVS_2	E	Fancy Intense pink	Inert	Inert	Weak blue	Very weak blue
79543	0.40	VS_1	F	Fancy Deep purplish pink	Inert	Inert	Moderate blue	Weak blue

[a] *Note that although these six samples were of relatively high color and clarity, the industry typically sends lower-quality diamonds for this coating treatment.*

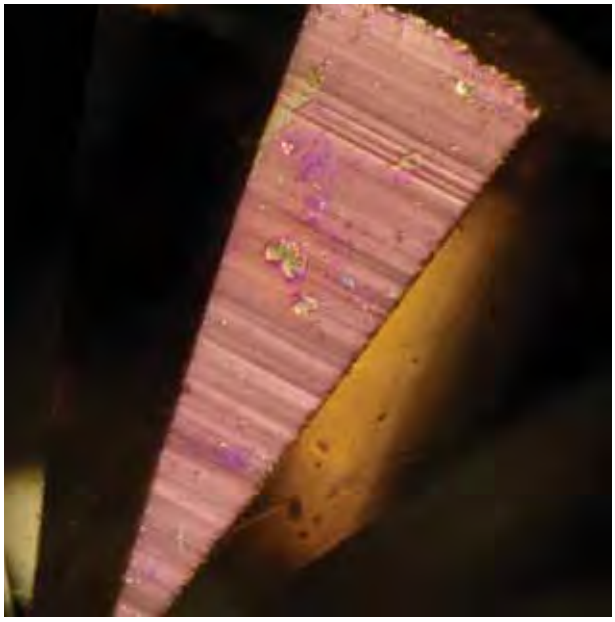

Figure 4. An interference-related colored film—here, a purple film on a green-coated diamond—was observed when the diamonds were viewed with diffused reflected light. Photomicrograph by W. Wang; magnified 105×.

Figure 5. Colorless spots, dark stains, and scratches occurred randomly on some coated facets. Photomicrograph by W. Wang; magnified 112×.

gray-violet color was produced on sample 79538, instead of the pure blue color we observed in many samples obtained from the market. Microscopic examination did not reveal any damage to the diamonds from this treatment process.

The color of all the coated samples appeared evenly distributed when they were examined face-up with magnification and diffused light. However, when their pavilion facets were viewed in diffused reflected light, the coating was visible as an interference-related colored film on the surface of all samples. This feature was particularly evident in the green-coated diamonds, which displayed an intense purple interference color (figure 4). Often, the color appeared bronzy. Randomly distributed colorless spots, dark stains, and scratch lines were also observed on some coated facets (figure 5), but many of the facets did not show such damage. For all the samples examined in this study, the coating was seen only on the pavilion facets; it was not observed on the table or crown facets.

Unlike natural-color pink diamonds, no pink graining was evident in the pink-coated diamonds when they were examined with magnification and darkfield illumination. Common internal features in natural-color diamonds (e.g., the high clarity observed in type IIb blue diamonds and the patchy distribution of color in natural yellow-orange diamonds) were generally missing in their coated counterparts. Instead, inclusions of varying sizes were typically seen, indicating the relatively low clarity of some of the stones selected for this treatment.

The coating had little effect on the UV-activated fluorescence in the six before/after samples (see table 1). After treatment, these six samples exhibited the same color of fluorescence to both long- and short-wave UV radiation, but the intensity to long-wave UV was weaker in two of them (nos. 79542 and 79543). In addition, chalky fluorescence developed in sample 79540 after the treatment.

Likewise, there seemed to be no correlation between UV-activated fluorescence and the coated color for the diamonds obtained from the market. Blue fluorescence of varying intensity was the most common (~80%) reaction to long-wave UV among the 102 diamonds, followed by weak yellow fluorescence (~20%). Weak-to-moderate yellow fluorescence to short-wave UV radiation was very common (~80%), while some samples appeared inert (~15%).

The DiamondView instrument did not show any obvious fluorescence variations on either the table or the pavilion after the coating treatment for any colors except orange. Before treatment, sample 79541 showed blue fluorescence in the DiamondView; after the orange coating was deposited, we observed a moderately strong orange fluorescence from the pavilion.

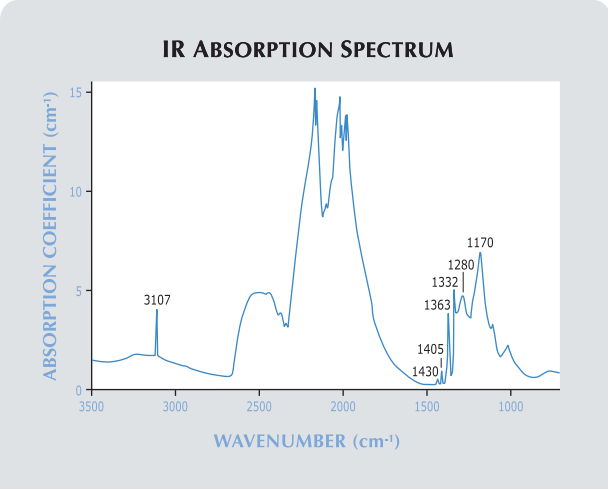

Figure 6. This absorption spectrum of a blue-coated diamond in the mid-infrared region shows that it is type IaAB with a moderately high to very high concentration of nitrogen (>250 ppm) and high hydrogen. No boron-related absorption was detected in any of the treated blue diamonds.

Spectroscopic Features. Infrared absorption spectra for the 21 randomly selected orange, purple-pink, and pink treated diamonds indicated that they were all type IaAB with very high concentrations of nitrogen. The spectral features of many samples (>50%) were similar to those of cape yellow diamonds. Eight blue samples analyzed in this study showed moderately high to very high concentrations (well over 250 ppm; type IaAB) of nitrogen. Two of these stones had higher concentrations of B-aggregate and were rich in hydrogen, as evidenced by the 3107 cm^{-1} peak in figure 6. No boron-related absorptions, such as those observed in natural or synthetic type IIb diamonds, were detected in any of the blue diamonds analyzed. Identical mid- and near-infrared absorption spectra were recorded in the six diamonds before and after treatment, and all showed cape series features. We did not observe any absorption features in these regions of the spectrum that could be attributed to the coatings.

Consistent absorption features in the UV-Vis-NIR region were recorded from samples of the same color categories; typically, they differed from those associated with their natural-color counterparts (figure 7). Absorption by the N3 system (zero phonon line at 415 nm) was detected in all of these samples with varying intensity, indicating the natural origin of these treated diamonds. The pink-coated diamonds showed an absorption band centered at ~525 nm that was so broad that a significant amount of blue light was absorbed (full width at half maximum [FWHM] ~89 nm). A similar broad absorption band occurred in the purplish pink diamonds. However, the center of this band shifted to ~540 nm, and it was slightly narrower (FWHM ~82 nm). As a result, absorption of blue light was less intense

Figure 7. The visible spectra of the Serenity coated diamonds (left) exhibited absorption features that were distinctly different from the spectra of their natural-color counterparts (right). Spectra are offset vertically for clarity.

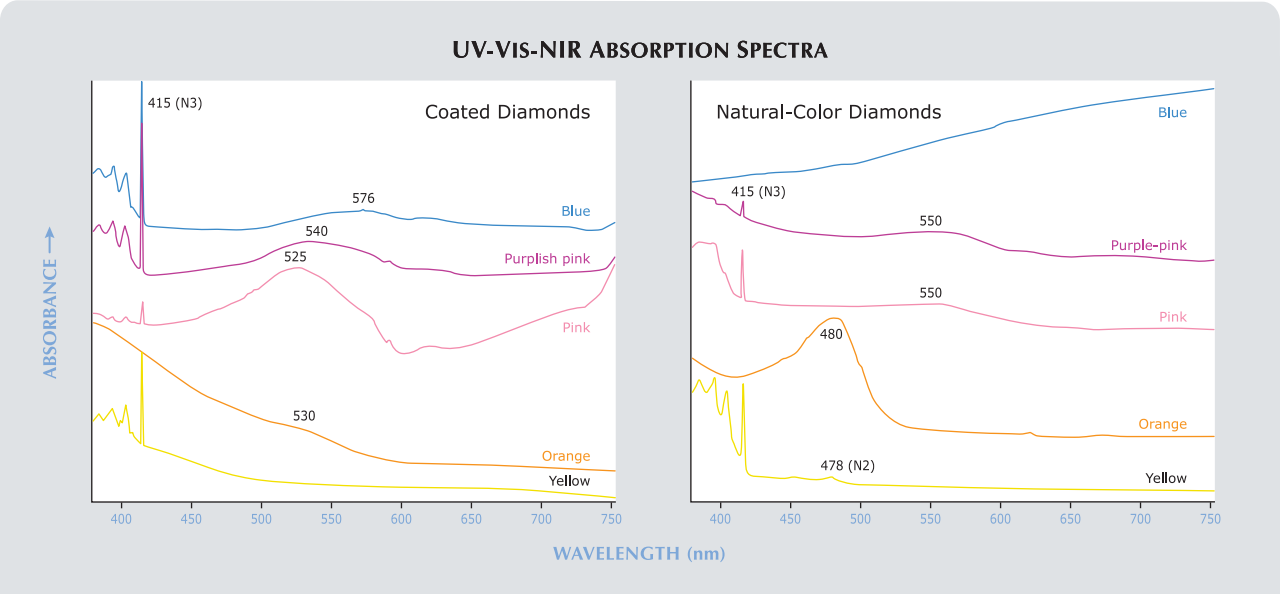

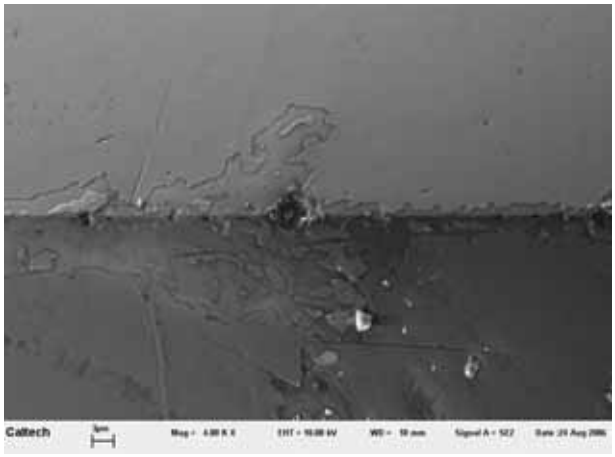

Figure 8. Backscattered electron imaging taken with the SEM reveals a thin film on the pavilion of this diamond. Some damage to the coating is visible along this facet junction. Image by Chi Ma.

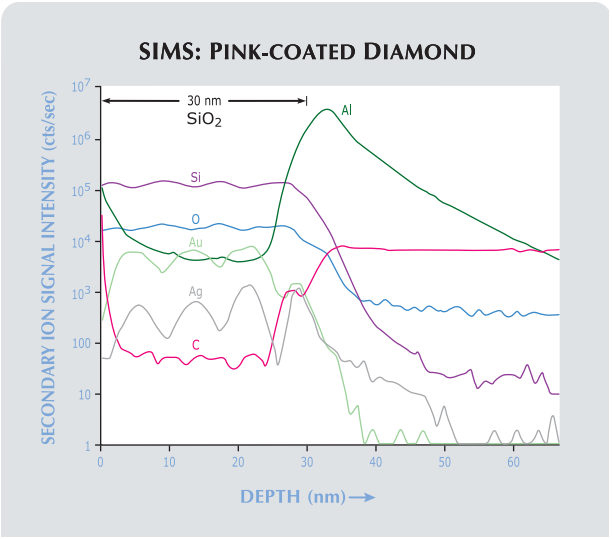

Figure 9. This SIMS depth profile reveals a silicon dioxide (SiO_2) coating with oscillating metal-bearing layers (Au>Ag) on one of the pink samples. The elemental intensities are shown on a logarithmic scale.

than in the pink-coated diamonds. In the blue samples, a broad band extended from 500 to ~700 nm, with the maximum at ~576 nm—absorbing a wide range of visible light and creating a transmission window in the blue region. In the orange-coated diamonds, we observed a decrease in absorption from the UV region to ~560 nm, as well as a weak feature at ~530 nm. The yellow-coated diamonds displayed a smooth decrease in general absorption from the UV region to ~550 nm. Although the other coated diamonds showed absorption features in the region of 520–580 nm, no such features were observed in the yellow-coated diamonds.

No Raman or photoluminescence signals attributable to the coatings were detected. The spectra before and after treatment were nearly identical.

Electron Imaging and Chemical Composition. The back-scattered electron images generated by the scanning electron microscope confirmed the presence of a thin surface film on the pavilion facets of all three diamonds tested (e.g., figure 8). The thickness of the coating could not be determined with this technique, but these images showed it to be <100 nm. Some visible damage to the coating, or lack of deposition, was seen along facet junctions of each of the three diamonds. The irregular embayments near the facet junctions are not known to occur on the surface of a polished diamond, and they are a strong indication that a coating has been applied. EDS chemical analysis detected Fe, Si, O, and C in the orange-coated diamond, and Si, Au, O, and C in the pink- and blue-coated diamonds. Since these films are very thin, the concentrations of these chemical elements could not be determined reliably. Only carbon was detected on the crown facets.

Using EDXRF analysis, we detected Fe and Si in an orange-coated diamond, and Au and Si in the

Figure 10. The SIMS depth profile of a blue coating shows similar chemical components as in the pink film, but with the added presence of Ti. (The boron signal is likely due to contamination.) However, the signal intensity of Ag is much higher than that of Au, and parallel trends for Al and Ti are observed. The blue coating also exhibits fewer variations in the apparent number of film layers. The elemental intensities are shown on a logarithmic scale.

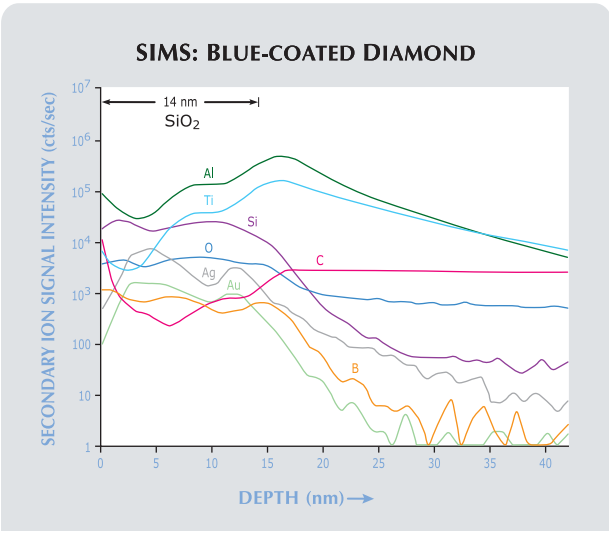

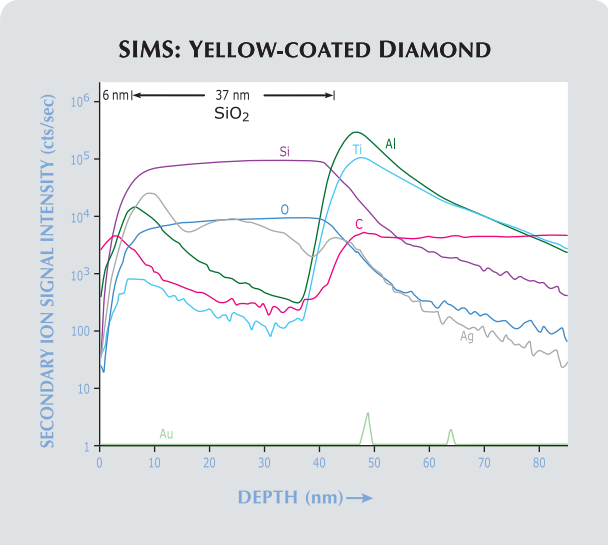

Figure 11. In the yellow coating, the concentration of Ag is very high, while Au is virtually undetectable. Unlike the other colors analyzed, the outermost layer (~6 nm) of the yellow coating appears to contain carbon. Two isotopes of silver (^{107}Ag and ^{109}Ag) were identified for this sample. The elemental intensities are shown on a logarithmic scale.

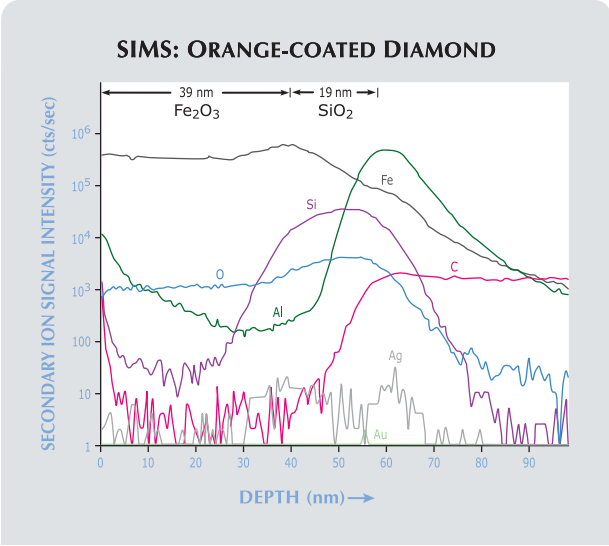

Figure 12. The orange coating was the only color analyzed that had a surface layer of iron oxide (likely as Fe_2O_3). Beneath the iron oxide layer is a SiO_2 film and an Al adhesion layer. The orange coating contains virtually no Au or Ag. The elemental intensities are shown on a logarithmic scale.

blue, pink, and purple-pink diamonds, similar to the observations of other researchers (Kitawaki, 2007). Signals of Fe and Au were usually very clear. Although Si has been shown by other techniques to be a major element of the coating, with this type of analysis it appeared as a weak "shoulder" beside a strong diffraction peak.

The depth profiles as measured by SIMS showed that these films, except the orange, consist of silicon and oxygen (likely as SiO_2) with various impurity elements added as coloring agents (figures 9–12). The interface between the coating and the diamond is marked by an increase in the intensity of the carbon signal, which then levels off within the diamond.

In the pink-coated diamond, Au had a higher intensity than Ag in the SiO_2 film (figure 9). Oscillations in the Au and Ag intensities with depth indicate that the film is composed of three SiO_2 layers (about 30 nm total thickness) that contain varying amounts of Au and Ag. A very thin layer of Al metal appears to be present between the diamond and the SiO_2 layers.

The blue-coated diamond had a SiO_2 layer only 14 nm thick that was doped with both Au and Ag (figure 10); Al is evident as well. This film also contained significant Ti. A very weak boron signal was also seen in the blue coating; this likely is due to contamination. Its intensity decreased gradually with depth before reaching the diamond, and then it decreased sharply. In addition, there was no increase in boron intensity as the sputtering ion beam reached the diamond surface, whereas the intensity of carbon increased gradually.

The SiO_2 film of the yellow-coated diamond was found to be Ag-doped, with virtually no Au detected (figure 11). It is interesting to note that a high concentration of carbon was observed in the outermost layer of the coating. After attaining a maximum in the near-surface region, the intensity of the carbon signal decreased with increasing sputtering depth before reaching the diamond—a profile that was not observed for other elements including Si. An ~9 nm layer of Al and Ti was identified between the SiO_2 coating and the diamond. The total thickness of the coating on the yellow diamond was about 52 nm.

In contrast to the other colored samples, the orange-coated diamond had a surface coating of nominally undoped iron oxide approximately 39 nm thick (figure 12). Beneath the iron oxide film was a SiO_2 film about 19 nm thick, with an underlying Al layer of ~4 nm.

DURABILITY TESTING

When a new gem treatment method is introduced, inevitably the question arises "Is it durable?" To test this, we set up a limited series of experiments that

focused mainly on the conditions such treated diamonds might encounter in real-life situations. The tests included controlled heating; standard jewelry setting, repair, and cleaning procedures; exposure to common household cleaners; and scratching.

Methods. *Controlled Heating.* Controlled heating experiments were performed using a Lindberg/Blue M Moldatherm box furnace. One sample of each color (pink, purple-pink, yellow, green, blue, and orange) was heated at 300–800°C for 30 minutes in air, with a 100°C increment between each step. In each experiment, the target temperatures were reached and then the samples were placed in the oven.

Jewelry Setting, Repair, and Cleaning. Three coated samples (pink, blue, and orange) were exposed to a series of procedures designed to assess this treatment's durability to standard jewelry manufacturing, repair, and cleaning practices. The samples had to be larger than 0.30 ct to fit in a standard solitaire setting that would allow adequate viewing of the pavilion. After each test, the stones were examined carefully with a standard gemological microscope and photographed as appropriate. Only one of the stones (the pink) was used for the rhodium plating test, and seven other coated diamonds were exposed to sulfuric acid.

1. *Setting:* The diamonds were mounted in standard 14K white gold rings, the prongs filed, and then one pavilion facet of each mounted diamond was polished using a wheel charged with a Tripoli or Rouge compound for about 5 seconds (as would be the case if the jeweler inadvertently touched the stone while polishing a prong).

2. *Retipping of Prongs:* The procedures used were similar to those previously performed on lead glass–filled rubies (McClure et al., 2006):
   A. The rings were soaked in a borax solution and gently heated. A small bead of low-temperature solder ("easy flow," melting temperature 621°C [1150°F]) was dipped in Battern's flux (a mixture of borax and ammonium chloride) and placed on top of a prong. Using a bench jeweler's torch, the solder was heated until it flowed around the broken prong.
   B. Following the same procedure, a high-temperature solder ("hard flow," melting temperature 788°C [1450°F]) was tested on a different prong, where the adjacent coating seemed undamaged.
   C. A small drop of Battern's flux was placed on the coating and the stone was heated to the melting temperature of the low-temperature solder.
3. *Rhodium Plating:* This simple electrode plating process for white-metal jewelry involves immersing the set object in a sodium hydroxide bath, as well as in a sulfuric acid bath containing dissolved rhodium. In both baths, the jewelry serves as an electrode with current passing through it. The ring set with the pink-coated diamond was plated and cleaned with ultrasonic and steam cleaners.
4. *Steam Cleaning:* A standard steam cleaner (40–50 psi) was used on the three mounted diamonds, held ~2.5 cm from the nozzle for 10–30 seconds.
5. *Immersion in a Pickling Solution (Sodium Bisulfate):* The three rings were immersed for one minute in a warm pickling solution after the low- and high-temperature retipping processes, and then steam cleaned for a several seconds.
6. *Exposure to Sulfuric Acid:* Seven other coated diamonds were boiled in sulfuric acid for 30 minutes, a method commonly used to clean master stones. We included one sample of each color (two were pink). Except for one orangy pink sample (0.50 ct), all of these samples were small (0.01–0.07 ct).

Exposure to Common Household Cleaners. The durability of 15 coated diamonds (pink, yellow, green, blue, and orange) was tested by exposure to kitchen detergent (water-diluted Palmolive), rubbing alcohol (isopropyl), acetone (reagent grade), and bleach (undiluted Clorox, which is 5.25% sodium hypochlorite). The diamonds were immersed in each substance and removed for observation after one minute, 5 minutes, and every 10 minutes up to one hour, then every hour for 6 hours. Another observation was made after 24 hours of immersion, and the last was made after 48 hours. All samples were then reimmersed and transferred to an ultrasonic cleaner for 60 minutes. Note that the limited time span of the testing may not correlate with the long-term durability of the coatings.

Scratch Tests. We tested seven coated diamonds of pink, blue, and orange colors using the following materials: a household sandpaper (Mohs hardness ~ 9), a synthetic corundum boule (Mohs hardness = 9), an abrasive powdered cleanser (Mohs hardness ~ 7), and a stainless steel needle (Mohs hardness ~ 5.5). The coated surface was gently rubbed against these materials. The powdered cleanser was made into a slurry and spread on a cloth, and the diamonds were gently rubbed between two layers of the cloth for 10 minutes.

TABLE 2. Summary of durability tests on different colors of coated diamonds.

Testing method	Blue	Green	Orange	Pink	Purple-Pink	Yellow
Jewelry setting and repair						
Controlled heating in air up to 500°C (figure 13)	No damage	No damage	No damage	No damage	No damage	No damage
Controlled heating in air from 600°C to 800°C (figure 13)	Color became pink at 600°C; cloudy appearance at 800°C	Cloudy appearance at 700°C, coating loss at 800°C	Cloudy appearance, coating loss at 800°C	Cloudy appearance, coating loss at 800°C	Cloudy appearance, coating loss at 800°C	Cloudy appearance, coating loss at 800°C
Setting—filing	No damage	N/T[a]	No damage	No damage	N/T	N/T
Setting—polishing (Tripoli or Rouge on metals)	No damage	N/T	No damage	No damage	N/T	N/T
Setting—polishing (Tripoli or Rouge on a pavilion facet; figure 15)	Damaged	N/T	Damaged	Damaged	N/T	N/T
Retipping—low-temperature (easy flow) solder	Color changed (figure 16)/reacted to flux	N/T	Burned appearance (figure 17)	Reacted to flux (figure 18)	N/T	N/T
Retipping—high-temperature (hard flow) solder	Color changed (figure 16)/reacted to flux	N/T	Changed color/burned appearance (figure 19)	Reacted to flux (figure 18)	N/T	N/T
Exposure to Battern's flux	Reacted	N/T	N/T	Reacted (figure18)	N/T	N/T
Rhodium plating	N/T	N/T	N/T	Dissolved (figures 20 and 21)	N/T	N/T
Jewelry cleaning						
Steam cleaning (10–30 seconds)	No damage	N/T	No damage	No damage	N/T	N/T
Pickling solution (one minute)	No damage	N/T	No damage	No damage	N/T	N/T
Sulfuric acid bath (boiling; 30 minutes)	Damaged	Damaged	Damaged	Damaged (figure 22)	Damaged	Damaged
Ultrasonic cleaning	No damage	No damage	No damage	No damage	No damage	No damage
Exposure to household chemicals						
Kitchen detergent (diluted Palmolive)	No damage	No damage	No damage	No damage	N/T	No damage
Isopropyl alcohol	No damage	No damage	No damage	No damage	N/T	No damage
Acetone	No damage	No damage	No damage	No damage	N/T	No damage
Bleach (undiluted Clorox—two days)	Color changed	Color changed (figure 23)	No damage	No damage	N/T	Color changed (figure 23)
Scratch tests						
Sandpaper (3M Wetordry Tri-M-ite silicon carbide paper)	Scratched	N/T	Scratched	Scratched	N/T	N/T
Synthetic corundum boule	Scratched	N/T	Scratched	Scratched	N/T	N/T
Powdered cleanser slurry (Waxie brand)	Scratched	N/T	Scratched	Scratched (figure 24)	N/T	N/T
Stainless steel needle point	Not scratched	N/T	Not scratched	Not scratched	N/T	N/T

[a] *N/T = not tested.*

Results. The results of the durability testing are listed in table 2 and summarized below.

Controlled Heating. All colors remained virtually the same up to 500°C (figure 13). Only the blue-coated stone turned pink after heating at 600°C. However, severe damage to the coatings (as well as the diamonds) was observed after heating at 700–800°C: Almost all samples became cloudy, and on all of them microscopic examination

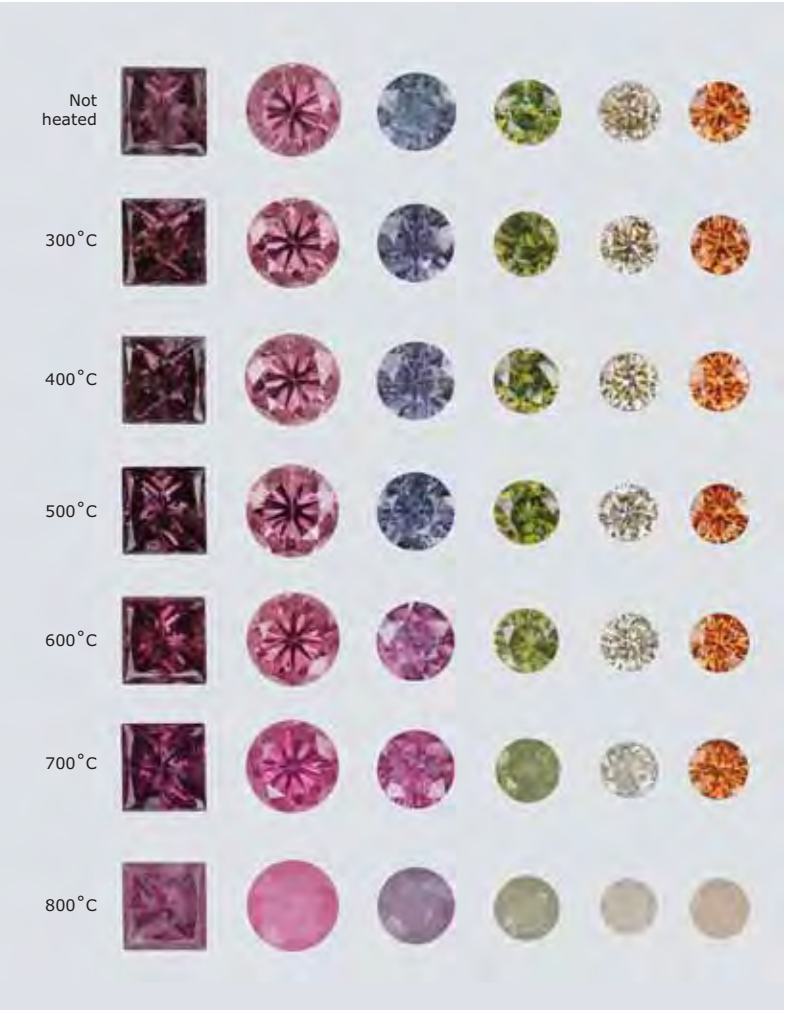

Figure 13. Heating of the coated diamonds in air demonstrated that the coatings are stable up to 500°C, as shown here, but substantial change could occur between 600°C and 800°C. The blue coating turned pink after heating at 600°C for 30 minutes. Composite photo by Jessica Arditi.

Figure 14. After heating at 800°C for 30 minutes, most of the green coating peeled off this diamond and only a small portion remained. Photomicrograph by W. Wang; magnified 70×.

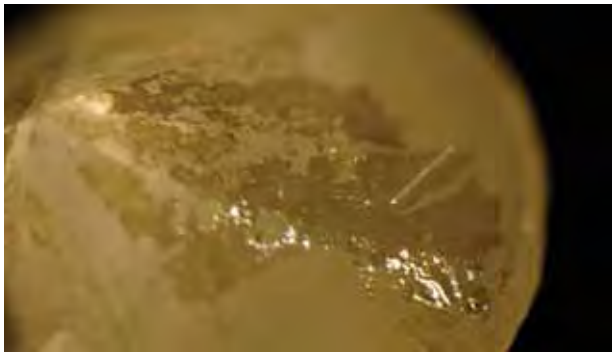

revealed that most of the coating had peeled off, with only small remnants remaining (figure 14). It should be mentioned that even untreated diamonds would display surface damage if heated at this temperature in air.

Epelboym et al. (2006) studied the impact of annealing similar coated diamonds in a vacuum, which reduced the effects of oxidation. They reported that while some stones began to change color at temperatures as low as 300°C, most changed color at 900–1000°C.

Jewelry Setting, Repair, and Cleaning. No damage was noted from the filing or polishing of the prongs, but the coatings on all three diamonds were removed where the pavilion facet was polished with a wheel charged with either Tripoli or Rouge (figure 15).

The most dramatic changes during retipping were seen in the blue-coated diamond. This Fancy gray-blue sample turned Fancy purplish gray after the low-temperature solder procedure (figure 16). This is not surprising, given the results of the heating tests (again, see figure 13). The blue-coated diamond turned pink at 600°C, and the easy-flow solder has a nominal melting temperature of 621°C. The orange coating showed a burned appearance on a relatively large area adjacent to the retipped prong (figure 17). The pink-coated diamond did not show any obvious color alteration after retipping with either type of solder. However, the pink and blue

Figure 15. Note the difference in reflection on this pavilion facet of the orange sample after polishing (with Tripoli), which removed the coating where it touched the stone. Photomicrograph by A. H. Shen; magnified 40×.

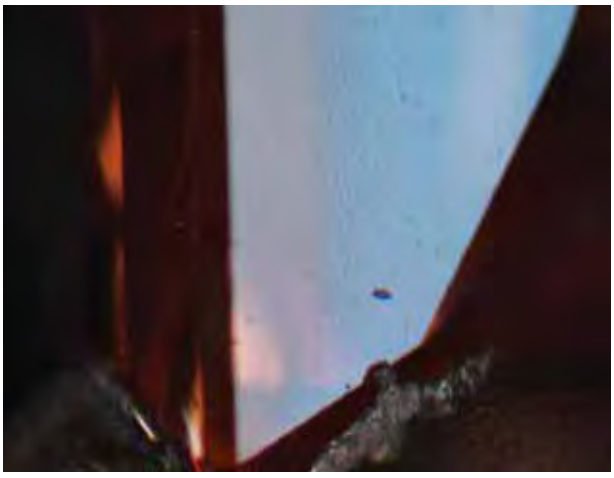

Figure 16. Retipping of a prong with a low-temperature solder caused a pronounced change in the appearance of this 0.36 ct coated diamond, from Fancy gray-blue (left) to Fancy purplish gray (center). The subsequent use of high-temperature solder caused the color to become slightly more purple (right). Photos by Jian Xin (Jae) Liao (left) and Robison McMurtry (center and right).

coatings reacted with the Battern's flux, as shown by mottled features that did not exist before testing (figure 18).

After the higher-temperature retipping process, the blue-coated diamond appeared more purple, but retained its equivalent grade of Fancy purplish gray (again, see figure 16). The original Fancy Vivid orange sample changed to a Fancy Intense yellowish orange and had a burned appearance (figure 19).

After retipping and rhodium-plating, the pink-coated diamond remained Fancy Intense pink, but there was a slight change of color and obvious damage to the surface (figure 20), as the film showed signs of dissolution (figure 21). This is not surprising because the coating can be completely dissolved in strong sulfuric acid, as described below.

No damage was seen in any of the stones with steam cleaning, ultrasonic cleaning, or immersion in a pickling solution. However, boiling in sulfuric acid entirely removed the coatings from six of the seven samples, restoring their original light yellow or light brown coloration (e.g., figure 22). However, a very light pink hue was preserved in the purplish pink coated diamond, and examination with the microscope revealed some coating remnants. In comparison, examination of such coated diamonds at intervals shorter than 30 minutes by Kitawaki (2007) found no effect after three minutes of boiling with aqua regia (25% nitric acid and 75% hydrochloric acid) and no macroscopic evidence of damage after 10 minutes of boiling.

Exposure to Common Household Cleaners. There was no observable damage to the pink and orange coatings with exposure to the various chemicals. The blue, green, and yellow samples were stable in

Figure 17. The film on the orange-coated diamond was damaged ("burned") over a relatively large area during the retipping process with a low-temperature solder. Photomicrograph by A. H. Shen; magnified 20×.

Figure 18. Exposure to Battern's flux, which was used during the retipping process, caused a mottled appearance on this area of the pavilion in the pink-coated stone. Photomicrograph by A. H. Shen; magnified 40×.

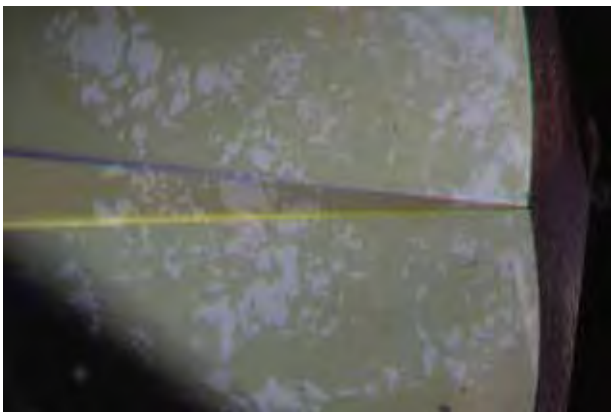

Figure 19. This orange-coated diamond (0.30 ct) was Fancy Vivid orange before the retipping test, but changed to Fancy Intense yellowish orange during exposure to the high-temperature solder. The sample also developed a burned appearance. Photos by Jian Xin (Jae) Liao (left) and Robison McMurtry (right).

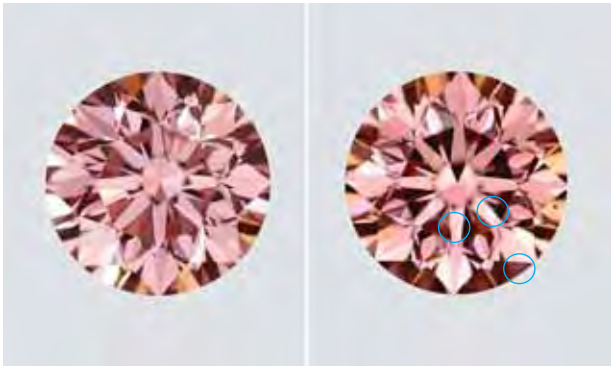

Figure 20. These images show that the jewelry repair tests had some effect on this 0.40 ct pink-coated diamond's apparent color. While the stone was graded Fancy Intense pink both before and after the tests, following rhodium plating approximately 10% of the surface showed evidence of damage in the form of uneven color distribution (see, e.g., circled areas). Photos by Jian Xin (Jae) Liao (left) and Robison McMurtry (right).

the detergent, alcohol, and acetone, but the colors of all three had faded after two days of immersion in the bleach (e.g., figure 23). Although prolonged exposure to bleach for this amount of time is unlikely in normal household use, regular exposure over months or years could produce the same result.

Scratch Tests. The stainless steel needle did not scratch the coatings, but the sandpaper, the tip of the synthetic corundum boule, and the powdered cleanser slurry did cause damage. For example, after the stones were rubbed with a powdered cleanser slurry, their coatings showed a mottled pattern (figure 24). According to the Materials Safety Data Sheets (MSDS) database, the powdered cleanser we used contained a bleach agent, calcium carbonate, and crystalline silica.

Figure 21. After the rhodium plating process, this pavilion facet on the pink-coated diamond in figure 20 showed damage that was not evident prior to the test. The pattern on the area adjacent to the girdle suggests dissolution of the coating. Photomicrograph by A. H. Shen; magnified 40×.

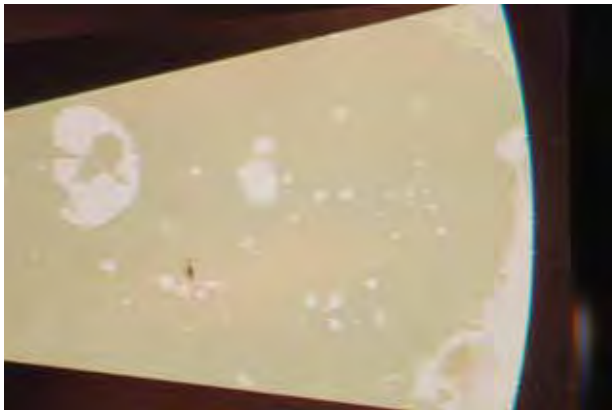

DISCUSSION

Nature of the Treatment. Diamond treatments to alter color are now routine. Well-known methods include irradiation (with and without subsequent heat treatment) and HPHT annealing. The treated colors produced by these methods generally are caused by defects similar to those present in natural diamonds. Consequently, most such treated colors are considered permanent with respect to the condi-

Figure 22. When this pink-coated diamond (0.50 ct) was boiled in sulfuric acid for 30 minutes, the coating was completely removed and the sample regained its original light yellow coloration. Photos by Jian Xin (Jae) Liao.

tions that a diamond would be subjected to during jewelry manufacture, repair, cleaning, and wear. In contrast, the treated diamonds in this study all received their perceived color from the presence of a thin coating, as confirmed by microscopic examination as well as SEM and SIMS analyses. Compared to some other coatings seen in the laboratory, the Serenity Technologies coating appeared to be very even, and the numerous colors produced were quite natural. Strong saturation was seen in all the hues except yellow.

The consistently high concentrations of Si and O in all the coatings demonstrate that the film has SiO_2 as a major component, while other metals or metal oxides appear to have been intentionally introduced as dopants or additional layers. Au and/or Ag likely are the major dopants in the purple-pink, blue, and yellow diamonds, while a high content of Fe was detected in an orange diamond. These thin coatings have strong selective absorptions in the visible light region, which induce the various colors that are observed. These observations are consistent with a recently published patent application (Neogi and Neogi, 2006).

According to the SIMS analyses, the coatings are very thin (<60 nm). Interference of light reflected from the coating surface and from the interface with the diamond creates the colors observed with diffused reflected light (again, see figure 4). However, the presence of the thin coatings cannot be detected using standard techniques for recording Raman spectra or infrared absorption spectra. The sampling depth of the Raman microspectrometer used in this study is ~3 µm, which is about two orders of magnitude thicker than the coatings. As a result, the Raman spectra were dominated by the underlying diamond, and no scattering signal could be detected from the coatings. Although many details, such as the presence of a silica layer and gold impurities, correspond to those reported by Epelboym et al. (2006), this study could not confirm their observation of a Raman peak associated with silicon carbide (SiC).

The SIMS depth profiles showed gradual, rather than abrupt, changes in the elemental concentrations at the transition between the coating and the diamond. However, this should be interpreted as an artifact of the SIMS sputtering method and resolution. In reality, there is likely a distinct interface between the coating and the diamond, with no significant interdiffusion of the elements.

Metal layers in these coatings are commonly used to help the subsequent nonmetal layers adhere to the underlying substrate material (Mattox, 1998). Most commonly, Cr, Ti, or Pt have been used as adhesion promoters; however, thin films of these metals may be more opaque than Al (Ohring, 1992). Very thin layers of Al and/or Ti (several nanometers) detected immediately above the diamond surface on all the samples we tested by SIMS were probably applied to help the coatings

Figure 23. The coatings were removed from these diamonds (0.01–0.02 ct) by immersion in undiluted Clorox bleach for 48 hours. Top—a Fancy Deep green-yellow diamond (left) received a color grade of N on the D-Z color scale (right). Bottom—a Fancy Light yellow diamond (left) was graded V color (right). Photos by Robison McMurtry.

Figure 24. A mottled pattern was evident on this pavilion facet of a pink-coated diamond after being rubbed with a slurry of a powdered household cleanser for 10 minutes. Photomicrographs by A. H. Shen; magnified 40×.

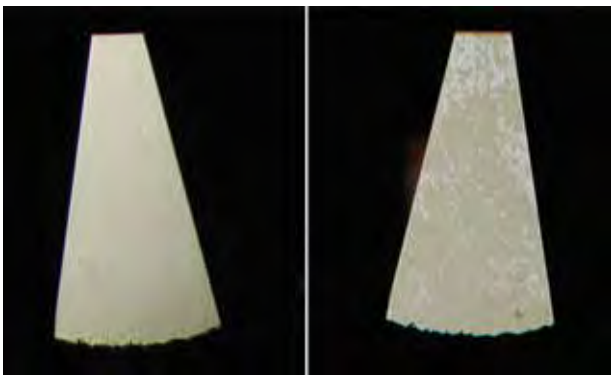

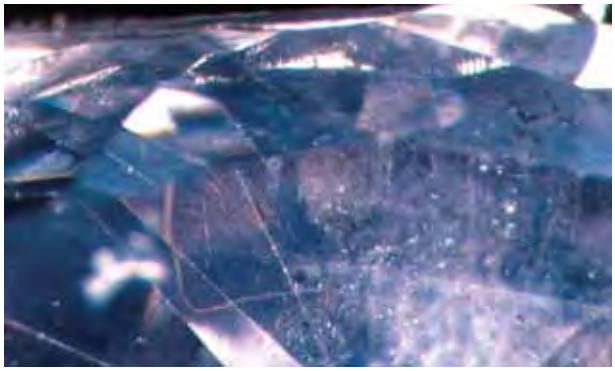

Figure 25. Sometimes surface features on the pavilion of a diamond are more visible when viewed through the table, as with these scratches in the coating on a 0.59 ct stone. Photomicrograph by S. F. McClure; magnified 26×.

adhere to that surface. The authors also detected a similar thin layer of Al in a pink diamond coated with CaF_2. We believe that the improved binding between the diamond and the coating that results from the use of metal adhesive layers is responsible for the greater evenness in color along the facet junctions than earlier coatings seen in the GIA Laboratory.

Identification. Microscopic examination should be the first step in the identification of any colored diamond. Unlike some of the pink CaF_2-coated diamonds, which could be difficult to detect with magnification, these silica-coated diamonds typically may be identified by an experienced gemologist using a gemological microscope. First, since these coatings were only found on the pavilion, it is important to examine the entire diamond when looking for treatment. Many gemologists will inherently begin examination of any stone with the microscope by looking at and under the table facet using darkfield illumination. What they often do not do is look deeper through the table to the pavilion. This type of examination is useful for several identification scenarios, but coatings in particular are often more visible in this viewing geometry (figure 25).

Flipping the stone over and examining the surface of the pavilion with diffused reflected light has proved to be the best method of detecting these coated diamonds. Transmitted light is also very helpful. With these two techniques, the coating is revealed by interference-related colors (again, see figure 4) or a bronze appearance at the surface (figure 26), small uncoated areas or irregularities in the coating (figures 27 and 28), and damage to the coating such as scratches or abrasions along facet junctions or elsewhere (figure 29). Additionally, the GIA sample that received an orange coating (no. 79541) showed whitish marks that made the stone look as if it needed to be cleaned, but they could not be wiped off (figure 30). These methods are similar to those recommended by Miles (1962 and 1964) for coated diamonds seen in the 1950s and '60s, which are also used to detect coatings on other gems, such as "Aqua Aura" quartz (Kammerling and Koivula, 1992). For additional confirmation, immersion in methylene iodide shows concentrated color in the surface region.

Part of the normal testing procedure for a pink diamond is to check for colored graining and the strain patterns typically associated with it. As stated earlier, the Serenity Technologies coated pink diamonds did not show any evidence of colored graining. However, a number of the CaF_2 coated diamonds we have seen (including some of those in figure 2) *did* display planar brown graining with associated strain patterns. We emphasize this as a word of caution, for if a gemologist was not careful, he or she might easily mistake this for the graining and strain present in most natural pink diamonds. Light brown diamonds typically show these features, and we believe these stones are likely candidates for coating.

By the same token, there is no assurance that a pink diamond that does not display colored graining or strain patterns is treated based on this fact alone.

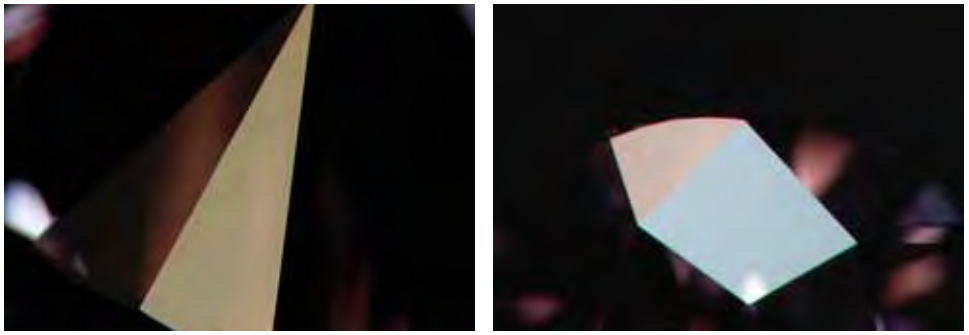

Figure 26. These coatings often have a bronze-colored appearance when viewed in reflected light (left), which makes their presence obvious when compared to the reflected-light appearance of an uncoated facet, here seen on the crown of the same diamond (right). Photomicrographs by S. F. McClure; magnified 23×.

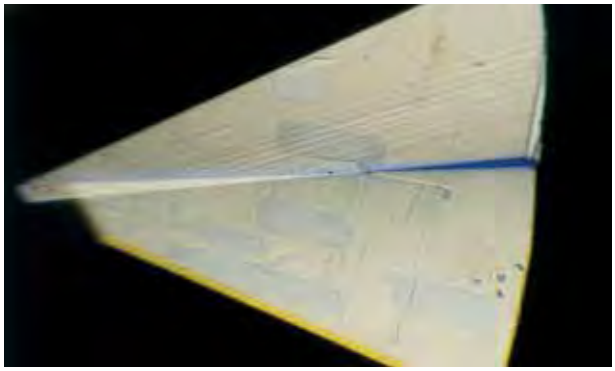

Figure 27. Occasionally, areas are left uncoated on these diamonds and can have several different appearances. Here, with reflected light, they are visible as rectangular patches on a blue-coated stone. Photomicrograph by John I. Koivula; magnified 10×.

A rare type of natural pink diamond, often referred to as a "Golconda pink," can follow this scenario, in which case the UV fluorescence becomes important. These diamonds fluoresce orange to both long- and short-wave UV radiation (stronger to long-wave), which would be an unlikely scenario for a coated diamond.

Other techniques that we used to characterize the coatings, such as SEM and SIMS, also can identify the presence of this treatment, but they are not available to the vast majority of gemologists and are not necessary. However, an anomalous IR or UV-Vis spectrum should alert the gemologist to the possibility of treatment, and EDXRF analysis will help determine if the coating is primarily CaF_2, SiO_2, or some other material.

Coating Durability. The color permanence of these diamonds is entirely determined by the durability of the coatings—how stable the films themselves are and how strongly they adhere to the diamond's surface. SiO_2 films, occurring either as amorphous silica or as quartz, have a Mohs hardness close to 7, which is significantly higher than the hardness of 4 for the CaF_2 diamond coating described by Evans et al. (2005), but considerably lower than that of diamond (10). Therefore, it was not surprising that these coatings were not damaged by scratching with a metal needle (~5.5 hardness), while the CaF_2 coatings we examined in the GIA Laboratory did show signs of damage when similarly tested. SiO_2 is also chemically more stable than CaF_2, but it still can be damaged by strong chemical solutions and harder materials such as abrasive cleaners.

The limited durability of coated diamonds, as revealed in this study and others (e.g., Epelboym et al., 2006; Kitawaki, 2007), is expected in accordance with the kind of coating material applied. When working with these coated diamonds, jewelers must be careful not to directly expose them to high heat and polishing compounds, to rhodium plating, or to cleaning in a sulfuric acid bath. Retailers should advise consumers not to wear the diamonds on their hands while doing household chores that involve bleach or abrasive cleansers.

Color Origin of the Coatings. Recently, SiO_2 films doped with Au and Ag have been extensively investigated for their interesting optical properties (Liz-Marzan, 2004; Yu et al., 2005; Armelao et al., 2006). When SiO_2 is doped with Au and then heated, the Au forms uniformly spaced nanoparticles within the film that create an apparent color due to Mie scattering (Simmons and Potter, 2000). Since the concentrations obtained from SIMS were not calibrated against known samples, it is difficult to calculate the exact composition of the coatings. In addition, one major drawback of SIMS is that sensitivity factors used to translate measured counts to actual concentrations may differ between elements by many orders of magnitude. However, Au and Ag have approximately equal sensitivity factors, so their relative intensities reasonably can be compared. Additionally, the presence of Au and Fe in

Figure 28. Reflected light (left) and transmitted light (right) can both be used to see the small rounded uncoated areas on these diamonds. Photomicrographs by John I. Koivula (left, 25×) and S. F. McClure (right, 23×).

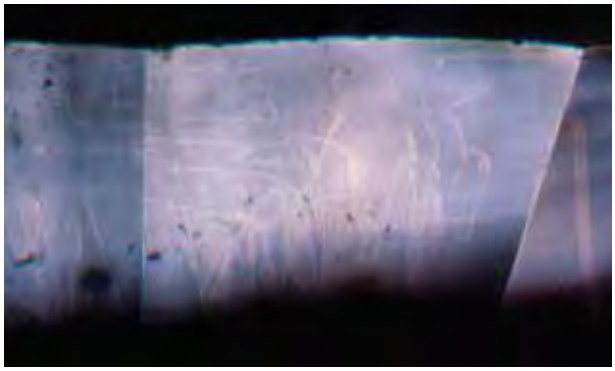

Figure 29. Scratches or other damage to a coating often make it easier to detect. Photomicrograph by S. F. McClure; magnified 35×.

the EDS and EDXRF analyses confirmed that these elements are major components of the coatings. Finally, it is important to reiterate that these analyses are based on depth profiles obtained at one location of one diamond for each color of coating.

Pink Coating. It has been reported that Au-doped films heated to 500°C acquire a light pink color due to an absorption peak at 533 nm (Yu et al., 2005). This is consistent with the absorption spectra of our pink-coated diamond (figure 7) and the concentration profile shown in figure 9. Interestingly, Au was first added to glass in Roman times to cause a red color (Wagner et al., 2000). Deposition of these thin films to create fancy-color diamonds therefore appears to be a modern application of an ancient practice.

Blue Coating. As the concentration of Ag nanoparticles increases within silica, the absorption band shifts toward the red region of the spectrum, to as high as 600 nm (Link and El-Sayed, 1999). This would make the color of the film appear blue. The intensity of the Ag signal (in absolute counts) in the blue film was the highest of any of the doped silica films we measured, and the blue color may be due to a high concentration of nanoparticles of Ag within this film (Link and El-Sayed, 1999). The change of color from blue to pink with heating at 600°C (figure 13) may indicate that such a nanoparticle configuration is unstable at these temperatures, possibly reverting to a more dispersed form similar to that of the pink film.

The apparent color of the blue-coated diamonds is not derived from boron. Extensive infrared absorption analysis confirmed that all the blue diamonds in this study were type IaAB with significant amounts of nitrogen (e.g., figure 6). None of the samples displayed electrical conductivity or exhibited any boron-related absorption features in their visible or infrared spectra. These observations rule out any involvement of ion-implantation of boron in this treatment. Additionally, these diamonds probably will not be confused with natural type Ia nonconductive gray-to-blue diamonds (see, e.g., Fritsch and Scarratt, 1992). In our experience, most of those diamonds show violet, gray, or greenish overtones and do not show the same blue hues that are observed in type IIb diamonds or these blue-coated diamonds.

Figure 30. The numerous irregularities on the surface of this orange-coated sample made the diamond appear to need cleaning, but the marks did not wipe off. Photomicrograph by S. F. McClure; magnified 22×.

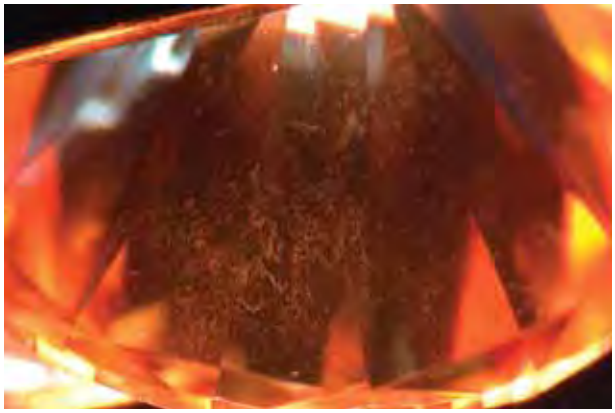

Yellow Coating. Silver was the major dopant in the SiO_2 film, and Au was not detected by SIMS. It is unclear if the elevated carbon peak near the surface is intentional or due to contamination, and additional experiments are needed to make that determination. Silver doping of silica produces nanoparticles with an absorption peak near 411 nm, which may cause the samples to appear yellow (Scalisi et al., 2004). This is not entirely consistent with the gradual increase in absorption from ~550 nm to lower wavelengths observed in this study (again, see figure 7).

Orange Coating. In contrast to the other colors, in which silica was the major component of the films, SIMS analysis revealed a high concentration of Fe in the orange coating. Deposited films of Fe_2O_3 appear brown or red-brown, whereas films of FeO and Fe_3O_4 are black (Peng et al., 2003). Therefore, it is reasonable to surmise that the coating on the orange diamond is composed of Fe_2O_3, with the thickness tailored to produce a desirable orange

color. Unfortunately, we could not measure the oxidation state of the iron, which would have confirmed this identification.

GEMOLOGICAL REPORTING ON COATED DIAMONDS

Due to the unstable nature of diamond coatings and the fact that a foreign material has been applied to the pavilion facets, all coated diamonds submitted to the GIA Laboratory are issued an identification report, but not a quality grading report. No color grade is provided. The identification report states that the diamond is "Surface Coated" and provides information about the diamond's carat weight, cutting style, and measurements. An additional comment explains that "A foreign material has been artificially applied to the surface, which precludes quality analysis." Other laboratories have similar practices and have indicated that coated diamonds either will not be issued a grading report (Kitawaki, 2007) or will be reported as "color-treated" (Epelboym et al., 2006).

CONCLUDING REMARKS

A new coating method has been developed to change the apparent color of diamonds. The coloration appears evenly distributed, and several colors have entered the marketplace, including blue, green, orange, pink, purple-pink, and yellow. The manufacturer reports that other colors, such as red (J. Neogi, pers. comm., 2007), can also be produced by this process. The coatings, which were applied only to the pavilions of the samples we examined, are very thin. They are composed mainly of multilayer doped SiO_2/metal and sometimes metal oxide films. No diffusion of elements into the diamond was detected.

A film-like coating on the pavilion, which can be seen with careful observation using a gemological microscope and diffused reflected light, is a good indication of this type of treatment. Damage to the film along facet junctions, as well as the presence of scratches and colorless and/or dark areas, are additional evidence of this type of treatment. Chemical analysis is required to confirm the specific identity of the coating material that has been applied to the diamond.

As the durability testing indicated, this is not a permanent treatment. Since a foreign material has been applied, the GIA Laboratory will only issue an identification report—not a grading report—on a diamond treated by this technique. The GIA Laboratory will continue to follow the development of this treatment technology to ensure that all diamonds submitted for examination are properly screened for these more sophisticated coatings.

ABOUT THE AUTHORS

Dr. Shen (andy.shen@gia.edu) is a research scientist, Mr. McClure is director of Identification Services, and Dr. Shigley is distinguished research fellow at the GIA Laboratory, Carlsbad. Dr. Wang is manager of Research Projects, and Mr. Hall is manager of Identification Services, at the GIA Laboratory in New York. Dr. Novak is senior specialist at the Evans Analytical Group, East Windsor, New Jersey. Mr. Moses is senior vice president, GIA Laboratory and Research, New York.

ACKNOWLEDGMENTS

The authors are grateful to the following individuals for their cooperation in this study: Jayant Neogi, Serenity Technologies, Temecula, California; Nilesh Sheth, Nice Diamond, New York; and Rahul Karnavat, Lotus Colors, Inc., New York. Special thanks to Gerald Golech and Don Hughes of GIA Education's Jewelry Manufacturing Arts Program, Carlsbad, for their assistance and helpful discussions in conducting the durability tests. We would also like to thank Yianni Melas for supplying useful and timely information on this new treatment. Paul Johnson of the GIA Laboratory in New York and Desiree Gontero of the GIA Laboratory, Carlsbad, were very helpful in characterizing the samples. Dr. Chi Ma and Dr. George Rossman of the California Institute of Technology, Pasadena, kindly provided the SEM analyses. We are grateful to Ken Scarratt of GIA Research (Thailand) for bringing this new product to our attention.

REFERENCES

Armelao L., Barreca D., Bottaro G., Gasparotto A., Gross S., Maragno C., Tondello E. (2006) Recent trends in nanocomposites based on Cu, Ag, and Au: A closer look. *Coordination Chemistry Reviews*, Vol. 250, No. 11/12, pp. 1294–1314.

Crowningshield G.R. (1959) Highlights at the Gem Trade Laboratory in New York: Coated blue diamond. *Gems & Gemology*, Vol. 9, No. 11, p. 343.

——— (1965) Developments and highlights at the Gem Trade Laboratory in New York: More painted diamonds. *Gems & Gemology*, Vol. 11, No. 10, pp. 310–311.

Epelboym M., Zaitsev A., Simic D., Deljanin D. (2006) Preliminary study on new generation of coated diamonds with limited color stability. EGL USA Group of Laboratories,

Nov. 14, www.eglcanada.ca/EN/research.
Evans D.J.F., Fisher D., Kelly C.J. (2005) Coated pink diamond—A cautionary tale. *Gems & Gemology*, Vol. 41, No. 1, pp. 36–41.
Fritsch E., Scarratt K. (1992) Natural-color nonconductive gray-to-blue diamonds. *Gems & Gemology*, Vol. 28, No. 1, pp. 35–42.
Fryer C. (1983) Gem Trade Lab Notes: Painted pink diamond—the big switch. *Gems & Gemology*, Vol. 19, No. 2, pp. 112–113.
Gübelin E.J. (1950) New process of artificially beautifying gemstones. *Gems & Gemology*, Vol. 6, No. 8, pp. 243–254.
Hargett D. (1989) Gem Trade Lab Notes: "Coated" diamond. *Gems & Gemology*, Vol. 25, No. 2, p. 104.
Kammerling R.C., Koivula J.I. (1992) An examination of "Aqua Aura" enhanced fashioned gems. *Journal of Gemmology*, Vol. 23, No. 2, pp. 72–77.
King J.M., Moses T.M., Shigley J.E., Liu Y. (1994) Color grading of colored diamonds in the GIA Gem Trade Laboratory. *Gems & Gemology*, Vol. 30, No. 4, pp. 220–242.
King J.M., Moses T.M., Shigley J.E., Welbourn C.M., Lawson S.C., Cooper M. (1998) Characterizing natural-color type IIb blue diamonds. *Gems & Gemology*, Vol. 34, No. 4, pp. 246–268.
Kitawaki H. (2007) New coating treatment on diamond. *Gemmology Journal*, Vol. 38, No. 448, pp. 6–7.
Liddicoat R.T. Jr. (1966) Developments and highlights at the Gem Trade Laboratory in Los Angeles: Coated diamond. *Gems & Gemology*, Vol. 12, No. 1, p. 26.
Link S., El-Sayed M.A. (1999) Spectral properties and relaxation dynamics of surface plasmon electronic oscillations in gold and silver nanodots and nanorods. *Journal of Physical Chemistry B*, Vol. 103, No. 40, pp. 8410–8426.
Liz-Marzan L.M. (2004) Nanometals—Formation and color. *Materials Today*, Vol. 7, No. 2, pp. 26–31.
Mattox D.M. (1998) *Handbook of Physical Vapor Deposition (PVD) Processing*. Noyes Publications, Westwood, NJ, 917 pp.
McClure S.F., Smith C.P., Wang W., Hall M.S. (2006) Identification and durability of lead glass–filled rubies. *Gems & Gemology*, Vol. 42, No. 1, pp. 22–34.
Miles E.R. (1962) Diamond-coating techniques and methods of detection. *Gems & Gemology*, Vol. 10, No. 12, pp. 355–364, 383.
——— (1964) Coated diamonds. *Gems & Gemology*, Vol. 11, No. 6, pp. 163–168.
Moses T., Shigley J.E., McClure S.F. (2007) A coat of many colors. *Rapaport Diamond Report*, Vol. 30, No. 5, pp. 1, 36–37.
Neogi S., Neogi J. (2006) *Abrasion Resistant Coatings with Color Component for Gemstones and Such*. U.S. Patent Application 20060182883, Aug. 16, 2006.
Ohring M. (1992) *The Materials Science of Thin Films*. Academic Press, San Diego, CA, 750 pp.
Peng Y., Park C., Laughlin D.E. (2003) Fe_3O_4 thin films sputter deposited from iron oxide targets. *Journal of Applied Physics*, Vol. 93, No. 10, pp. 7957–7959.
Scalisi A.A., Compangnini G., D'Urso L., Puglisi O. (2004) Nonlinear optical activity in Ag-SiO_2 nanocomposite thin films with different silver concentration. *Applied Surface Science*, Vol. 226, No. 1/3, pp. 237–241.
Sheby J. (2003) Gem Trade Lab Notes: Coated diamonds. *Gems & Gemology*, Vol. 39, No. 4, pp. 315–316.
Simmons J.H., Potter K.S. (2000) *Optical Materials*. Academic Press, San Diego, CA.
Wagner F.E., Haslbeck S., Stievano L., Calogero S., Pahnkhurst Q.A., Martinek K.-P. (2000) Before striking gold in gold-ruby glass. *Nature*, Vol. 407, No. 6805, pp. 691–692.
Wang W., Moses T., Shen A. (2006a) From GIA Research—New "coated" diamonds. *GIA Insider*, Dec. 1, 2006, www.gia.edu/newsroom/issue/2798/2675/insider_newsletter_details.cfm#5.
Wang W., Gelb T., Dillon S. (2006b) Lab Notes: Coated pink diamonds. *Gems & Gemology*, Vol. 42, No. 2, pp. 162–163.
Welbourn C.M., Cooper M., Spear P.M. (1996) De Beers natural versus synthetic diamond verification instruments. *Gems & Gemology*, Vol. 32, No. 3, pp. 156–169.
Wilson R.G., Stevie F.A., Magee C.W. (1989) *Secondary Ion Mass Spectrometry: A Practical Handbook for Depth Profiling and Bulk Impurity Analysis*. John Wiley & Sons, New York.
Yu G.Q., Tay B.K., Zhao Z.W., Sun X.W., Fu Y.Q. (2005) Ion beam co-sputtering deposition of Au/SiO_2 nanocomposites. *Physica E*, Vol. 27, No. 3, pp. 362–368.

TRAPICHE TOURMALINE FROM ZAMBIA

Thomas Hainschwang, Franck Notari, and Björn Anckar

Well-formed crystals of green tourmaline from northwestern Zambia show a growth pattern reminiscent of trapiche emerald/ruby when sliced perpendicular to the c-axis. In fact, such slices were originally encountered in parcels sold as emerald in Zambia. The trapiche appearance most likely originates from skeletal growth, with the pattern formed by a black carbonaceous substance (mostly graphite) that partially filled growth tubes concentrated in three areas: (1) along the three edges of the trigonal pyramids *r* {$10\bar{1}1$} or *r'* {$01\bar{1}\bar{1}$}, (2) at the interface between the trigonal pyramids and the prism *a* {$11\bar{2}0$}, and (3) between individual growth sectors of the prism *a*. Spectroscopic and chemical analyses indicate that the tourmaline is uvite that is colored green by a vanadium-related mechanism. To the authors' knowledge, this is the first occurrence of trapiche tourmaline.

Tourmaline is one of the most complex minerals in terms of its chemical composition and color distribution. The extraordinary color zoning of many tourmalines was illustrated by Benesch (1990). Triangular zones containing a trigonal star-like pattern (following the edges of the trigonal pyramid) are common in some multicolored tourmalines, particularly in liddicoatite from Madagascar. Other growth phenomena are not common in tourmaline, so two of the authors (TH and FN) were interested when, in November 2005, they encountered some sliced crystals of green tourmaline from Africa that exhibited a growth structure similar to the trapiche pattern known to occur in emerald and ruby (see, e.g., figure 1). The third author (BA) first saw such material in 2004 and 2005 in Lusaka, Zambia, within "salted" parcels of rough emerald and as separate lots of this green tourmaline that were being offered as emerald (figure 2). Zambian gem traders called the material "Mercedes Benz tourmaline" (or "emerald") due to the shape of the trapiche-like inclusions in the cores of the slices, which may resemble this automobile company's logo (again, see figure 1).

LOCATION AND PRODUCTION

Most of this trapiche tourmaline reportedly comes from the Kavungu mine adjacent to the tiny village of Jivunda in Chief Sailunga's area, which lies southeast of Mwinilunga in northwestern Zambia (figure 3). The locality is accessed by driving 230 km west from Solwezi on the Mwinilunga road and turning south for 35 km to reach Jivunda on the road going toward Ntambu. Local gem traders also report another locality for this tourmaline in the Kampanda area, which is located southwest of Mwinilunga near the border with Angola.

According to the Jivunda villagers, the Kavungu deposit has been known for at least 10 years, but it was not significantly exploited until 2004, when commercial mining was attempted under the assumption the material was emerald. However, this activity was short-lived, and the equipment was removed when the mine investor realized that the gems were another mineral altogether. Children

See end of article for About the Authors and Acknowledgments.
GEMS & GEMOLOGY, Vol. 43, No. 1, pp. 36–46.

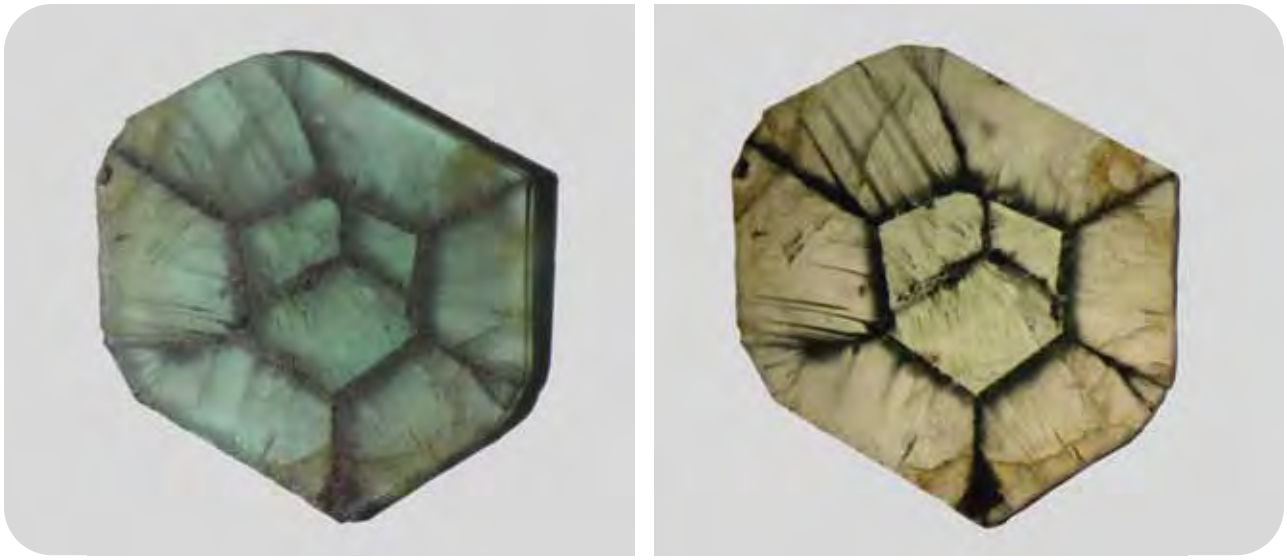

Figure 1. A distinct trapiche pattern is seen in this tourmaline slice (12.8 × 10.6 mm) from Zambia. Photos by T. Hainschwang (left—overhead light; right—transmitted light).

from Jivunda continue to recover the tourmaline by hand from the various pits dug over the years (see, e.g., figure 4), which they sell to passing traders. The tourmaline is fairly abundant; during a two-hour mine visit in December 2006, one of the authors (BA) witnessed the recovery of more than 100 crystals by a few of the children. It must be noted, though, that only about 1–2% of the tourmaline is found as near-euhedral to euhedral crystals that are suitable for slicing or cutting thin cabochons that show the trapiche pattern. Facetable material is extremely rare and restricted to small pieces (<0.10 ct), due to the dark color of the tourmaline. For these reasons, the trapiche tourmaline is seldom encountered on the international market.

GEOLOGY

The bedrock at the Kavungu mine consists of an impure and distinctly banded marble that has been selectively weathered into a typical karst landform, with solution-resistant areas of marble that are surrounded by lateritic soil (figures 4 and 5). The tourmaline has been found only in these residual laterite

Figure 2. Well-formed crystals of green tourmaline—which may display a trapiche appearance when cut into slices—have been sold as emerald in Zambia. The crystals shown here range from 0.8 to 2.6 cm long. In general, only a small percentage of the tourmaline shows a near-euhedral shape and a noticeable trapiche pattern when sliced. Gift of Björn Anckar, GIA Collection no. 36754; photo by Robert Weldon.

Figure 3. The trapiche tourmaline studied in this report came from the Kavungu mine, located southeast of Mwinilunga in northwestern Zambia. Similar tourmaline has also reportedly been found in the Kampanda area, which lies southwest of Mwinilunga near the Angolan border.

Figure 4. Previous mining efforts have left several pits at the Kavungu site. Tourmaline is encountered in the lateritic soil between the marble outcrops. Photo by B. Anckar, December 2006.

layers, so its precise petrologic setting is unknown. Villagers report that the tourmaline crystals are occasionally seen "in the hard rock," but no such sample was encountered at the time of the visit by author BA.

The Kavungu mine area is underlain by metasedimentary rocks of the Wamikumbi Formation of the Neoproterozoic Katanga System (Klinck, 1977). The Katanga System has been affected by three deformation phases of the Lufilian orogeny. The immediate area of the Kavungu mine was initially mapped as biotite schists (see map appended to Klinck, 1977). More recently, the Geological Survey Department remapped the Kavungu mine area as dolomitic marbles (D. Lombe and E. Mulenga, pers. comm., 2006). Klinck (1977) studied the area but did not encounter the tourmaline locality. He did, however, describe a location only 2 km southeast of the Kavungu mine with outcrops of banded calcite and calcite-scapolite marbles that he called the "Mujimbeji Marble Member." Both of these marbles contain abundant phlogopite, minor quartz, and accessory pyrite. Klinck (1977) also

reported that they contain minor bands of dolomitic marble and very fine-grained graphitic schist.

It is reasonable to believe that the tourmaline (which was identified as uvite; see below) is metamorphic in origin and formed within these impure Mg-bearing marbles (see, e.g., Gübelin, 1939; Anovitz and Grew, 1996), where it was most likely hosted by local graphite-bearing zones (as shown by the presence of graphite in the trapiche inclusions). Boron, which is an essential element for tourmaline crystallization, is highly mobile in metamorphic aqueous fluids. Klinck (1977) speculated that the abundance of scapolite in the marble is due to evaporite layers in the original sediments; evaporites are commonly enriched in boron.

MATERIALS AND METHODS

For this study, we examined two doubly terminated crystals (5.01 and 12.74 ct) and 30 slices of trapiche tourmaline (0.33–5.29 ct), 28 of which were cut from three similar crystals. The slices were 1–1.5 mm thick and cut perpendicular to the c-axis. In addition, 16 trapiche emeralds (14 cabochons and two crystals) from Muzo, Colombia, were examined microscopically to provide a comparison of their growth patterns and structures.

The trapiche tourmaline samples were tested by standard gemological methods for refractive index (on two polished slices) and specific gravity (determined hydrostatically for the two crystals). The fluorescence of all samples was observed using a standard long- and short-wave UV lamp (365 and 254 nm, respectively). Microscopic examination of all samples was performed in both reflected and transmitted light with a Leica MZ12 binocular microscope.

The trace-element composition of three samples (one crystal and two slices from two different crystals) was measured qualitatively with a Thermo Noran QuanX energy-dispersive X-ray fluorescence (EDXRF) system, using a Si detector cooled by a Peltier cooling stage. Quantitative chemical analysis of two other slices (26 spots total) by electron microprobe was obtained with an ARL-SEMQ instrument (15 kV accelerating voltage, 15 nA beam current, and 3 µm beam diameter). Analyses were calibrated with natural mineral and synthetic compound standards; ZAF and MAN correction procedures were applied to the data (see, e.g., Donovan and Tingle, 1996).

Polarized specular reflectance infrared spectra were recorded for three samples (one from each of the three crystals that were sliced) at 4 cm^{-1} resolution with a Perkin Elmer Spectrum BXII FTIR (Fourier-transform infrared) spectrometer equipped with a DTGS (deuterium triglyceride sulfate) detector and a fixed-angle specular reflectance accessory. We used reflectance mode, because these spectra give more precise information about the structure of the samples—specifically, detection of the intrinsic one-phonon absorptions of tourmaline—than do spectra in transmission mode.

Figure 5. Local miner and gem dealer Stanley Kabwita is shown next to an outcrop of distinctly banded marble in a pit at the Kavungu tourmaline mine. Photo by B. Anckar, December 2006.

Visible–near infrared (Vis-NIR) absorption spectra in the 400–1000 nm range were recorded for two slices (both of which had been analyzed by EDXRF and FTIR spectroscopy) on a custom-made system equipped with an Ocean Optics SD2000 dual-channel spectrometer that had a resolution of 1.5 nm. A 2048-element linear silicon charge-coupled device (CCD) detector was also used. We employed a Hitachi U-3000 spectrophotometer to collect polarized spectra of the same two slices in the UV-Vis-NIR range from 250 to 800 nm. Only the ordinary ray was determined, owing to the dark color of the tourmaline.

Micro-Raman spectra of the inclusions in one slice were recorded with a Renishaw 1000 Raman microscope using a 514 nm laser. Integration times of 10 seconds and up to three scans per spectrum were used.

For X-ray diffraction analysis, a crystal fragment of the tourmaline was mounted on a Nonius Kappa CCD diffractometer equipped with graphite-monochromated Mo-Kα radiation.

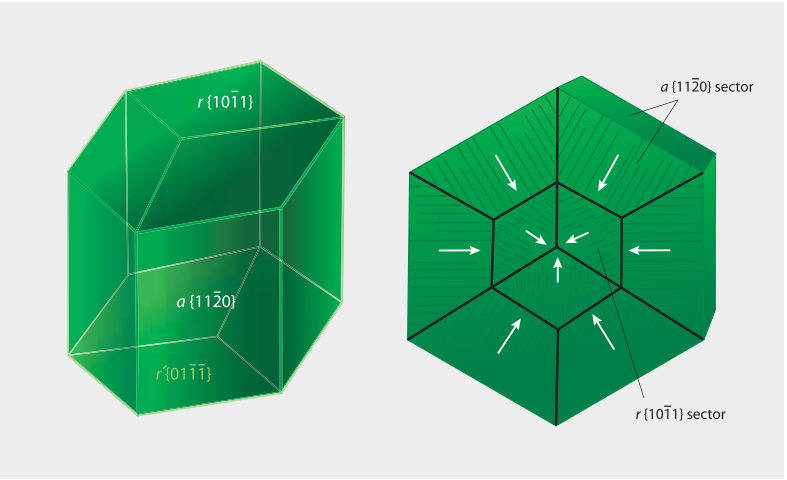

Figure 6. The trapiche tourmaline crystals consisted of the hexagonal prism a {11$\bar{2}$0} and the trigonal pyramids r *{10$\bar{1}$1} and* r′ *{01$\bar{1}\bar{1}$}; the 180° rotation of the pyramids is evident (left). An idealized drawing of a slice cut perpendicular to the c-axis is shown on the right. The arrows indicate the orientation of the channels; in the inner sectors, they are nearly parallel to the c-axis, while those in the outer sectors are close to perpendicular to the c-axis.*

RESULTS

Crystal Morphology and Trapiche Pattern. The tourmaline crystals showed an unusually well-formed and simple habit consisting of the hexagonal prism *a* {11$\bar{2}$0} that was terminated by the positive (on one end) and negative (on the other end) trigonal pyramids *r* {10$\bar{1}$1} and *r′* {01$\bar{1}\bar{1}$} (figure 6, left). As the indices of the pyramids indicate, the pyramids were rotated 180° to one another; thus, the term *polar* or *hemimorph* for tourmaline crystals in general. The prism faces were smooth, as is typical of uvite but uncommon for most other tourmalines, which have striated and rounded faces (Benesch, 1990). The basal pinacoid *c* {0001} was well developed in some crystals seen by one of the authors (BA).

The trapiche motif was formed by black inclusions that were concentrated along the three edges of the trigonal pyramid (forming the central trigonal "star"), at the interface between the trigonal pyramid and the hexagonal prism (hexagon surrounding the trigonal star), and extending from the six edges of the internal prism toward the six edges of the external prism (six outer "arms"; figure 6, right). The black inclusion material appeared to be hosted by growth channels that showed two crystallographic orientations. One set followed the vertical growth direction of the pyramidal faces (parallel to the "faces" of the core formed by the *r* sectors) making up the central trigonal star. The other set appeared at first glance to be perpendicular to the prism, but was likely inclined at the same angle as the pyramidal faces; these channels formed the six "arms" connecting the *r* sectors with the prism, and accentuated the hexagon surrounding the trigonal star. The progression of slices from each crystal showed that the pyramidal faces were dominant at one end and decreased in importance toward the other end, where growth of the prism strongly dominated (see, e.g., figure 7). This structural arrangement was present in all samples, including the two unsliced crystals. The trapiche

Figure 7. These series of slices were cut perpendicular to the c-axes of two crystals of trapiche tourmaline. Each series shows a progression in the dominance of various growth sectors, as marked by the black inclusions that form the trapiche patterns. Photos by T. Hainschwang (upper row—FN 7665–7674, up to 13.4 × 10.6 mm; lower row—TH 682–6810, ~8.4 mm in diameter).

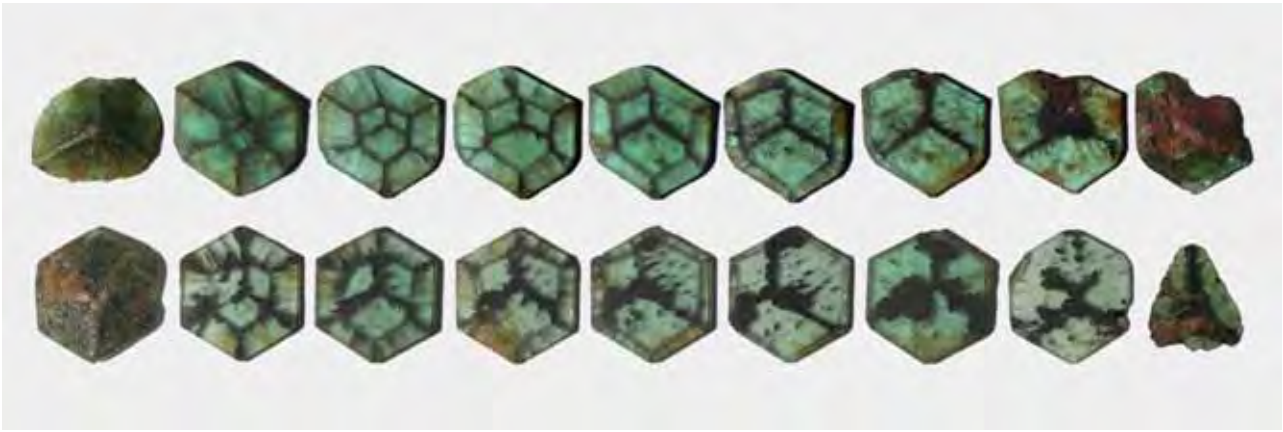

Figure 8. Chalky yellow short-wave UV fluorescence was shown by the slices and crystals of trapiche tourmaline. However, the faces of the trigonal pyramid were inert. Photos by T. Hainschwang (samples TH 682–6810; ~8.4 mm in diameter).

pattern was clearly visible only in the relatively thin slices, since the very dark green color impeded observation of the gray-to-black trapiche pattern in the uncut crystals unless they were examined with very strong transmitted light.

Standard Gemological Testing. The trapiche tourmaline had a deep green bodycolor with very weak pleochroism. The refractive indices were 1.620–1.640, yielding a birefringence of 0.020. The specific gravity varied from 2.82 to 2.99. The samples were inert to long-wave UV radiation, but they fluoresced a weak-to-moderate chalky yellow to short-wave UV on the prism faces only. However, the pyramidal faces did not show UV fluorescence (figure 8). Microscopic observation revealed that the black inclusion material responsible for the trapiche pattern was concentrated in elongate growth channels within the tourmaline (figure 9).

Chemical Analysis. EDXRF spectroscopy of the three samples identified them as Mg-Ca tourmaline with minor Na in two cases. Electron-microprobe analyses (table 1) of two other slices gave chemical compositions that correspond to near end-member uvite (Dunn, 1977a). All of the analyses performed on both slices showed nearly identical compositions, regardless of spot location (e.g., whether on the dark trapiche pattern or the green central area). Traces of the chromophores vanadium, chromium (with V>Cr), titanium, iron, and sometimes Mn also were detected in these two samples. In addition, traces of strontium were detected by EDXRF spectroscopy, and minor fluorine and traces of sodium and zinc were measured by electron microprobe; the latter technique also found minute amounts of potassium and bismuth in the dark trapiche pattern areas.

FTIR Spectroscopy. The polarized specular reflectance FTIR spectra of the trapiche tourmaline samples were almost identical to the reference spectra of most of the "chrome" tourmalines (uvite to intermediate uvite-dravite) from Landanai, Tanzania, in the authors' database. The polarized spectra showed strongly pleochroic absorptions, with the ordinary and extraordinary rays being distinctly different (figure 10). Besides the widely varying intrinsic bands between 1500 and 450 cm^{-1}, the peak at 3550 cm^{-1} (related to structural hydroxyl groups; Rosenberg and Foit, 1979) was only detected in the extraordinary-ray spectrum.

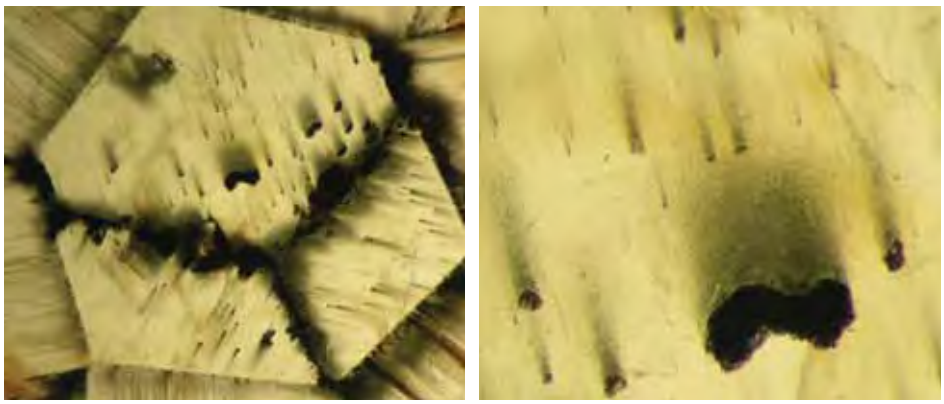

Figure 9. As seen here in transmitted light, two sets of growth channels are apparent in the trapiche tourmaline (left), one following the vertical growth direction of the pyramidal faces, and one nearly perpendicular to the prism. Some channels are empty, while others are filled with a black carbonaceous material (right). Photomicrographs by T. Hainschwang; magnified 10× (left) and 40× (right).

TABLE 1. Representative chemical composition by electron microprobe of two trapiche tourmaline slices.[a]

Chemical composition	Slice 1		Slice 2	
	Green central region[b]	Black trapiche ray	Green central region	Black trapiche ray
Oxide (wt.%)				
SiO_2	36.03	35.96	36.06	36.10
TiO_2	0.33	0.19	0.15	0.12
B_2O_3 (calc)	10.55	10.51	10.57	10.56
Al_2O_3	26.73	26.74	26.70	26.70
Cr_2O_3	0.15	0.13	0.06	0.06
Bi_2O_3	nd	nd	nd	0.08
V_2O_3	0.34	0.28	0.35	0.32
FeO	0.01	nd	0.01	nd
MnO	0.01	nd	nd	nd
MgO	15.12	14.99	15.10	15.09
CaO	5.03	4.96	5.39	5.28
ZnO	nd	nd	0.03	0.07
Na_2O	0.43	0.43	0.62	0.60
K_2O	nd	0.08	nd	0.02
H_2O (calc)	3.11	3.09	3.13	3.21
F	1.12	1.13	1.09	0.91
Subtotal	98.96	98.49	99.26	99.12
-O=F	0.47	0.48	0.46	0.38
Total	98.49	98.01	98.80	98.74
Ions on the basis of 31 (O,OH,F)				
Si	5.934	5.949	5.931	5.942
Ti	0.041	0.024	0.018	0.014
B	3.000	3.000	3.000	3.000
Al	5.190	5.214	5.177	5.180
Cr^{3+}	0.020	0.017	0.007	0.007
Bi^{3+}	nd	nd	nd	0.003
V^{3+}	0.044	0.038	0.047	0.042
Fe^{2+}	0.001	nd	0.001	nd
Mn	0.001	nd	nd	nd
Mg	3.712	3.695	3.701	3.701
Ca	0.887	0.878	0.949	0.931
Zn	nd	nd	0.003	0.008
Na	0.138	0.137	0.199	0.191
K	nd	0.018	nd	0.003
F	0.584	0.593	0.565	0.475
OH	3.416	3.407	3.435	3.526

[a]*Contents of B_2O_3 and H_2O were calculated by stoichiometry. Abbreviation: nd=not detected. Detection limits (wt.%): FeO=0.005, MgO=0.014, MnO=0.005, K_2O=0.015, ZnO=0.029, and Bi_2O_3=0.020. In addition, Cu was analyzed but below the detection limit (0.009 wt.% Cu_2O).*

[b]*The chemical composition recorded in this analysis corresponds to the following formula: $(Ca_{0.887}Na_{0.138})_{1.025}(Mg_{2.712}Al_{0.188}Ti_{0.041}Fe_{0.001}Mn_{0.001})_{2.943}(Al_{4.936}Mg_{1.00}V^{3+}{}_{0.044}Cr^{3+}{}_{0.020})_6(BO_3)_3(Si_{5.934}Al_{0.066})_6O_{18}(OH_{3.416}F_{0.584})_4$. End-member uvite has the general formula $CaMg_3(Al_5Mg)(BO_3)_3(Si_6O_{18})(OH)_4$.*

UV-Vis-NIR Spectroscopy. The ordinary-ray spectrum of the tourmaline was characterized by two broad bands, one centered at 415 nm and the other at 610 nm (figure 11). The resulting strong broad transmission window centered at 520 nm is responsible for the green coloration.

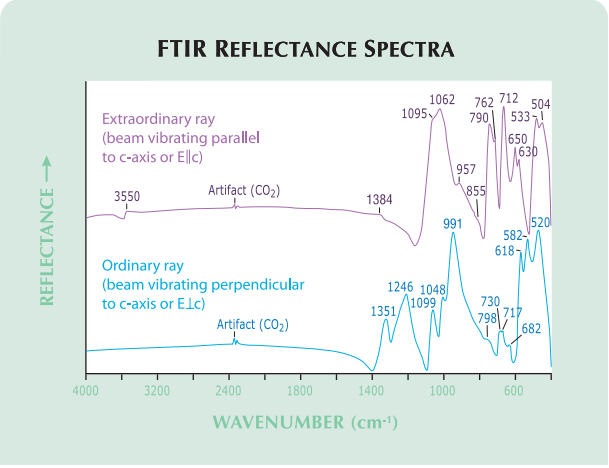

Figure 10. These polarized specular reflectance FTIR spectra are indicative of uvite. The spectral bands are very pleochroic, as shown by the variations in the absorption characteristics of the ordinary and extraordinary rays. The x-axis scale is compressed in the 4000–2000 cm^{-1} region.

Micro-Raman Spectroscopy. The Raman spectra of the black inclusions in the trapiche pattern were characterized by graphite peaks mixed with multiple unknown peaks. Raman analysis also revealed rare iron oxide inclusions—most likely hematite—and inclusions of dolomite within the trapiche pattern.

X-Ray Diffraction. X-ray diffraction analysis gave lattice parameters of a = 15.96(1) Å and c = 7.20(1) Å. The relatively high value of the lattice parameter c

Figure 11. The polarized UV-Vis-NIR spectrum of a trapiche tourmaline (ordinary ray) shows two broad bands centered at approximately 415 and 610 nm, which are characteristic for vanadium-colored green gems such as tsavorite and some tourmaline.

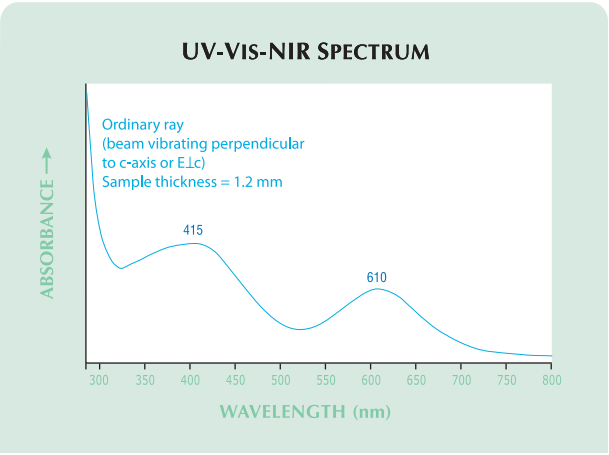

clearly indicated that there was some Mg at the Z site (~1 atom per formula unit). These parameters are consistent with the uvite species of tourmaline.

DISCUSSION

Win (2005) documented a sample of green tourmaline from Mong Hsu, Myanmar, that appeared to show a trapiche pattern. However, the authors of the present article believe that the star-like motif in that sample is due to color zoning rather than the skeletal growth that is associated with trapiche material.

The chemical and spectroscopic properties of the Zambian trapiche tourmaline identify it as near end-member uvite, with traces of Na, Fe, V, and Cr. Chemically, uvite is distinguished from other tourmalines by its Ca-Mg content, and the dravite component is indicated by Na. The identification as uvite was verified by X-ray diffraction analysis and lattice parameter calculations.

Standard gemological, spectral, and chemical data for the trapiche tourmalines correspond to those recorded for the majority of "chrome" tourmalines from Landanai, Tanzania, from the authors' database; these are, in most cases, colored by vanadium, with a minor influence from chromium (Schmetzer and Bank, 1979). The deep green color of the trapiche tourmaline also is most likely due to vanadium (V^{3+}). Although chromium and vanadium both cause broad absorption bands centered at about the same position in the UV-Vis-NIR spectrum (e.g., 600–610 [V^{3+}] and 588 nm [Cr^{3+}]; 418–440 nm [V^{3+}] and 417 nm [Cr^{3+}]; Schmetzer, 1978), the characteristic weak Cr^{3+} absorption at 687 nm (Schmetzer, 1978) was not apparent. And while the presence of Fe and Ti was confirmed by chemical analysis, the 438–444 nm band due to $Fe^{2+} \rightarrow Ti^{4+}$ charge transfer (Schmetzer, 1978) was not evident in the absorption spectra of the chemically analyzed samples. Additionally, the ratio of V:Cr determined by the chemical analyses showed that vanadium is strongly dominant. This is consistent with the UV-Vis-NIR spectra, which were uniquely characterized by the two broad bands due to V^{3+} (see also Schmetzer and Bank, 1979; Schmetzer, 1978).

Dietrich (1985) described the yellow UV fluorescence in some tourmaline (particularly uvite) as "mustard-yellow"; a similar hue was apparent in our samples (again, see figure 8). The lack of this chalky yellow luminescence on the pyramidal faces can most probably be explained by a higher iron content in those sectors at the end of crystal growth; iron impurities are known to quench yellow fluorescence in dravite and uvite (and in many other gems; Dunn, 1977a,b).

Figure 12. The trapiche pattern in the tourmaline is particularly evident when slices of the material are observed with strong transmitted light. Photo by Robert Weldon.

The trapiche pattern most likely formed by skeletal growth, resulting in microscopic channels with two crystallographic orientations: one following the vertical growth direction of the pyramidal faces (parallel to the "faces" of the core formed by the $\{10\bar{1}1\}$ sector); and one nearly perpendicular to the prism, most likely inclined at the same angle as the pyramidal faces (again, see figure 9). These channels are responsible for the significant variations in specific gravity; the greater their abundance, the lower the measured S.G. value.

The trapiche pattern is emphasized by the presence of a black carbonaceous material within these channels (figure 12). These inclusions are most likely related to the lithology of the host rock, as in trapiche emeralds from Colombia. This is supported by the presence of layers and bands of very fine-grained graphitic schist in the marble at the mine site. Our visual and microscopic observations suggest a formation process very similar to that of trapiche emeralds from Muzo, Colombia (see also box A). Muzo trapiche emerald formed in beds of carbonaceous limestone intercalated with black shale (Pogue, 1917). Another trapiche gem related to carbonates is corundum (ruby and violet-to-purple sapphire) from Myanmar, which formed in marbles via contact metasomatism (Sunagawa, 2005). The trapiche tourmaline described here most likely formed in impure Mg-bearing marbles. The close association of all three trapiche gem varieties with limestone or marble suggests that they share a similar formation mechanism.

BOX A: THE TRAPICHE GROWTH PHENOMENON

The trapiche growth phenomenon in gems is commonly associated with emeralds showing a black "fixed star"–like pattern that originate from the Muzo, La Peña, and Coscuez mines in Colombia (e.g., figure A-1). The earliest observation of such emeralds was made by Bertrand (1879). Subsequent work led to much confusion and error, such as ascribing their unusual pattern to twinning (Muñoz, 1948). The first thorough analysis of this material, with the logical conclusions pointing toward a growth phenomenon due to different growth rates, was published by Nassau and Jackson (1970).

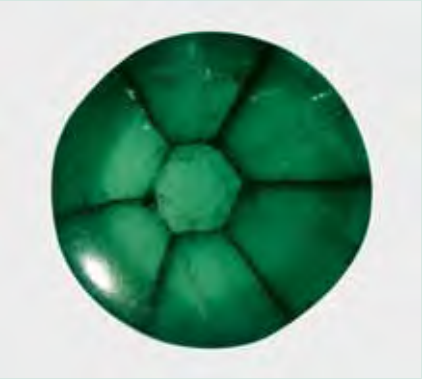

Figure A-1. These trapiche emeralds are representative of such material from Colombia. The observed pattern and the presence and orientation of growth channels are similar to the ones seen in the trapiche tourmalines. Photos by T. Hainschwang (left—TH A15, 10.8 × 8.4 mm; right—FN 6776, 8.6 × 8.4 mm).

Figure A-2. In these trapiche rubies from Mong Hsu, skeletal growth is responsible for the "star." On the left (5.7 × 5.0 mm), typical skeletal growth formed a simple star; on the right (8.2 × 6.6 mm), very strongly developed skeletal growth resulted in a star motif of the gemmy sectors that is created by triangular opaque skeletal arms. Photos by T. Hainschwang.

Figure A-3. Much of the material currently sold as "trapiche" sapphire is in fact not the result of skeletal growth. Only the star in the unusual sample on the right is due to skeletal growth; in the sample on the left, the star-shaped pattern is due to the variable exsolution of inclusions. Photos by T. Hainschwang (left—TH A18, 9.2 × 9.1 mm; right—TH A17, 6.5 × 5.7 mm).

Sunagawa (2005) attributed the trapiche phenomenon in both beryl and corundum to skeletal (or dendritic) growth, in which the edges and corners grow much faster than the faces of a crystal. This phenomenon typically occurs on rough interfaces, under conditions of rapid growth due to local buildup of undissipated latent heat on crystal faces, or simply due to undersaturation of the surrounding solution of a fast-growing crystal. In extreme cases, it can cause fine, tree-like protuberances and branching growth forms (see, e.g., Libbrecht and Rasmussen, 2003).

Trapiche rubies from Mong Hsu (Myanmar) and Vietnam were described by Schmetzer et al. (1996; see also figure A-2). An explanation for their formation was given by Sunagawa et al. (1999), who proposed dendritic (skeletal) growth followed by layer-by-layer growth. Subsequent publications cited basically the same explanation—rapid growth and changes in growth conditions—to explain the trapiche pattern in these rubies. The interpretations differed slightly from author to author (see, e.g., Garnier et al., 2002; Sunagawa, 2005), especially concerning the different growth stages and whether the skeletal arms were formed before, or at the same time as, "regular" growth.

Similar-appearing "trapiche" sapphires are also present on the market. However, these sapphires owe their "star" to variable exsolution of mineral inclusions within the different sectors (figure A-3, left; see also Schmetzer et al., 1996). In some unusual "trapiche" sapphires from Mogok, the pattern results from the distribution of chromophores, resulting in a white star-shaped pattern on a blue background (sample in author TH's collection). True trapiche sapphires resulting from skeletal growth are very rare, and the only samples the authors know of are violet-to-purple sapphires from Mong Hsu (figure A-3, right).

It is not yet clear whether there should be different nomenclatures for the various "fixed star" patterns that are being offered as "trapiche" in the marketplace, especially for sapphire. It *is* evident that true trapiche corundum (i.e., formed by skeletal growth) is much rarer than the others described above; this is particularly true for the violet-to-purple trapiche sapphires.

The trapiche phenomenon is also known in other minerals, such as quartz and andalusite, which the authors are currently studying.

Our comparison of the tourmalines to trapiche emeralds showed nearly identical growth patterns, with tubes filled by carbonaceous inclusions oriented in two crystallographic directions in both gems. The same is true for the development of the pinacoid in emerald versus the development of the trigonal pyramidal faces in tourmaline: In both, from the beginning to the end of growth, a cone-like sector developed as the result of a decrease in the pinacoid/pyramid in the positive c-axis direction and their enlargement in the negative direction. This is most evident when a crystal is sliced parallel to the prism faces (Nassau and Jackson, 1970). In the trapiche tourmaline studied here, the pyramid sector could be reconstructed by observation of the slices cut perpendicular to the c-axis (figure 7). It has been determined that in doubly terminated uvite crystals the positive direction grows about twice as fast as the negative one (Takahashi and Sunagawa, 1998). Since fast-growing faces diminish in crystals (and eventually disappear; Sunagawa, 2005), we concluded that the direction with the diminishing $\{10\bar{1}1\}$ sector core was the positive c-axis direction, and the direction with the growing $\{10\bar{1}1\}$ sector core was the negative c-axis direction.

A distinctive feature of the trapiche pattern in this tourmaline is the presence of a trigonal "star" within the core formed by the $\{10\bar{1}1\}$ sector, corresponding to the edges of the trigonal pyramid. Such a pattern is not known in either corundum or beryl; when a central sector is present in those gems, it is always free of trapiche motifs. One possible scenario for the development of trapiche tourmaline appears to be rapid crystal growth (i.e., somewhere between normal growth and skeletal growth; see also Sunagawa et al., 1999, and box A). The presence of this skeletal motif within the core formed by the $\{10\bar{1}1\}$ sector indicates that this trapiche tourmaline grew rapidly from the beginning of crystallization. Slightly faster growth at the edges would result in the formation of growth channels and the trapping of black inclusions to form the trapiche pattern. Evidence for rapid growth rates can be seen in snowflakes, which can show all stages from normal hexagonal growth to entirely dendritic growth (Libbrecht and Rasmussen, 2003). The channels were formed by rapid growth and the associated black inclusions were trapped in the tourmaline at the faster-growing edges, since a rapid growth rate is one factor that causes more inclusions to be trapped within a gem (Nassau and Jackson, 1970; Sumiya et al., 2005). The accumulation of black inclusions on the faces of the core formed by the $\{10\bar{1}1\}$ sector is likely related to a change in growth conditions.

CONCLUSION

These unusual green tourmalines from Zambia provide a rare example of tourmaline containing a skeletal trapiche pattern. The tourmaline samples analyzed are nearly pure uvite, colored by vanadium. The black pattern shown by slices of this trapiche tourmaline is formed by growth channels that contain carbonaceous material. The pattern is unusual in that there is a trigonal "star" in the core of the slices. The complex trapiche pattern is indicative of rapid growth of the tourmaline from the beginning of crystallization. Although tourmaline is relatively abundant at Kavungu, to date there has been very little organized mining and only a small percentage of the crystals recovered are suitable for slicing to show the trapiche pattern.

ABOUT THE AUTHORS

At the time this article was prepared, Mr. Hainschwang (thainschwang@yahoo.com) was research gemologist, and Mr. Notari was research manager, at GIA GemTechLab in Geneva, Switzerland. They are now research manager and laboratory manager, respectively, at GemTechLab in Geneva. Mr. Anckar worked for the European Union Mining Sector Diversification Programme in Lusaka, Zambia, and is currently a consulting geologist and gemologist residing in Göteborg, Sweden.

ACKNOWLEDGMENTS

The authors are grateful to Denis Gravier (Gravier & Gemmes, Poncin, France) for supplying samples; Andreas Ertl (Institut für Mineralogie und Kristallographie, Geozentrum–University of Vienna, Austria) for X-ray diffraction analysis and lattice parameter calculations; Dr. William B. Simmons and Alexander U. Falster (University of New Orleans, Louisiana) for electron-microprobe analysis; Dr. Andy H. Shen (GIA Laboratory, Carlsbad) for Raman analysis; and Elizabeth Quinn (GIA Laboratory, New York) for determination of standard gemological data. One of the authors (BA) gratefully acknowledges Stanley Kabwita, an amethyst miner and gem dealer from Solwezi, Zambia, for guiding him to the tourmaline locality, as well as Daniel Lombe and Emanuel Mulenga (both of the Geological Survey of Zambia, Lusaka) for fruitful comments on the mining area.

REFERENCES

Anovitz L.M., Grew E.S. (1996) Mineralogy, petrology and geochemistry of boron: An introduction. In E.S. Grew and L.M. Anovitz, Eds., *Boron—Mineralogy, Petrology and Geochemistry*, Reviews in Mineralogy, Vol. 13, Mineralogical Society of America, Washington, DC, pp. 1–40.

Benesch F. (1990) *Der Turmalin: Eine Monographie*. Verlag Urachhaus, Stuttgart, Germany, 380 pp.

Bertrand E. (1879) Compte-rendu de la séance du 13 Février 1879 [Report of the meeting of February 13, 1879]. *Bulletin de la Société Minéralogique de France*, Vol. 2, p. 31.

Dietrich R.V. (1985) *The Tourmaline Group*. Van Nostrand Reinhold Co., NY, 300 pp.

Donovan J.J., Tingle T.N. (1996) An improved mean atomic number background correction for quantitative microanalysis. *Journal of Microscopy*, Vol. 2, No. 1, pp. 1–7.

Dunn P.J. (1977a) Uvite, a newly classified gem tourmaline. *Journal of Gemmology*, Vol. 15, No. 6, pp. 300–308.

Dunn P.J. (1977b) Chromium in dravite. *Mineralogical Magazine*, Vol. 41, pp. 408–410.

Garnier V., Ohnenstetter D., Giuliani G., Schwarz D. (2002) Rubis trapiches de Mong Hsu, Myanmar. *Revue de Gemmologie a.f.g.*, No. 144, pp. 5–11.

Gübelin E.J. (1939) Die Mineralien im Dolomit von Campolungo (Tessin) [The minerals in the dolomite of Campolungo (Tessin)]. *Schweizerische Mineralogische und Petrographische Mitteilungen*, Vol. 14, pp. 326–442.

Klinck B.A. (1977) The geology of the Kabompo Dome area—Explanation of Degree Sheet No. 1224 NE Quarter. *Report of the Geological Survey of Zambia*, No. 44, 27 pp. Appended to report: Geological Map of the Kabompo Dome Area (1992), Geological Survey Department, Lusaka, Zambia.

Libbrecht K., Rasmussen P. (2003) *The Snowflake: Winter's Secret Beauty*. Voyageur Press, Stillwater, MN, 115 pp.

Muñoz G.O. (1948) *Esmeralda de Colombia*. Bank of the Republic of Colombia, Bogotá, pp. 122–123.

Nassau K., Jackson K.A. (1970) Trapiche emeralds from Chivor and Muzo, Colombia. *American Mineralogist*, Vol. 55, No. 3–4, pp. 416–427.

Pogue J.E. (1917) The emerald deposits of Muzo, Colombia. *Transactions of the American Institute of Mining Engineers*, Vol. 55, pp. 42–45.

Rosenberg P.E., Foit F.F. (1979) Synthesis and characterization of alkali-free tourmaline. *American Mineralogist*, Vol. 64, No. 1–2, pp. 180–186.

Schmetzer K. (1978) Vanadium III als Farbträger bei natürlichen Silikaten und Oxiden—ein Beitrag zur Kristallchemie des Vanadiums [Vanadium III as color carriers in natural silicates and oxides—A contribution to the crystal chemistry of vanadium]. Ph.D. dissertation, University of Heidelberg, Germany, 277 pp.

Schmetzer K., Bank H. (1979) East African tourmalines and their nomenclature. *Journal of Gemmology*, Vol. 16, No. 5, pp. 310–311.

Schmetzer K., Hänni H.A., Bernhardt H.-J., Schwarz D. (1996) Trapiche rubies. *Gems & Gemology*, Vol. 32, No. 4, pp. 242–250.

Sumiya H., Toda N., Satoh S. (2005) Development of high-quality large-size synthetic diamond crystals. *SEI Technical Review*, No. 60, pp. 10–16.

Sunagawa I., Bernhardt H.J., Schmetzer K. (1999) Texture formation and element partitioning in trapiche ruby. *Journal of Crystal Growth*, Vol. 206, No. 4, pp. 322–330.

Sunagawa I. (2005) *Crystals—Growth, Morphology and Perfection*. Cambridge University Press, Cambridge, UK, 295 pp.

Takahashi Y., Sunagawa I. (1998) Tourmaline: Morphological and compositional variations during the growth history of uvite single crystals. *Journal of Gemmology*, Vol. 26, No. 4, pp. 226–236.

Win K.K. (2005) Trapiche of Myanmar. *Australian Gemmologist*, Vol. 22, pp. 269–270.

LAB NOTES 2007

EDITORS
Thomas M. Moses and
Shane F. McClure
GIA Laboratory

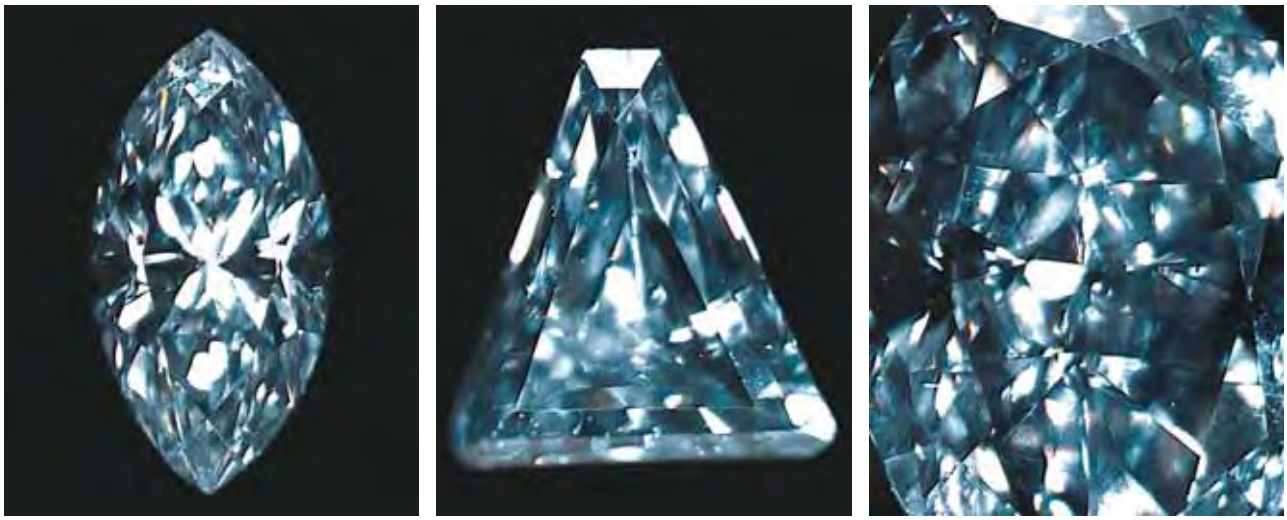

Figure 1. These three blue diamonds (0.42, 0.55, and 2.03 ct), which were color graded Fancy Light blue (marquise) and Fancy Intense blue (triangular and pear shapes), showed unusual phosphorescence in the DiamondView.

DIAMOND

Blue Diamonds Showing Multiple Colors of Phosphorescence

Recently, three blue diamonds—a 0.42 ct marquise, a 0.55 ct triangular step cut, and a 2.03 ct pear shape (figure 1)—were submitted to the East Coast laboratory for diamond grading (0.42 and 2.03 ct) and identification and origin (0.55 ct) reports. The 0.42 ct diamond was color graded Fancy Light blue, and the 0.55 and 2.03 ct diamonds were graded Fancy Intense blue. Gemological examination and photoluminescence spectra proved that the three stones were natural-color diamonds. No color zoning was observed. There was no reaction to long-wave ultraviolet (UV) radiation, and the 0.55 and 2.03 ct samples fluoresced very weak yellow to standard short-wave UV; no phosphorescence was observed.

Since phosphorescence in the Diamond Trading Company (DTC) DiamondView can be a useful means of separating natural from synthetic blue diamonds, as part of our examination we used this instrument to excite the samples with high-energy short-wave (<230 nm) UV radiation for five seconds at room temperature. After the UV source was turned off, individual images were taken with 1, 4, and 10.2 seconds of camera exposure time at different time delays (from 0.1 to 10 seconds) in an attempt to record the decay of the phosphorescence. We were surprised to see different colors of phosphorescence at various time delays in all three diamonds (see, e.g., figure 2): blue phosphorescence from 0.1 to 1 second, purplish blue and pink after 2 seconds of delay, and orangy red and red between 5 and 10 seconds of delay. The latter colors

Editor's note: All items are written by staff members of the GIA Laboratory, East Coast (New York City) and West Coast (Carlsbad, California).

GEMS & GEMOLOGY, *Vol. 43, No. 1, pp. 47–55*

were easier to see with longer exposure times (again, see figure 2).

Generally, natural blue diamonds are observed to phosphoresce blue to green or, rarely, red and orangy red, whereas synthetic blue diamonds usually phosphoresce blue or sometimes orange (J. M. King et al., "Characterizing natural-color type IIb blue diamonds," Winter 1998 *Gems & Gemology*, pp. 246–268). S. Eaton-Magaña et al. ("Luminescence of the Hope diamond and other blue diamonds," Fall 2006 *Gems & Gemology*, pp. 95–96) recently reported that the phosphorescence spectra of natural blue diamonds typically show a blue-green band centered at 500 nm and an orange-red band centered at 660 nm. The variation in relative intensities of these two bands, along with their respective decay times, creates the different colors of *observed* phosphorescence. Thus, although orangy red phosphorescence may be seen only rarely by visual observation, it is almost always present.

K. Watanabe et al. ("Phosphorescence in high-pressure synthetic diamond," *Diamond and Related Materials*, Vol. 6, No. 1, 1997, pp. 99–106) reported observing a change in phosphorescence colors from blue to orange in synthetic blue diamonds. However, the latter hue was not the orangy red phosphorescence seen in natural diamonds; nor did the luminescence peak reported for this color (2.1 eV or 590 nm) match that for the red phosphorescence in natural diamonds (660 nm). Our ongoing DiamondView studies indicate that natural blue diamonds usually show consistent phosphorescence colors, either blue or red, although sometimes in slightly different hues of each during the decay period. However, these three blue diamonds showed multiple colors of phosphorescence: Combinations of the colors blue and red were observed as the two peaks decayed at different rates.

Interestingly, photoluminescence spectra of the three diamonds did not show the 776.5 nm peak that has been associated with red phosphorescence in natural blues (Fall 2005 Lab Notes, pp. 258–259). The phenomenon of multiple phosphorescence colors is rare in natural blue diamond, but it can be explained by the presence of the 500 and 660 nm luminescence bands, and the fact that the 500 nm band decays before the 660 nm band.

Kyaw Soe Moe and Paul Johnson

Figure 2. DiamondView images of the 0.42 ct blue diamond, taken with various camera exposure times and time delays, reveal a progression of phosphorescence colors. The phosphorescence color changed from blue to red as the decay time increased from 0.1 to 10 seconds.

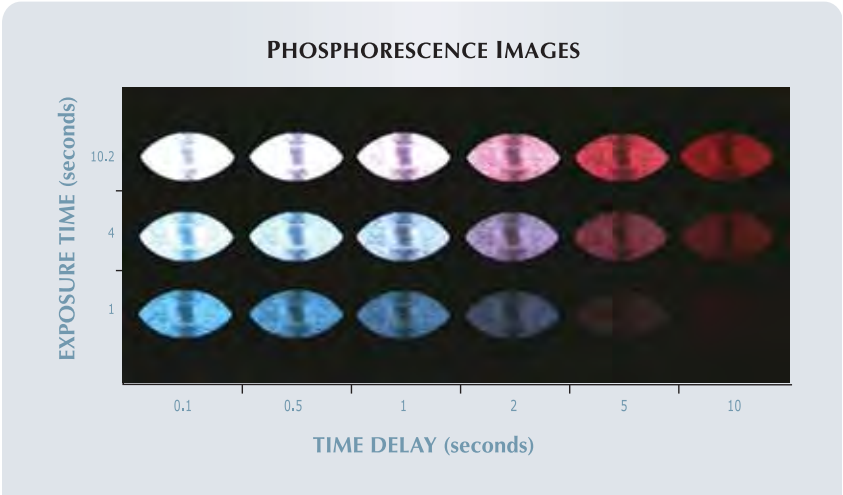

Diamond with "Etched Dislocation Loops"

While gemologists are familiar with common diamond clarity characteristics such as cleavage cracks (feathers) and mineral inclusions (crystals and pinpoints), microscopically visible features that appear to have resulted from structural dislocations are much more unusual. The West Coast laboratory recently received for grading a near-colorless round brilliant–cut diamond that fell into this "unusual" category. What made this diamond interesting was a formation of filamentary curved loops clearly visible through a gemological microscope (figure 3). These loops seemed to defy the monocrystalline structure of gem-quality diamonds, where angular and straight-edged internal features are the norm and distinctly curved structural features are unexpected.

Dislocations are defects in the crystal lattice structure of a mineral. Whether natural or synthetic, truly perfect crystals are almost unknown, and dislocations are very common. This is as true of diamond as it is of any other crystalline material.

It is also well known that diamonds often undergo plastic deformation in the earth; linear surface graining and internal graining are visual manifestations of this. During diamond growth, plastic deformation as well as the precipitation of microscopic-to-submicroscopic foreign matter on growing surfaces can increase dislocation density, and the presence of a dislocation can itself cause the development of additional dislocations.

Most individual dislocations cannot be seen with an optical microscope unless their density in a particular area is sufficiently high. In that case, they may produce visible strain in their host or, if they are subjected to etching and become hollowed out, may scatter light and appear white. The curved features in this diamond seem to fall into the latter group, in that they appeared white when examined through a gemological microscope. This contributor welcomes any alternate hypothe-

Figure 3. Microscopically visible filamentary "dislocation trails," like the curved loops shown here, are very unusual internal features in diamond. Magnified 15×.

ses that might explain these unusual distinctly curved features that are sometimes seen in diamonds.

John I. Koivula

HPHT-Annealed Yellow-Orange Diamond with a Strong 480 nm Absorption Band

Diamonds with a strong absorption band centered at 480 nm usually show chameleon behavior or a yellow-orange coloration with a brown component of varying saturation. Typically, they also show strong yellow to yellow-orange fluorescence to both long- and short-wave UV radiation and weak yellow phosphorescence to short-wave UV. Little is known about the defect(s) responsible for this absorption band and the typical luminescence features, but—unlike many other defects—the artificial inducement of this defect (or defects) has never been reported. In addition, significant concentrations of this defect are only rarely seen in color-treated diamonds.

The East Coast laboratory recently examined a known high-pressure, high-temperature (HPHT) annealed diamond with a strong 480 nm absorption band, which provided a special opportunity to examine the response of this feature to HPHT annealing. This 0.88 ct emerald-cut was color graded Fancy Intense yellow-orange (figure 4). The color distribution was patchy, and some areas were more intensely colored than others, with clear and distinct boundaries. Observation with the microscope revealed many tiny pinpoint inclusions in a linear arrangement; some pinpoints had surrounding haloes. Strong linear graining dominated in one direction throughout the entire stone, a good indication that the diamond had a strong brown hue before HPHT treatment. In contrast to most diamonds with the 480 nm absorption band, this stone displayed strong orange fluorescence to long-wave UV radiation and a moderately strong orange reaction to short-wave UV, and no phosphorescence was observed. The fluorescence image seen when the diamond was exposed to the high-energy short-wave

Figure 4. The absorption band centered at 480 nm in the visible spectrum of this 0.88 ct HPHT-annealed Fancy Intense yellow-orange diamond (figure 5) is rarely seen in a treated diamond.

Figure 5. The UV-Vis absorption spectrum of the diamond in figure 4 showed a strong, broad 480 nm band despite HPHT annealing. The band centered at ~270 nm and the peak at 271.5 nm are due to isolated nitrogen. The spectrum also showed several other sharp absorption features that could not be assigned to particular defects.

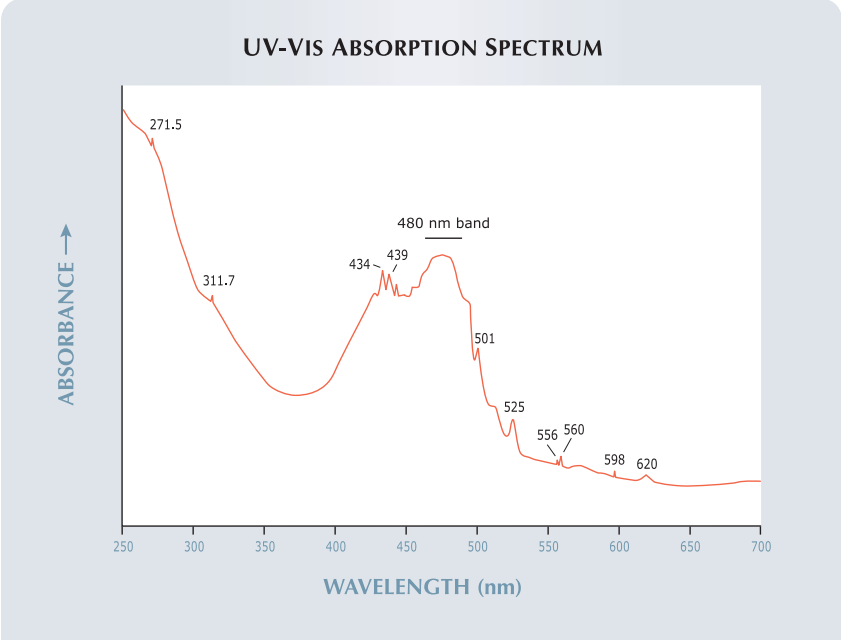

UV radiation of the DiamondView was dominated by a strong orange color with many unevenly distributed sharp, parallel green lines.

The UV-Vis absorption spectrum (taken at –196°C) showed a strong and broad band centered at 480 nm, in addition to some sharp peaks in the 430–600 nm range. There were many moderately strong and broad bands in the 420–530 nm region, as well as one at ~620 nm (figure 5). A broad band centered at ~270 nm and a sharp peak at 271.5 nm were due to trace isolated nitrogen, a common feature of this type of natural diamond that can be additionally enhanced by HPHT treatment. The infrared absorption spectrum showed a weak peak at 1332 cm^{-1} and a relatively strong peak at 1085 cm^{-1}; the assignment of the latter peak is unclear. In contrast, the IR absorption spectra of natural-color diamonds with a 480 nm absorption band usually have some unassigned peaks in the 1330–1100 cm^{-1} region.

Study of this interesting diamond strongly indicated that the defect(s) responsible for the 480 nm absorption band and yellow or yellow-orange fluorescence persisted through HPHT treatment. Despite the differences in the IR absorption spectra and the absence of phosphorescence, identification of a diamond showing the 480 nm band as HPHT-treated could be a challenge in the laboratory.

Wuyi Wang

Translucent Greenish Yellow Diamonds

Translucent diamonds bearing micro-inclusions are not encountered often in the laboratory, but they have been reported from time to time. As the popularity of colored diamonds increases, we are seeing a broader range of them with this feature (see, e.g., the following Lab Notes: Winter 2004, pp. 325–326; Summer 2005, pp. 165–167; and Spring 2006, pp. 57–59). We recently examined two large diamonds with such micro-inclusions, and it appears that both were cut from the same piece of rough.

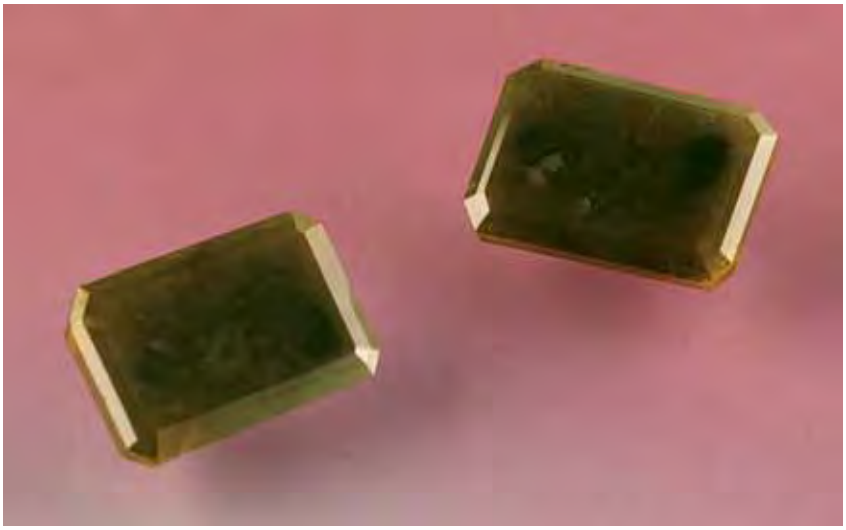

Figure 6. These two translucent greenish yellow diamonds—10.95 ct (left) and 11.40 ct (right)—have some unusual inclusions as well as gray zones on their tables that seem to mirror each other.

The two translucent greenish yellow stones (10.95 and 11.40 ct; figure 6) were submitted to the East Coast laboratory for identification reports. Microscopic examination revealed small black inclusions and numerous fractures, some of which contained orange stains (figure 7). We also saw gray zones, which were darkest in their centers, on the table facets (again, see figures 6 and 7). When observed in the DiamondView instrument with high-energy short-wave UV radiation, these gray zones corresponded to growth sectors (figure 8). The fluorescence images

Figure 7. Numerous orange-stained fractures and small black inclusions (graphite) were present in the two diamonds (left, magnified 30×). Note how this irregularly shaped gray zone is darker in the center (right, magnified 15×).

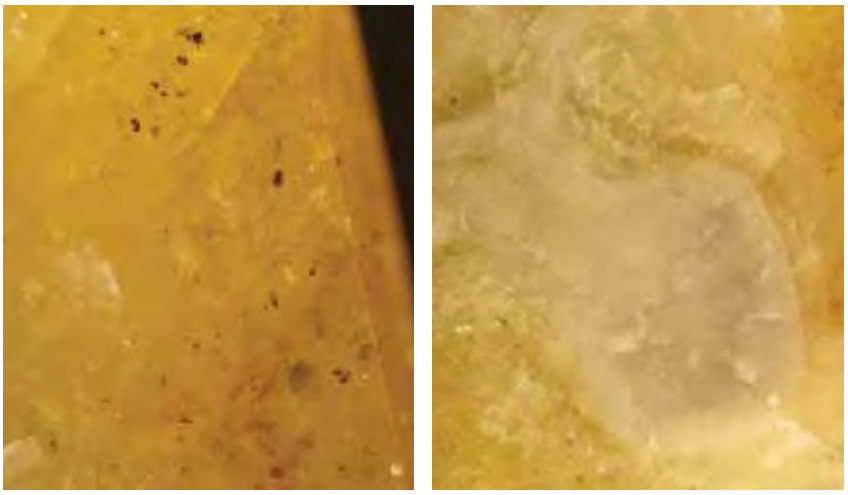

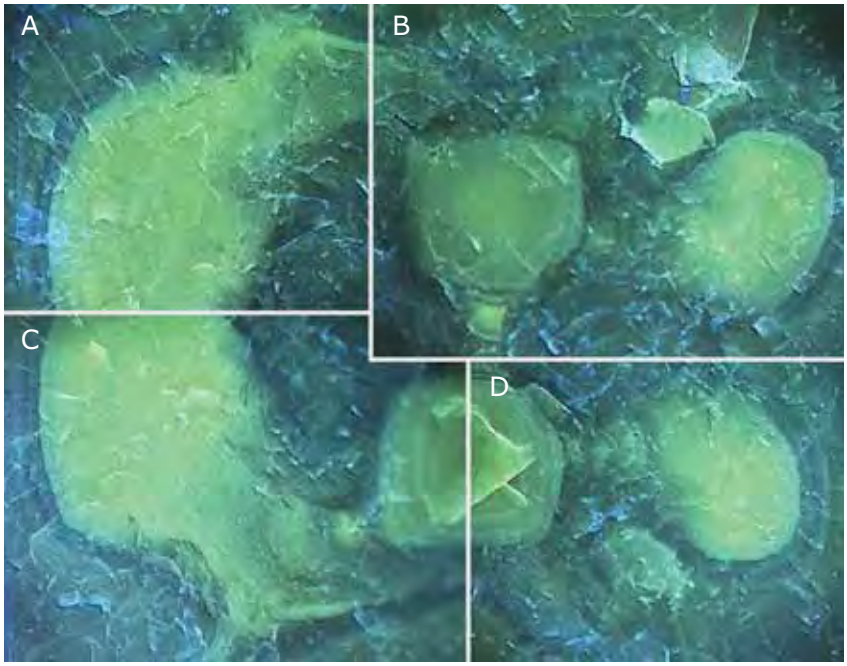

*Figure 8. When the table facets were examined in the DiamondView, the gray zones (see figures 6 and 7) proved to be growth sectors. Note how they are indeed mirror images of each other in the two stones (*A *and* B *= 11.40 ct;* C *and* D *= 10.95 ct). All the growth sectors originated from cubic growth and later developed into octahedral growth.*

of the two diamonds actually mirrored each other, which suggests that they were cut from the same crystal.

The small black inclusions were identified as graphite by Raman spectroscopy. The micro-inclusions were identified as water, carbonates, calcite, quartz, and micas by Fourier-transform infrared spectroscopy (figure 9). The broad OH-stretching (3600–2800 cm^{-1}) and the HOH-bending (~1650 cm^{-1}) bands indicated the presence of different water phases and suggested that these diamonds were formed progressively through different growth events (see D. A. Zedgenizov et al., "Water-related IR characteristics in natural fibrous diamonds," *Mineralogical Magazine*, Vol. 70, 2006, pp. 219–229). The quartz bands at 808 and 783 cm^{-1} were shifted from their normal positions of 798 and 778 cm^{-1}. The shifted positions correspond to a residual pressure of 1.5 GPa (at room temperature) inside the diamond; this suggests that high internal pressure was trapped in these diamonds during growth in the earth's upper mantle (see M. Schrauder and O. Navon, "Hydrous and carbonatitic mantle fluids in fibrous diamonds from Jwaneng, Botswana," *Geochimica et Cosmochimica Acta*, Vol. 58, 1994, pp. 761–771).

The fibrous texture is not associated with this micro-inclusion assemblage. As seen in figure 8, the cubic growth developed into octahedral growth at later growth stages. A diamond showing a similar growth sequence was reported in the Spring 2006 Lab Note mentioned above. The yellow color, which was unevenly distributed throughout the two diamonds, was caused by C-centers (i.e., single substitutional nitrogen, at 1344 cm^{-1}).

Diamonds such as these create special concerns during cutting. It is recommended that a diamond with two growth sectors be sawn between the two sectors to avoid causing cracks (see G. P. Bulanova et al., "A venture into the interior of natural

Figure 9. The mid-infrared spectra of both diamonds (top, 11.40 ct, bottom, 10.95 ct) revealed the presence of numerous micro-inclusions. The different modes of the water bands suggest that they were formed by different growth events. The spectra have been offset for clarity.

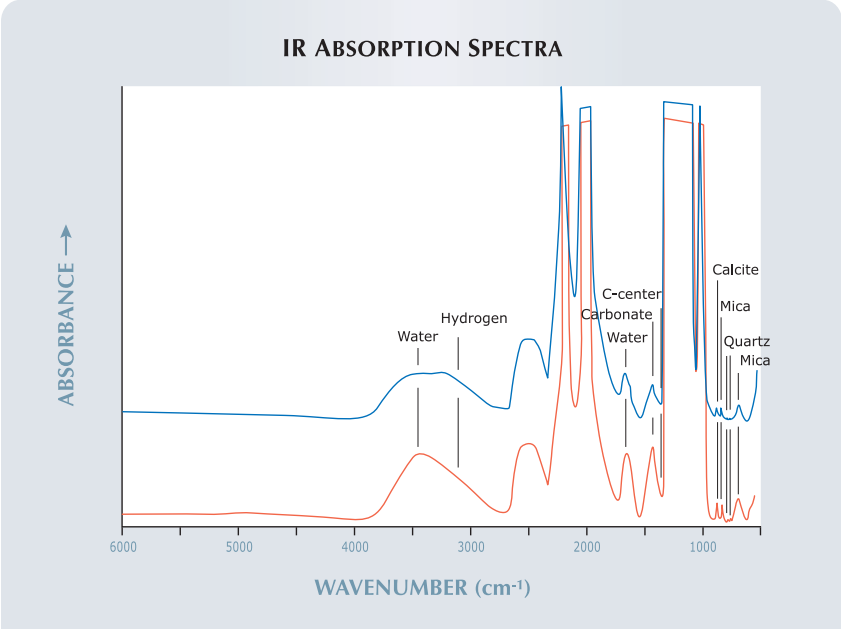

diamond: Genetic information and implications for the gem industry [Part I: The main types of internal growth structures]," *Journal of Gemmology*, Vol. 29, 2005, pp. 377–386). Likewise, the elevated temperatures used for cutting can release the high pressure trapped inside fluid-bearing micro-inclusions, which could also have contributed to the numerous fractures in these two diamonds.

The DiamondView images and infrared spectra proved that the diamonds were natural, with natural color. The micro-inclusions were formed from the trapped fluids in which the diamonds grew (again, see Schrauder and Navon, 1994). Even though these diamonds were translucent, their micro-inclusions and growth sectors provided us with valuable geologic information related to the growth environment of diamond crystals and the challenges that crystals grown in some environments can pose for the cutting process.

Kyaw Soe Moe, Paul Johnson, and HyeJin Jang-Green

Unusual Natural-Color Black Diamond

Black diamonds in the market today commonly receive their color from heat treatment at ambient pressure or intense irradiation. These treatments create either graphite inclusions or absorption centers (from the damaged diamond lattice) that strongly absorb visible light and result in a black appearance. In comparison, we see very few gem-quality black diamonds of natural color in the lab, and the natural color is usually ascribed to graphite inclusions (R. C. Kammerling et al., "An investigation of a suite of black diamond jewelry," Winter 1990 *Gems & Gemology*, pp. 282–287) or metallic inclusions such as magnetite (S. V. Titkov et al., "An investigation into the cause of color in natural black diamonds from Siberia," Fall 2003 *Gems & Gemology*, pp. 200–209). Recently, the East Coast laboratory examined a 3.14 ct natural-color black cut-cornered rectangular brilliant diamond (figure 10) that showed some interesting gemological features and yet another cause of color.

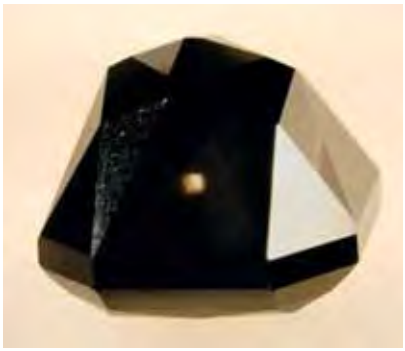

Figure 10. This 3.14 ct black diamond is colored by extremely dense clouds of micro-inclusions. The small "window" on the pavilion is an area that did not contain inclusions.

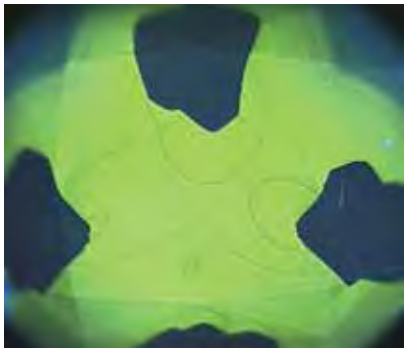

Figure 11. When exposed to high-energy short-wave UV radiation in the DiamondView, the black diamond in figure 10 exhibited typical greenish yellow fluorescence in its cubic growth sectors.

Unlike most natural diamonds, in which octahedral growth is well developed, this black diamond was dominated by cubic growth and had a high concentration of hydrogen. These cubic growth sectors exhibited greenish yellow fluorescence to short-wave UV radiation in the DiamondView instrument (figure 11). They also contained dense clouds of tiny inclusions that were readily visible with magnification. These small inclusions were evenly distributed in the cubic growth sectors and absorbed almost all the light entering the diamond. As a result, it was graded Fancy black.

Micro-inclusions occur frequently in natural diamonds and normally induce an overall brownish or grayish hue (see Winter 2004 Lab Notes, pp. 325–326; Spring 2006 Lab Notes, pp. 57–59; and Spring 2006 Gem News International, pp. 73–74), but a resulting black appearance is rare (when examined with very strong lighting, areas along the edges of the octahedral growth sectors were seen to be dark brown). The spectrum in the mid-infrared region for this diamond displayed extremely strong hydrogen-related absorptions (e.g., 3107 cm^{-1}), a common feature of natural diamonds with micro-inclusions that are restricted to certain growth sectors. The mineralogy of these tiny inclusions is not well known.

Another unusual feature of this diamond was its poorly developed octahedral growth sectors. These were much smaller than the cubic sectors, and contained almost none of the micro-inclusions. As a result, these transparent areas formed small, symmetrical colorless "windows" in the diamond (figures 10 and 12).

The well-developed cubic growth

Figure 12. Unlike the cubic growth sectors, the black diamond's octahedral sectors contained no micro-inclusions, and these areas consequently formed transparent "windows" through the stone. Magnified 45×.

pattern, unusual inclusions, and interesting color distribution combined to make this natural-color black diamond gemologically interesting.

Chincheung Cheung and QianWen (Mandy) Liu

SYNTHETIC DIAMOND, Possibly Grown at Higher Temperatures

The gemological features of most synthetic diamonds show little variety. Many articles have been written on the subject, and most of the features are quite familiar to gemologists, which is why a synthetic diamond recently submitted to the East Coast laboratory was so interesting.

Figure 13. The Vivid yellow color of this 1.35 ct cut-cornered rectangular modified brilliant is unusual for a synthetic diamond.

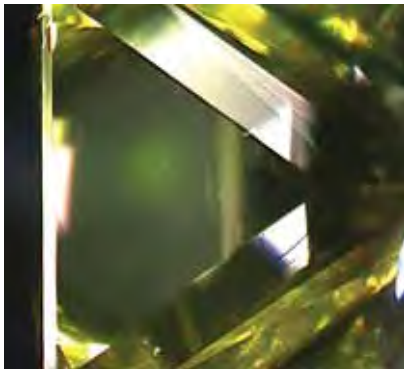

Figure 14. When the synthetic diamond in figure 13 was illuminated using a fiber-optic light, unevenly distributed moderate green luminescence was seen to correspond to the patchy color zoning.

Standard testing procedures established that the 1.35 ct cut-cornered rectangular modified brilliant in figure 13 was a synthetic diamond. The sample was color graded Vivid yellow, which in itself was unusual, as most HPHT synthetic diamonds we see have an orangy component to their color. Examination with 60× magnification did not reveal any large metallic inclusions, but numerous pinpoint-like micro-inclusions were present. Also seen was a subtle yellowish patchy color zoning in a very limited region in the center; this is not common in yellow synthetic diamonds. When illuminated with a fiber-optic light, the sample showed unevenly distributed moderate green luminescence that corresponded to the color zoning (figure 14). Notably absent was the characteristic hourglass-like color zoning seen in most HPHT-grown synthetic diamonds (see J. E. Shigley et al., "An updated chart on the characteristics of HPHT-grown synthetic diamonds," Winter 2004 *Gems & Gemology*, pp. 303–311). Also, in contrast to type Ib synthetic diamonds, which are inert or display weak fluorescence when exposed to long-wave UV radiation, this synthetic diamond displayed unevenly distributed moderate-to-strong green fluorescence. Furthermore, also unlike most other synthetic diamonds, the intensity of the fluorescence was *weaker* when exposed to short-wave UV.

Observation with the DiamondView instrument revealed an internal growth-sector arrangement showing well-developed octahedral growth zonation and a four-fold cross-shaped pattern from very poorly developed cubic growth sectors (figure 15).

In further contrast to typical HPHT-grown synthetic yellow diamonds, which are dominated by isolated nitrogen, the nitrogen in this sample was highly aggregated. Its mid-infrared absorption spectrum was dominated by A-form nitrogen (>200 ppm as shown by the 1282 cm^{-1} peak), and only an extremely weak absorption due to isolated nitrogen at 1344 cm^{-1} was detected (figure 16). When viewed with a handheld spectroscope, a weak but sharp band at 546 nm was observed, which is evidence of nickel impurities. Many other Ni-related defects were present in the sample's photoluminescence spectrum.

These observations indicated that this synthetic diamond likely was grown at a relatively high temperature, ~1700°C, compared to the 1400–1500°C for typical synthetic diamonds (see, e.g., J. E. Shigley et al., "The gemological properties of Russian gem-quality synthetic yellow diamonds," Winter 1993 *Gems & Gemology*, pp. 228–248). At very high temperatures, octahedral growth sectors are selectively developed and cubic growth sectors are minimized (H. Sumiya et al., "Growth rate of high-quality large diamond crystals," *Diamond and Related Materials*, Vol. 237/239, 2002, pp. 1281–1285). Most nitrogen in synthetic diamonds grown at such a high temperature is aggregated.

Another possibility is prolonged

Figure 15. In the DiamondView instrument, the synthetic diamond showed green fluorescence with a cross-shaped pattern.

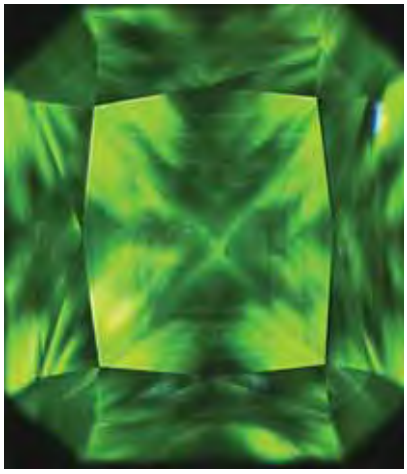

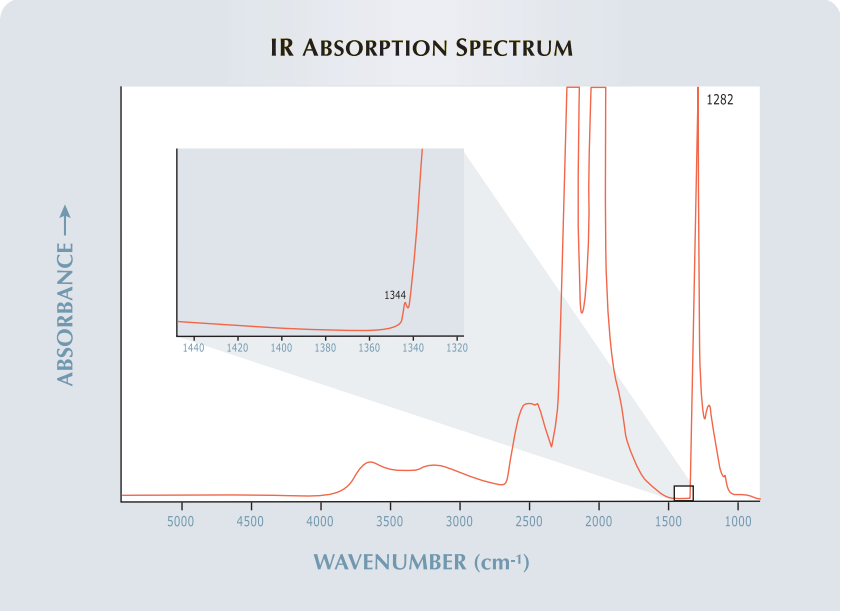

Figure 16. While many HPHT-grown synthetic yellow diamonds are predominantly type Ib due to isolated nitrogen, this sample proved to be type IaA with a trace of type Ib (the small peak at 1344 cm^{-1}); the peak intensity at 1282 cm^{-1} indicated a nitrogen concentration of >200 ppm in the A centers.

annealing at high temperatures after initial growth, but the very limited development of cubic growth in this synthetic diamond indicated that it was more likely to have crystallized at higher temperatures directly. While HPHT-grown synthetic yellow diamond is becoming more common in the jewelry market, samples such as this one are encountered only rarely.

QianWen (Mandy) Liu

Heat-Treated Blue SAPPHIRE with Unusual Dendrites

The laboratory routinely receives large numbers of blue sapphires for examination. Many of these stones show relatively typical signs of heat treatment in the form of melted and resolidified mineral inclusions, heat-decrepitated primary and secondary fluid inclusions, and color zoning attributed to internal diffusion.

It has also been demonstrated through experimentation with synthetic corundum that the precipitation of inclusions formed by exsolution, such as fine needles of silk-like rutile, can be controlled during the growth process. As would be expected, this is true of natural corundum as well.

During the heat treatment of natural corundum, preexisting exsolved rutile can be dissolved back into the corundum lattice structure to clarify a rutile-clouded stone. This "breakdown" begins to occur at approximately 1250°C and progresses more rapidly as the temperature and time-at-temperature both increase.

In some instances, however, the rutile is not completely reabsorbed, leaving behind tiny crystallite remnants aligned in typical corundum exsolution patterns; these are sometimes accompanied by clouds of color resulting from internal diffusion. The rutile may also partially *re*crystallize back into the corundum host. When this occurs, the rutile usually reappears as very fine, short needles or extremely small dust-like, light-scattering particles. Good examples of this type of controlled exsolution can be found in both flame-fusion (Verneuil) grown star sapphires and rubies and cabochon-cut natural stones that have asterism induced by lattice diffusion.

Recently the laboratory received a relatively large (20+ ct), faceted, transparent blue sapphire for identification. The many inclusions, all of which showed evidence of heat treatment, made the identification as a natural but heat-treated stone relatively easy.

Figure 17. The rows of unusual tree-like inclusions in this sapphire probably formed through exsolution as a result of the heat-treatment process. Their composition is unknown. Magnified 10×.

However, the examination also revealed an inclusion with a dendritic pattern that was unique in our experience. This feature was very elusive in that it was only visible when a fiber-optic light was directed at a specific angle oblique to the plane of the table facet. These dendrites were arranged in consecutive rows and displayed an obvious arborescent habit, as illustrated in figure 17. They also appeared to occupy the same plane in their host. This, combined with their reflective thin-film behavior and crucial directional visibility, led to the conclusion that they were the result of post-treatment exsolution. The fact that they were composed of numerous tiny individual disk-like crystallites also suggested that they originally formed as continuous branching dendrites that then contracted down into individual droplets as the corundum cooled before they finally solidified.

This is only one theory, of course. Readers are invited to convey their own thoughts as to the origin of these unusual inclusions.

John I. Koivula

Figure 18. This unusual elongated dislocation spiral was discovered in a faceted green YAG. It appears to consist of numerous minute particles of growth residue, as well as gas bubbles that were captured as the spiral developed. Magnified 10×.

YTTRIUM ALUMINUM GARNET (YAG) with a Dislocation Spiral

Crystalline compounds, whether natural or synthetic, can show two main types of structural dislocations. The first, *edge dislocations*, are offsets within atomic planes; these can be thought of as an extra half-plane of atoms inserted between two parallel planes in an otherwise "perfect" crystal structure. The other type, *screw dislocations*, are helical in nature; these can be compared to a spiral staircase or the auger-like pattern on a screw, hence the name. As far as gemstones are concerned, the screw dislocation is visually the most interesting of the two types.

A screw dislocation forms in a gem crystal when a helical pattern develops around a linear defect that starts at a point source, such as an inclusion or a strain knot. The spiral form becomes visible when there is sufficient strain to cause small fractures to develop along the central dislocation line and/or when fluid inclusions are captured along it as the crystal grows.

While we occasionally encounter beautifully formed dislocation spirals decorated by fluid inclusions and minute fracture patterns in gems such as topaz (orthorhombic) and beryl (hexagonal), these are somewhat expected, since both minerals have central axes of symmetry around which a spiral structure might form. However, using a gemological microscope, we had never seen an inclusion spiral in a material formed in the isometric (cubic) crystal system. It was, therefore, somewhat surprising when just such a spiral-shaped inclusion formation (figure 18) was observed during the otherwise routine identification of a faceted transparent green yttrium aluminum garnet (YAG).

Whether it is a doubly refractive synthetic such as corundum or chrysoberyl, or a singly refractive material such as spinel or YAG, if a melt-grown crystalline rod is sawn in two lengthwise and both halves are polished, the sawn sections will sometimes display centrally located strain oriented parallel to their length. During growth, this central strain zone could develop as a visible spiral in the host, which would explain this unusual inclusion in a YAG. From that, we surmised the green YAG was probably grown by a melt technique rather than from a flux.

John I. Koivula

PHOTO CREDITS
Kyaw Soe Moe—1, 2, 7, and 8; John I. Koivula—3, 17, and 18; Jian Xin (Jae) Liao—4 and 13; Jessica Arditi—6; QianWen (Mandy) Liu—10; Chincheung Cheung—11, 12, 14, and 15.

Tucson 2007

The 2007 Tucson gem shows brought together the usual fantastic quality and quantity of gems and minerals, but there was little in the way of new gem localities or varieties. Instead, additional production from known localities was brought to market, with the most exciting example being the widespread availability of copper-bearing tourmaline from Mozambique (see Gem News International, Winter 2005, pp. 360–361, and Spring 2006, p. 62), which was available from numerous dealers mainly as heated blue-to-green material. One notable stone at this year's American Gem Trade Association (AGTA) show was a 325.13 ct tsavorite from Merelani, Tanzania (figure 1), that was reportedly cut from the same piece of rough as the 62.81 ct stone pictured in last year's Tucson report (Spring 2006 GNI, pp. 62–63). Also of interest were two enormous slabs of Australian tiger's-eye in jasper (e.g., figure 2) that were displayed at the 53rd Tucson Gem & Mineral Show, where this year's theme was the minerals of Australia. The specimens were mined from the Marra Mamba Formation at Mt. Brockman in Western Australia. Another example of minerals at Tucson on a grand scale are the amethyst and citrine crystal "cathedrals" from Brazil in figure 3, which were on display at the JG & M Expo show. Additional items are described below, with more to be included in the Summer 2007 GNI section. *G&G* thanks the many friends who shared material and information with us this year.

Figure 1. This 325.13 ct tsavorite is from Merelani, Tanzania. Courtesy of Michael Couch & Associates, West Des Moines, Iowa; photo by Robert Weldon.

COLORED STONES AND ORGANIC MATERIALS

"Emerald" green fluorite from India. Although green fluorite is rather common, saturated "emerald" green stones are known mainly from the emerald mines of Colombia

Editor's note: The initials at the end of each item identify the editor or contributing editor who provided it. Full names and affiliations are given for other contributors.

Interested contributors should send information and illustrations to Brendan Laurs at blaurs@gia.edu or GIA, The Robert Mouawad Campus, 5345 Armada Drive, Carlsbad, CA 92008. Original photos can be returned after consideration or publication.

GEMS & GEMOLOGY, Vol. 43, No. 1, pp. 56–80


Figure 2. Shown here is one of two large slabs of Australian tiger's-eye in jasper (220 cm × 50 cm × 4 cm) that were displayed at this year's Tucson Gem & Mineral Show. The photo on the right highlights some of the details of the piece. Courtesy of David Vaughan, Australian Outback Mining, Perth, Western Australia; photos by Robert Weldon.

(see, e.g., P. Vuillet, "La fluorite verte de Peñas Blancas," *Revue de Gemmologie*, No. 140, 2000, pp. 21–25). We were therefore interested to receive a 3.99 ct bright green fluorite (figure 4) reportedly from Bihar, India, that was donated to GIA by Dudley Blauwet (Dudley Blauwet Gems, Louisville, Colorado) at the AGTA show. Mr. Blauwet obtained the stone in Jaipur, India, in November 2006. He was shown approximately 1,000 carats of the cut green fluorite, and obtained 200–300 carats ranging from 2 to 58 ct each. The material showed various degrees of saturation of the green color, and some of the larger stones were color zoned, with blue bands seen in certain orientations. No treatments were indicated by the dealer.

Examination of the 3.99 ct fluorite by one of us (EAF) showed the following properties: color—green; R.I.—1.439; hydrostatic S.G.—3.19; Chelsea filter reaction—none; fluorescence—inert to long- and short-wave UV radiation; and no absorption lines visible with the desk-model spectroscope. Microscopic examination revealed planar fluid inclusions, traces of the characteristic cleavage exhibited by fluorite, and minute primary three-phase inclusions (figure 5). Many of these inclusions exhibited a tetrahedral or modified tetrahedral habit, which is a relatively well-known identifying characteristic of fluorite. Judging from the low relief of the fluid inclusions, the liquid filling them appeared to be a saturated brine with a refractive index less than, but very near to, that of the fluorite host. In addition to the transparent daughter phase(s), some of the three-phase inclusions appeared to contain a tiny opaque solid phase with a brassy color and metallic luster (probably a sulfide mineral). Vuillet (2000) also reported seeing three-phase inclusions in green fluorite from Colombia. However, several other properties

Figure 3. Displayed within their shipping crates are three large crystal "cathedrals" of amethyst and citrine, with owner Tina Sim shown for scale. The citrine color was created in Brazil by heating amethyst; it undoubtedly required a very large oven. Courtesy of Gemstone Material Interiors, Tucson, Arizona; photo by B. Laurs.

Figure 4. This 3.99 ct "emerald" green fluorite is reportedly from Bihar, India. Gift of Dudley Blauwet, GIA Collection no. 36751; photo by C. D. Mengason.

Figure 5. The green fluorite contained numerous tiny three-phase inclusions. Photomicrograph by John I. Koivula; magnified 40×.

reported by Vuillet (2000) were not observed in our green fluorite: a "rose" Chelsea filter reaction, absorption at 560–580 nm, intense blue long-wave UV fluorescence, and moderate blue-violet short-wave UV fluorescence. Therefore, we suspected that the origin of color in the Indian fluorite might be different from that of the Colombian material examined by Vuillet.

Fluorite can show a variety of colors that are caused by complex centers involving rare-earth ions and/or oxygen; green is commonly due to traces of Sm^{2+} (H. Bill and G. Calas, "Color centers, associated rare-earth ions and the origin of coloration in natural fluorites," *Physics and Chemistry of Minerals*, Vol. 3, 1978, pp. 117–131). Indeed, Vuillet (2000) indicated that the green fluorite from Colombia is colored by Sm^{2+} (green), with a blue-violet component caused by luminescence from traces of Eu^{2+}. However, a UV-Vis-NIR spectrum of our 3.99 ct fluorite (figure 6) did not show features consistent with Sm^{2+}. Instead, the spectrum indicated the presence of yttrium (Y)- and cerium (Ce)-associated centers (Bill and Calas, 1978), with absorptions recorded at 335, 400, ~590, and ~710 nm. As expected, EDXRF spectroscopy showed traces of Y and very minute amounts of Ce; no Sm was detected. According to Bill and Calas (1978), the production of deep green to yellowish green coloration in fluorite by Y- and Ce-associated centers is quite rare.

Eric A. Fritz (eric.fritz@gia.edu)
and John I. Koivula
GIA Laboratory, Carlsbad

BML

Figure 6. This UV-Vis-NIR spectrum of the green fluorite shows absorption features at 335, 400, ~590, and ~710 nm, which are consistent with yttrium- and cerium-associated color centers as the cause of the bright green coloration.

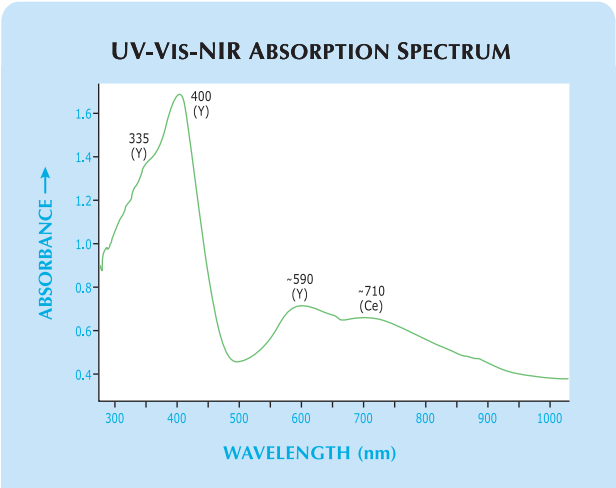

Cat's-eye leifite from Mont Saint-Hilaire, Canada. Leifite, $Na_2(Si,Al,Be)_7(O,OH,F)_{14}$, is an alkali pegmatite mineral that has been found rarely as transparent facetable pieces at Mont Saint-Hilaire, Quebec, Canada (see Gem News, Spring 1993, p. 60, and Spring 1995, pp. 65–67). At the Gem & Jewelry Exchange (GJX) show, gem cutter Brad Wilson (Coast to Coast Rare Stones International, Kingston, Ontario, Canada) showed this contributor two cat's-eye leifite cabochons that he had recently cut from Mont Saint-Hilaire material. He noticed the potential for chatoyancy in a few small pieces of rough that he acquired over the past few years, and stabilized this fibrous material with epoxy prior to cutting. So far he has cut seven pieces of the cat's-eye leifite, ranging from approximately 0.5 to 2.78 ct; the best two stones are shown in figure 7. Mr. Wilson reported that most of the leifite production at Mont Saint-Hilaire took place between 1988 and 1991, and that the fibrous

Figure 7. These cabochons of the rare mineral leifite (1.60 and 0.62 ct) are notable for their chatoyancy. Courtesy of Coast to Coast Rare Stones International; photo by Robert Weldon.

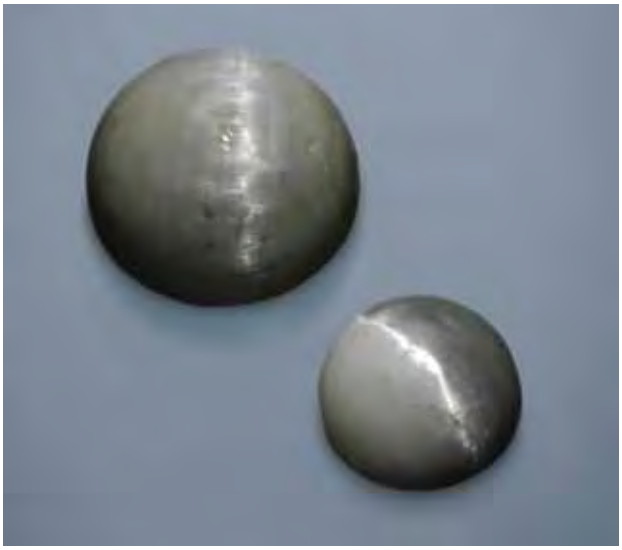

Figure 8. These recently mined opals from Piauí, Brazil, are notable for their high quality, as shown by their strong play-of-color (left, 38.36 ct), transparency (center, 18.42 ct), and even chatoyancy (above, 15.90 ct). Courtesy of Opalas Pedro II; photos by Robert Weldon.

material was found at the end of this period. The leifite finds in 1988–1990 were described by L. Horváth and R. A. Gault ("The mineralogy of Mont Saint-Hilaire, Quebec," *Mineralogical Record*, Vol. 21, No. 4, 1990, pp. 284–359). While the transparent leifite documented in the Spring 1995 Gem News entry was light purplish pink, all the fibrous material obtained by Mr. Wilson was white to light gray.

BML

Play-of-color opal from Piauí, Brazil. A variety of opals are known from Brazil's Piauí State, which is that country's most important source for this gem (see J. Knigge and C. C. Milisenda, "Brazilian opals from Pedro II," *Gemmologie: Zeitschrift der Deutschen Gemmologischen Gesellschaft*, Vol. 46, No. 2, 1997, pp. 99–105). These include white or light opal (see reference above and Spring 1991 Gem News, p. 49, as well as Spring 1999 Gem News International, pp. 53), fire opal ("Reporter's Notebook," *Colored Stone*, Vol. 15, No. 3, 2002, p. 44–45), and matrix opals (Fall 2002 Gem News International, pp. 268–269).

During the AGTA show, Juscelino Souza (Opalas Pedro II, Pedro II, Piauí, Brazil) and Robb Darula (From Earth To Art and Mystic Jewelry and Gemstones, Mystic, Connecticut) showed this contributor some rough and cut play-of-color Piauí opals that were notable for their unusually high quality, including one cabochon with a cat's-eye (figure 8). Their samples were obtained since mid-2006 from some new mines in the same area near Pedro II (or Pedro Segundo) that has historically produced play-of-color opal (e.g., figures 9–10). The gentlemen had approximately

Figure 9. Workers use hand tools and dry sieves to mine for opals at this alluvial deposit near Pedro II in Piauí, Brazil. Courtesy of Opalas Pedro II.

Figure 10. This alluvial mining operation for Piauí opal employs a pump to remove groundwater from the workings. Courtesy of Opalas Pedro II.

2,000 carats of polished opal that were cut from the top 2% of the production. The samples were derived from about 30 mining sites that are exploring alluvial deposits. The opal is typically recovered at least 0.5 m below the surface, with some of the pits reaching as deep as 3 m. There has also been opal production from primary deposits in the area.

Carvings of some older Piauí opal were featured in a jewelry series called the Opal Natural Wonder Collection that was also seen in Tucson. The pieces were created by Judy Wallace (Wallace Goldsmithing, Sarasota, Florida) using material that was mined in the early 1970s, and demonstrated how the opal carvings can be creatively incorporated into wearable designs (e.g., figure 11).

In the future, more opal production from the Pedro II area is anticipated as additional mines are rejuvenated. Mr. Darula reported that the renewed mining efforts are in part due to cooperation from the state government, which is interested in promoting awareness of Piauí's opals and has recently published a pamphlet on them in Portuguese (*Pedra Primeira de Pedro Segundo*, Serviço de Apoio às Micro e Pequenas Empresas do Piauí, Sebrae, Piauí, 2007, 44 pp.).

BML

Prehnite from Merelani, Tanzania. At the Pueblo Gem & Mineral Show, Steve Ulatowski (New Era Gems, Grass Valley, California) had rough and cut prehnite from the tanzanite mines at Merelani, Tanzania. He obtained a total of about 20 kg of mixed-grade rough prehnite while on buying trips to Tanzania in November 2006 and January 2007. The prehnite formed aggregates that were mostly yellow, with white areas on some pieces. Some of these aggregates were intergrown with violet tanzanite, gray graphite, and/or pale green diopside (identified based on their visual appearance and typical mineral association at Merelani). So far, he has cut five pieces into faceted stones and cabochons.

Mr. Ulatowski loaned one faceted stone, one cabochon, and several pieces of rough to GIA for examination (e.g., figure 12). Characterization of the two polished stones by one of us (EAF) showed the following properties: color—greenish yellow, with no pleochroism; R.I.—1.617 to 1.639 and a spot reading of 1.62; birefringence 0.022; hydrostatic

Figure 11. Carved Piauí opals have been incorporated into some creative jewelry designs. The opal in the moth brooch weighs 25.00 ct, and the frog is 43.88 ct. Courtesy of Wallace Goldsmithing; photos by Robert Weldon.

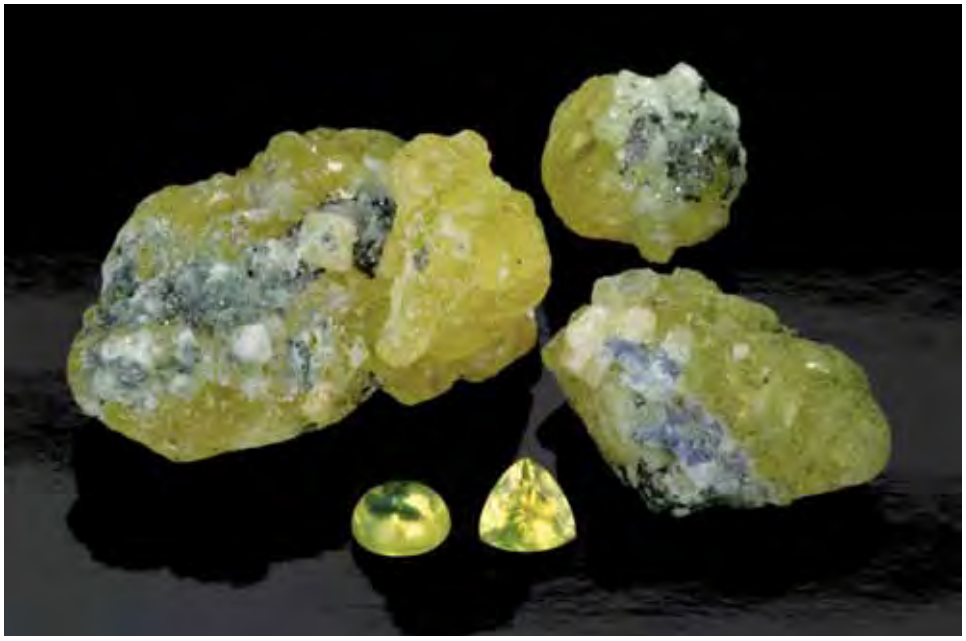

Figure 12. The tanzanite mines at Merelani, Tanzania, are the source of this prehnite. The polished stones weigh 1.62 and 2.14 ct. The rough pieces consist of yellow-to-white prehnite aggregates that in some cases are intergrown with violet tanzanite, gray graphite, and/or pale green diopside. Courtesy of New Era Gems; photo by Robert Weldon.

S.G.—2.91 and 2.96; Chelsea filter reaction—none; fluorescence—inert to long-wave UV radiation and weak yellow to short-wave UV; and no absorption features visible with the desk-model spectroscope. Microscopic examination revealed fine oriented fibers throughout the stones, numerous fractures, and planar fluid inclusions. These properties are comparable to prehnite from Mali (see Summer 2006 Gem News International, pp. 178–179), and similar to prehnite from Australia (see Spring 2001 GNI section, pp. 71–72), except for the fluorescence; the Australian stones described in 2001 fluoresced weak yellow to long-wave UV radiation and weak orange to short-wave UV.

To the best of our knowledge, this is the first report of gem-quality prehnite from Tanzania.

Eric A. Fritz and BML

Colorado rhodochrosite near end of availability. The Sweet Home mine in Colorado's Alma mining district has been known since 1872, when it was initially exploited for silver. More recently, however, the mine has become famous for producing world-class rhodochrosite crystals (see T. Moore et al., "The Sweet Home mine," *Mineralogical Record*, Vol. 29, No. 4, 1998, entire issue). In their best qualities, rhodochrosite crystals from Sweet Home are well-formed, largely translucent-to-transparent rhombohedrons, with a saturated orangy red color (e.g., figure 13).

In 1991 the mine was taken over by an investment corporation called Sweet Home Rhodo Inc. and overseen by veteran miner Bryan Lees (The Collector's Edge, Golden, Colorado). In 1992, the company reached its heyday after producing a series of magnificent crystal specimens. Although the corporation's main objective was to recover mineral specimens for collectors, broken crystals were sent for cutting; approximately 100 cut stones over half a carat were produced annually between 1992 and 1996 (K. Knox and B. Lees, "Gem rhodochrosite from the Sweet Home mine, Colorado," Summer 1997 *Gems & Gemology*, pp. 122–133). The Sweet Home mine finally ceased operations after the 2004 mining season and the site has been

Figure 13. A gem rhodochrosite crystal (33.9 g, with embedded tetrahedrite crystals) from the Sweet Home mine in Colorado is shown here with a trilliant weighing 7.14 ct. Courtesy of Beija-flor Gems; photo by R. Weldon.

reclaimed, including the closure of the portal and removal of the dumps. Mr. Lees' company still owns the mine and the property, and he is investigating ways of turning the site into an open-space park.

The cut rhodochrosite and material suitable for cutting was sold to a group of investors that includes gem dealer Robert Van Wagoner (Beija-flor Gems, Haiku, Hawaii), who was exhibiting at the GJX show. Because the stock was sold to the group as a single parcel, and because the mine is no longer in production, Mr. Van Wagoner and his associates are now the main dealers trading in cut rhodochrosite from the Sweet Home mine.

Rhodochrosite is soft and has perfect cleavage in three directions, so it is notoriously difficult to facet (again, see Knox and Lees, 1997). Mr. Van Wagoner reported that cut yields can range between 5% and 20%, depending on the quality of the rough and the expertise of the cutter. The smaller material (i.e., <2 ct) is faceted into calibrated sizes, in 0.5 mm increments, as oval, round, princess, cushion, and emerald cuts, as well as some trilliants. Stones >2 ct are cut in free sizes (again, see figure 13); so far, the largest clean rhodochrosite they have cut weighed 12 ct, although they have faceted heavily included gems up to 30–40 ct. In addition, cabochons (in both calibrated and free sizes) and polished rhombohedra are produced. Mr. Van Wagoner indicated that some of the cabochons have shown chatoyancy and four-rayed stars. He added that some of the cabochons and polished rhombohedrons are stabilized during the cutting process, while the faceted stones are completely untreated.

The cut rhodochrosite is being sold by Mr. Van Wagoner and his associates mostly as loose gems, although some jewelry pieces have been manufactured from the material. They expect that stocks of cut Sweet Home rhodochrosite will not last beyond two-to-three years, after which relatively few stones will be available in the market.

Robert Weldon (rweldon@gia.edu)
GIA Library, Carlsbad

Serpentinite from Argentina, marketed as "Andes Jade." At the Arizona Mineral & Fossil Show (InnSuites Hotel venue) and Tucson Electric Park, Jorge Dascal (Patagonia Minerals, Buenos Aires, Argentina) had some serpentinite from central-western Argentina that he was selling with the marketing name "Andes Jade." The material ranged from light-to-dark green, to bluish green, to black; Mr. Dascal has recognized 12 specific color varieties. The diaphaneity was nearly opaque to translucent. He had 11 tonnes available in Tucson, as rough blocks ($25 \times 20 \times 20$ cm to $50 \times 40 \times 35$ cm), broken polished pieces ($15 \times 10 \times 10$ cm), sawn slices, and a few cabochons, as well as an interesting carving that was crafted by Mark Zirinsky of Denver, Colorado (figure 14).

Mr. Dascal indicated that X-ray diffraction analyses of several samples performed at the University of Bonn in Germany showed the material to be a mixture of the serpentine minerals antigorite and lizardite, together with magnesite and minor magnetite. Some of the pieces were strongly magnetic. Light red-brown specks in some of the

Figure 14. A variety of colors and textures are shown by this serpentinite from Argentina, which is marketed as "Andes Jade." The image on the right shows the translucency and execution of detail in the carving by Mark Zirinsky, which measures 5.5 × 3.5 cm. Courtesy of Patagonia Minerals; photos © Jeff Scovil.

serpentinite were identified as garnets by a local university laboratory. A Mohs hardness of 5½–6 has been suggested by experienced local artisans and Chinese carvers, with the lighter green material being harder than the darker colors.

Mr. Dascal reported that he first found the Andes Jade in early 2004, received mining rights in early 2006, and constructed a road to the deposit in preparation for mining in late 2006. The deposit has been worked as an open cut, using hand tools and pneumatic drills. The reserves appear to be extensive, and Mr. Dascal plans to start mining soon on a full-time, year-long basis.

BML

New variscite production from Western Australia. At the Arizona Mineral & Fossil Show (Mineral & Fossil Marketplace venue), Glenn Archer and David Vaughan (Australian Outback Mining, Perth, Western Australia) had some attractive green variscite that they recently mined from the Meekatharra District in central Western Australia. Although variscite has been known from this area for decades, they have been exploring a part of the district that had not previously been mined, at Woodlands Station, located 100 km east of Mt. Augustus. They started prospecting in 2002 in an area where a mining company had mapped a phosphatic shale horizon, but it took more than a year of exploration before they found a vein system containing high-quality variscite. After a lengthy process that involved pegging the claim, negotiating for the native title, and obtaining the necessary permits, they began exploratory mining with a backhoe in late 2004. However, little production was obtained initially due to the very hard nature of the rock.

In 2005 they brought in larger machinery, including a D-8 bulldozer, and produced 8 tonnes of various grades of variscite mixed with matrix material. Mining in 2006 yielded 4–5 tonnes of mixed-grade variscite, which was greener and of better quality than the previous material. Although this material was obtained from a maximum depth of just 3 m, it required moving a substantial amount of overburden to follow the vein system under the neighboring hillside.

The variscite has been recovered from a <1-m-wide layer containing several veins ranging from 2.5 to nearly 4 cm thick. So far the variscite has been mined over a 50-m-long area of the vein system, but the material is present along strike for 8,500 m. Due to the remoteness of the area and the oppressively hot climate, mining has taken place for only a 10-day period once a year during the cool season (May through September). During the 2006 campaign, the mining crew consisted of five people and employed a bulldozer, backhoe, and two trucks.

The variscite from Australian Outback Mining's claim was first sold at the 2006 Tucson show as broken pieces, slabs, and partially polished pieces. During the 2007 show, they had both rough and polished variscite; they reported that about 10 kg had been fashioned thus far as cabochons and carvings (see, e.g., figures 15–16). The color ranged from light-to-dark yellowish green, with attractive patterns created by orangy brown veining. The variscite reportedly is not treated or stabilized in any way.

Figure 15. Attractive patterning and a range of color is shown by this variscite, which was recently mined from a new claim in central Western Australia. The cabochon in the center is 56 × 25 mm; the specimen on the left was carved by Dalan Hargrave. Courtesy of Australian Outback Mining; photo © Jeff Scovil.

In March 2007, particles of native gold were discovered in this variscite by researchers at CSIRO (Australia's Commonwealth Scientific and Industrial Research Organisation). Working under a funded research grant, the origin, characterization, and formation of the gold particles in the variscite is being investigated by Drs. Ernie Nickel,

Figure 16. This toad (5 × 7 × 8 cm) was carved from the new Australian variscite in Idar-Oberstein, Germany. Courtesy of Australian Outback Mining; photo by Robert Weldon.

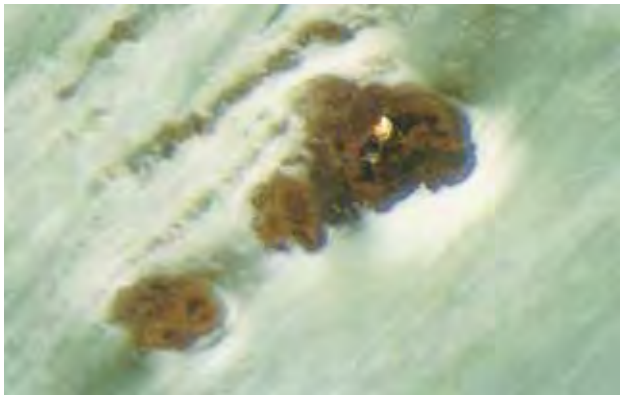

Figure 17. Tiny inclusions of native gold are present in some of the Australian variscite. Photomicrograph by J. I. Koivula; magnified 20×.

Robert Hough, and Elena Hancock at the Australian Resources Research Centre in Perth. GIA also recently documented gold inclusions in the variscite, after receiving a donation of several polished plates from gem cutter Dalan Hargrave (GemStarz Jewelry, Spring Branch, Texas). Microscopic examination revealed isolated tiny brassy inclusions in three of the slabs (e.g., figure 17), and EDXRF spectroscopy detected traces of gold in those samples, along with Fe and As with the expected Al and P. LA-ICP-MS analysis of an inclusion in one sample by GIA research scientist Dr. Andy Shen confirmed its identity as gold.

BML, Eric A. Fritz, and John I. Koivula

INSTRUMENTS AND TECHNIQUES

Portable Raman spectrometer and the CrystalSleuth software. At the AGTA show, Bear and Cara Williams (Bear Essentials, Jefferson City, Missouri) showed this contributor a portable Raman spectrometer (figure 18) they had recently purchased for their own gemological research and in-house laboratory. Their instrument, the Enwave Optronics EZRaman L System, uses a 785 nm laser excitation source (532 and 670 nm lasers are also available) and is operated with a standard laptop computer. It is used in conjunction with a comprehensive Raman spectral library that is freely downloadable from the RRUFF Project web site at http://rruff.info/about/about_software.php. (For more on the RRUFF Project, see the abstracts by R. T. Downs and M. B. Denton in the Fall 2006 issue of *G&G*, pp. 89–90.) The Windows-based software, called CrystalSleuth, is capable of analyzing and manipulating Raman spectra, as well as powder X-ray diffraction data. It can be used to remove background noise, compare multiple spectra, and identify an unknown sample by referencing peak positions against the on-line RRUFF Project database. While the current database is strongly oriented toward mineralogy, there are obvious overlaps with gemology.

Mr. Williams indicated that it typically takes about five minutes to get a well-defined Raman spectrum that can then be saved to his database or compared to the RRUFF database using the CrystalSleuth software. He is in the process of building his own Raman spectral database that includes information on the origin and any known treatment of every gem sample that he analyzes.

This portable Raman spectrometer was purchased for under $20,000, and continued technological advances are expected to make such instrumentation even smaller and more affordable in the future. This, combined with the availability of the free CrystalSleuth software, is poised to make Raman spectroscopy a more accessible tool for the professional gemologist and conscientious gem dealer.

BML

Figure 18. Bear Williams set up his portable Raman spectrometer at the AGTA show in Tucson. Photo by Robert Weldon.

GNI Regular Features

COLORED STONES AND ORGANIC MATERIALS

Amethyst from the Democratic Republic of the Congo. During a buying trip to Tanzania in mid-2006, gem dealer Farooq Hashmi (Intimate Gems, Jamaica, New York) obtained some rough amethyst that was reportedly mined from the Democratic Republic of the Congo. He noted that in recent years up to several hundred kilograms of gem-quality rough amethyst from the DRC has been sold in Tanzania annually, in addition to even larger quantities from Zambia.

Mr. Hashmi loaned us a crystal fragment and three faceted stones (3.31–22.11 ct; figure 19) that were representa-

Figure 19. This amethyst (3.31–22.11 ct) was reportedly sourced from the Democratic Republic of the Congo. Courtesy of Intimate Gems; photo by Robert Weldon.

Figure 20. The DRC amethyst contained sprays of reddish needles that resemble the hematite inclusions commonly encountered in amethyst. Photomicrograph by Robert Weldon; magnified 10×.

tive of the more attractively colored DRC amethyst. The cut stones were examined by one of us (EAF), and gave typical properties for amethyst: color—purple; R.I.—1.546–1.555; birefringence—0.009; hydrostatic S.G.—2.65; and inert to both long- and short-wave UV radiation. Microscopic examination revealed "fingerprints" consisting of minute two-phase (liquid and gas) inclusions, as well as a few sprays of reddish needles (e.g., figure 20) that had the appearance of the hematite inclusions commonly found in amethyst (see also E. J. Gübelin and J. I. Koivula, *Photoatlas of Inclusions in Gemstones*, Vol. 2., Opinio Publishers, Basel, Switzerland, 2005, p. 562). The stones did not exhibit Brazil-law twinning in the polariscope, but they did produce a typical quartz "bull's-eye" uniaxial optic figure. FTIR spectroscopy showed typical features for amethyst and no unusual peaks (e.g., no 3543 cm^{-1} peak, as has been documented in material from a few localities as well as in some synthetic amethyst).

Eric A. Fritz and BML

Figure 21. These faceted brown-orange andradites from Iran (1.25 and 1.64 ct) contain striking green color zones. Photo by M. Douman.

Color-zoned andradite from Iran, with calcite inclusions. The recent GIA Gemological Research Conference included a poster describing Iranian demantoid (G. Du Toit et al., "Demantoid from Iran," Fall 2006 *Gems & Gemology*, p. 131). Since then, one of the poster authors and present contributors (MD) obtained some unusual andradite samples from Iran, including two faceted brown-orange stones (1.25 and 1.64 ct; figure 21) with distinct zones of green color centered under their tables. The 1.25 ct sample was examined in detail for this report. The specific gravity (3.79) and refractive index (1.86) values confirmed that it was andradite. Magnification revealed parallel, nearly parallel, and curved fibrous inclusions with some associated fractures (figure 22).

Figure 22. Parallel, nearly parallel, and curved fibrous inclusions were present in the color-zoned andradite, together with associated fractures. Photomicrograph by E. Gaillou; magnified 20×.

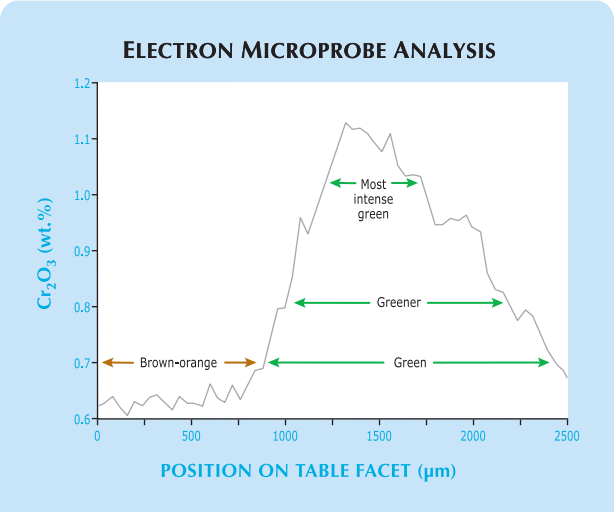

Figure 23. This graph shows the Cr_2O_3 content inferred from 64 point analyses that were performed across the 2.5-mm-diameter table of the 1.25 ct color-zoned andradite. The green color was apparent in regions where the Cr_2O_3 concentration exceeded 0.7 wt.%, and the saturation of the green color correlated well with chromium content.

To explore the possible correlation between chemical composition and color, we obtained numerous microanalyses of this sample using a Princeton Gamma Tech energy-dispersive detector attached to a JEOL 5800 scanning electron microscope. In addition to the Si, Ca, Fe, and Al expected for andradite, both the brown and green zones contained traces of Mg, Mn, and V. However, the green areas also contained Cr_2O_3 concentrations above 0.7 wt.%, and the color intensity increased with chromium content (figure 23). There was no correlation between the green color and other elements. This is in agreement with previous studies stating that the green color of demantoid is caused by Cr^{3+} (see E. Fritsch and G. R. Rossman, "An update on color in gems. Part 3: Colors caused by band gaps and physical phenomena," Summer 1988 *Gems & Gemology*, pp. 81–102), and it was supported by visible absorption spectroscopy. The spectrum of the stone showed a broad band with two apparent maxima at 620 and 640 nm that are likely due to Cr^{3+}. There was also total absorption in the violet and blue regions of the spectrum, presumably due to Fe^{2+}-Ti^{4+} charge transfer (see S. M. Mattson and G. R. Rossman, "Fe^{2+}-Ti^{4+} charge transfer in stoichiometric Fe^{2+}, Ti^{4+}–minerals," *Physics and Chemistry of Minerals*, Vol. 16, No. 1, 1988, pp. 78–82); this caused the areas of brown color in the stone.

The Raman spectrum of the entire 1.25 ct sample (taken without the use of a microscope) showed the

Figure 24. This 4.77 ct emerald exhibited some unusual growth features. Photo by G. Choudhary.

Figure 25. The emerald contained parallel jagged three-phase inclusions, as are commonly seen in Colombian emeralds. Photomicrograph by M. Vyas; magnified 25×.

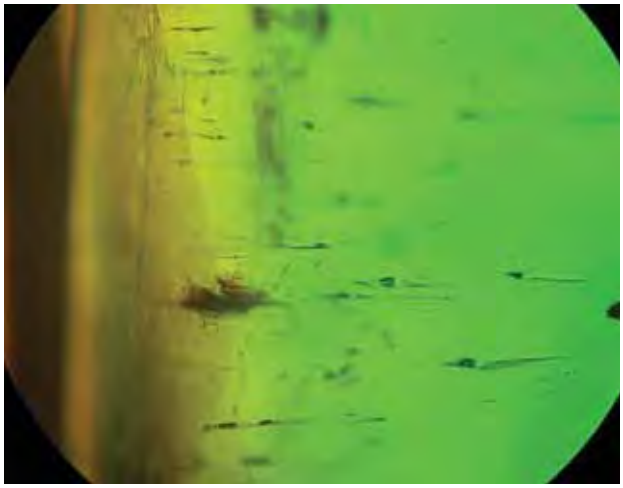

Figure 26. Rain-like growth tubes oriented parallel to the three-phase inclusions were also present in the emerald. Photomicrograph by G. Choudhary; magnified 30×.

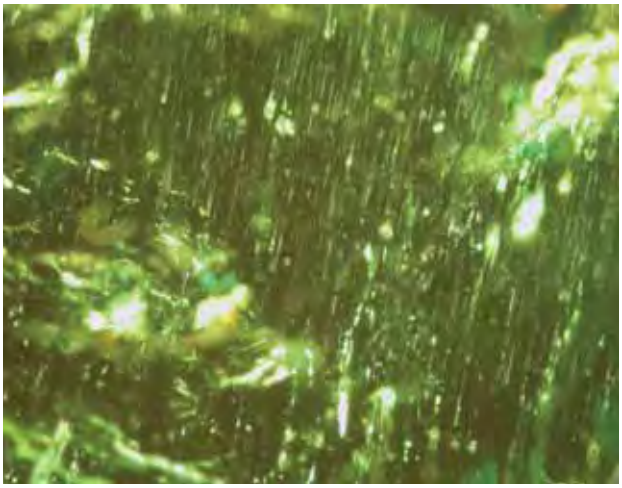

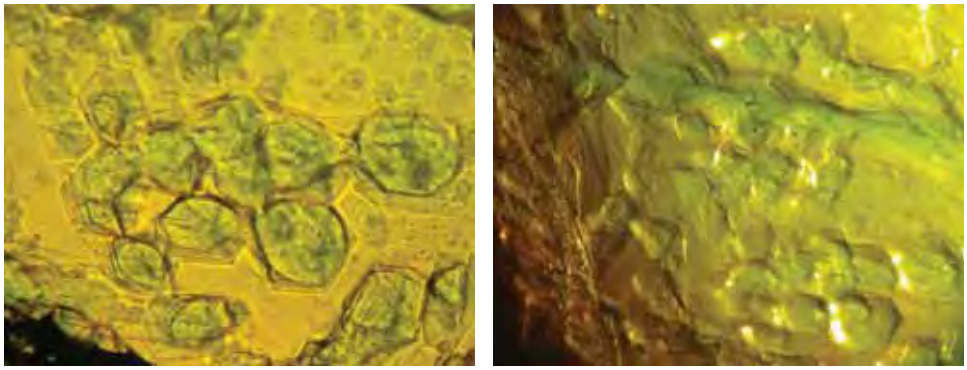

Figure 27. These unusual growth features in the emerald appear to be formed by an aggregation of hexagonal subcrystals. Also note the six-fold sector zoning within the individual subcrystals (left). Photomicrograph by G. Choudhary, magnified 40×, crossed polarizers (left); and C. Golecha, magnified 25×, transmitted light (right).

expected andradite peaks, as well as smaller peaks correlating to calcite. Although calcite inclusions have been described in garnet previously, they are found mostly in grossular (especially hessonite and tsavorite; E. J. Gübelin and J. I. Koivula, *Photoatlas of Inclusions in Gemstones*, Vol. 2, Opinio Publishers, Basel, Switzerland, 2005, pp. 471–475). To our knowledge, calcite has not been reported previously in demantoid. Further research is necessary to determine if the calcite is present as the fibrous inclusions mentioned above, or as micro-inclusions that were not visible with a gemological microscope. Additional research is also needed to determine if calcite is present in andradite/demantoid from other localities, or if it is characteristic of the material from Iran.

Stefanos Karampelas (steka@physics.auth.gr)
Department of Geology
University of Thessaloniki, Greece;
Institut des Matériaux Jean Rouxel (IMN)
Université de Nantes, France

Eloïse Gaillou and EF
IMN

Makhmout Douman
Arzawa Mineralogical Inc., New York

Emerald with unusual growth features. Recently, the Gem Testing Laboratory, Jaipur, India, received a 4.77 ct green gem for identification (figure 24). Its refractive index was 1.571–1.577, giving a birefringence of 0.006; the hydrostatic S.G. was 2.67. The stone had a strong chromium spectrum and was inert to UV radiation. These properties are consistent with emerald, natural or synthetic. Notably, when viewed with the polariscope, it exhibited strong strain patterns with patches of color in the optic axis direction (i.e., perpendicular to the table facet).

With magnification, the stone revealed a number of jagged three-phase inclusions oriented parallel to the optic axis (figure 25). Such inclusions are common in Colombian emeralds. Parallel growth tubes with a rain-like appearance (figure 26) were present in the same orientation; these are often observed in beryl, but they are unusual in Colombian emerald. The stone also had a roiled appearance (or "heat-wave" effect) when viewed table-up.

Although the inclusions indicated a natural origin, the causes of the unusual polariscope reaction and heat-wave effect were not clear. Examination of the stone with crossed polarizers while immersed in bromoform revealed a mosaic pattern when viewed along the optic axis (figure 27, left), somewhat similar to that seen in some Colombian emeralds (see, e.g., E. J. Gübelin and J. I. Koivula, *Photoatlas of Inclusions in Gemstones*, Vol. 1, ABC Edition, Zurich, p. 252). In plane-polarized transmitted light, these features appeared to be formed by the boundaries of intergrown columnar hexagonal subcrystals (figure 27, right). Most of these subcrystals followed the same orientation as the two-phase inclusions described above. When viewed with diffuse illumination (still in immersion), the hexagonal columns appeared slightly darker green than the interstitial areas and could be seen extending throughout the stone. Although the crystals followed the same orientation, some irregular boundaries between individual subcrystals were also visible, as was six-fold sector zoning (again, see figure 27, left).

It was clear that the roiled appearance of this emerald was due to intergrowth of the hexagonal subcrystals when viewed table-up (i.e., along the optic axis), while wavy growth features were seen in a direction perpendicular to the optic axis (figure 28). The latter patterns were similar to the chevron-like growth zoning that is typically seen in

Figure 28. Wavy growth features similar to the chevron-like growth zoning associated with synthetic emeralds were prominent when this natural emerald was viewed from the side (i.e., perpendicular to the optic axis). Such features indicate disturbed or rapid growth. Photomicrograph by C. Golecha; magnified 35×.

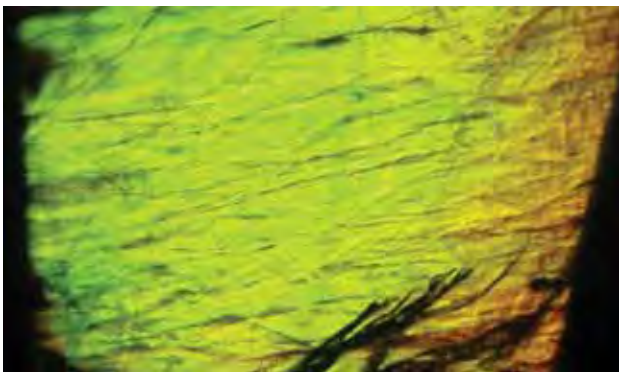

Figure 29. Attractive grossular (hessonite) has been produced recently from the Anza Borrego Desert in San Diego County, California. The cut stones shown here weigh 1.31–6.26 ct, and the etched crystal weighs 3.5 g. Courtesy of Paul Vollom; photo by R. Weldon.

Figure 30. These 2.24 and 0.74 ct clinozoisite samples from the Anza Borrego Desert were examined for this report. Courtesy of Paul Vollom; photo by R. Weldon.

synthetic emerald, and are indicative of disturbed or rapid growth. However, FTIR spectra taken in various directions showed that the strength of the peak at approximately 5270 cm^{-1} was characteristic of natural emerald (see, e.g., Fall 2005 Gem News International, pp. 265–266). The IR spectrum, as well as the overall inclusion pattern, confirmed the natural origin of this emerald.

Gagan Choudhary and Chaman Golecha
(gtl@gjepcindia.com)
Gem Testing Laboratory, Jaipur, India

Grossular and clinozoisite from San Diego County, California. For decades, small quantities of gem-quality grossular (hessonite) have been intermittently produced from skarn deposits in southeastern San Diego County (J. Sinkankas, *Gemstones of North America*, Van Nostrand Co., Princeton, NJ, 1959, pp. 288–289). Since 2004, renewed mining at one such claim has yielded good-quality hessonite as well as facetable clinozoisite. Paul Vollom (Omega Gems & Minerals, San Diego) and Roger Smith (Bishop, California) have been working the claim using hand tools and a portable gasoline-powered drill and jackhammer. The deposit is situated in a rugged area east of Jacumba, near the border with Mexico, in the Anza Borrego Desert. In some regards, this area conspires to limit human access to its mineral wealth, presenting an array of obstacles such as huge boulders, cholla cacti, rattlesnakes, and scorpions. Nevertheless, Mr. Vollom has recovered 7 kg of hessonite (e.g., figure 29), including a 46.8 g etched crystal. He estimated that 2 kg of this production would be suitable for cutting cabochons between 0.33 and 0.50 ct, and 1 kg could be faceted into the following sizes: >5 ct (5%), 2–5 ct (20%), <2 ct (35%), with the remaining 40% consisting of smaller stones. So far he has cut 36 hessonites, most ranging from 2 to 6 ct each. In addition, he has obtained 50 g of clinozoisite, and by the end of 2006 he had faceted 10 stones weighing ~0.75–3.00 ct (e.g., figure 30).

In January 2007, Mr. Vollom supplied several rough and cut samples of each gem to GIA for examination. Four faceted hessonites (1.31–6.26 ct) and one etched

Figure 31. In addition to "fingerprints," one of the garnets contained a primary two-phase fluid inclusion. Photomicrograph by J. I. Koivula; magnified 20×.

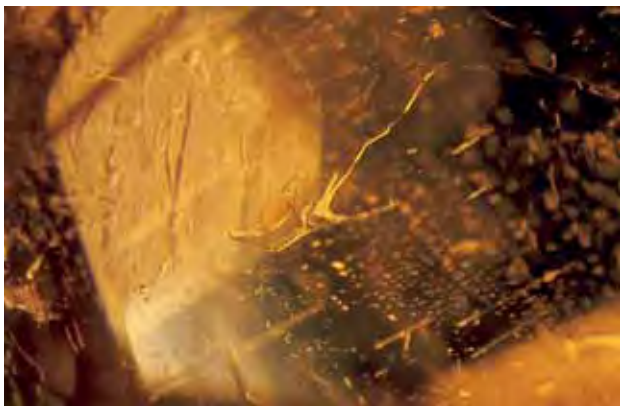

Figure 32. Lamellar color zoning is evident in this Anza Borrego hessonite. Photomicrograph by J. I. Koivula; magnified 10×.

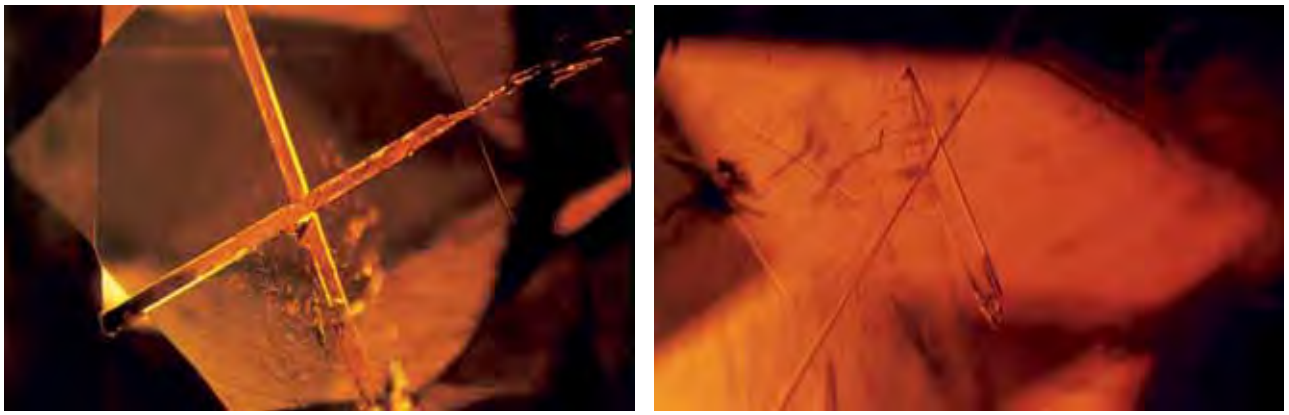

Figure 33. Needle-like quartz inclusions form a conspicuous intersection in the image on the left; the high relief and apparent orange color of these inclusions is due to the presence of an air interface with the host garnet. The more typical low-relief appearance of the quartz inclusions in the Anza Borrego hessonite is shown on the right. Photomicrographs by J. I. Koivula; magnified 10× (left) and 15× (right).

crystal (3.5 g), which represented the range of color from this locality (again, see figure 29), were selected for characterization by one of us (EAF). The following properties were obtained on the cut stones: color—yellowish orange to orange to reddish orange; R.I.—1.743 to 1.747; hydrostatic S.G.—3.63 to 3.65; fluorescence—inert to both long- and short-wave UV radiation; and weak general absorption to 520 nm observed with the desk-model spectroscope. These properties are consistent with those reported for grossular by C. M. Stockton and D. V. Manson ("A proposed new classification for gem-quality garnets," Winter 1985 *Gems & Gemology*, pp. 205–218). Microscopic examination revealed growth tubes, two-phase (liquid and gas) inclusions (figure 31), transparent planar growth zoning, lamellar color zoning (figure 32), and colorless needles (figure 33) that were identified as quartz by Raman spectroscopy.

Examination of two cut clinozoisites (0.74 and 2.24 ct; again, see figure 30) showed the following properties: color—brownish greenish yellow to brownish yellow-green, with moderate colorless to greenish yellow or yellow-green pleochroism; R.I.—n_o=1.711 and 1.712, n_e=1.720; birefringence—0.008 and 0.009; hydrostatic S.G.—3.40; Chelsea filter reaction—none; fluorescence—inert to long- and short-wave UV radiation; and an absorption line at 455 nm visible with the desk-model spectroscope. Microscopic examination revealed transparent angular growth structures and "fingerprints" consisting of two-phase (liquid and gas) inclusions. The physical properties are consistent with those reported for clinozoisite by W. A. Deer et al. (*Rock-Forming Minerals—Vol. 1B, Disilicates and Ring Silicates*, 2nd ed., The Geological Society, London, 1997, pp. 44–134). The R.I., birefringence, and S.G. of clinozoisite increase with iron content; the values of the samples tested here correlate to the lower range of iron that has been measured in clinozoisite (i.e., ~4 wt.% Fe_2O_3; see Deer et al., 1997).

Eric A. Fritz, John I. Koivula, Robert Weldon, and BML

New pegmatite gem production from Tsarafara, Madagascar. Spodumene, tourmaline, and morganite were recently recovered as well-formed crystals and gem rough from a pegmatite at Tsarafara, near Mount Ibity in the Sahatany Valley of central Madagascar. The gems came from two pockets that were found in September 2006. The mine has been worked by local miners, using hand methods, in shafts down to 20 m deep (figure 34). This contributor visited the mine three times in October 2006 to document the production. Tsarafara is also known as Ankadilava or Ambalaroy in the literature.

Figure 34. A weathered pegmatite at Tsarafara, Madagascar, recently produced some fine spodumene, tourmaline, and morganite. The miners constructed a simple windlass to remove the material from each of the two shafts shown here. Photo by F. Danet.

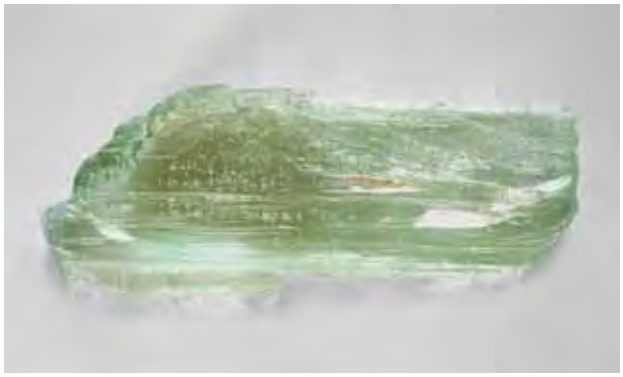

Figure 35. This green spodumene crystal from Tsarafara measures 7 cm long. Photo by F. Danet.

Figure 36. Tourmaline from Tsarafara has been cut into colorful slices (here, 1–4 cm in diameter). Photo by F. Danet.

The spodumene ranged from colorless to pale green (e.g., figure 35), pale blue, and pink (rarely bicolored blue-pink). At least 150 kg were produced, in translucent to eye-clean crystals up to 50 cm long. The largest crystal (not seen by this author) reportedly measured about 80 cm long. Most of the spodumene was exported as mineral specimens for collectors and as rough for Asian lapidaries; only a few cut stones have been seen in Madagascar.

Hundreds of tourmaline crystals were produced, commonly with a black "skin" and concentric internal layers of violet-pink, dark green, grayish green to bluish green, brownish yellow, and/or colorless. Although some of the tourmaline has been faceted into multicolored gems (grayish green, dark green, and violet) weighing up to 30 ct, a significant amount of the material has been cut into attractive slices that typically measure 1–8 cm in diameter (e.g., figure 36). Most of the rough, which was of low quality and recovered in small sizes, was sold to African traders for the Asian market (to make carvings and beads).

The Tsarafara pegmatite also yielded a few kilograms of morganite, mostly with a pale yellowish orange color. The best morganite consisted of eye-clean orangy pink crystals that measured up to 10 cm in diameter. In December 2006, this contributor saw a clean 66 g yellowish orange piece of morganite that would probably yield an ~100 ct faceted stone. Most of the well-formed crystals have been retained as specimens for collectors, with some broken pieces cut into faceted stones (e.g., figure 37).

Figure 37. The best-quality morganite from Tsarafara is notable for its transparency and orangy pink color (here, 31.8 ct). Photo by F. Danet.

By the end of 2006, almost all of the deep workings had collapsed due to flooding from the rainy season. The miners therefore shifted to higher ground in the southern part of the mine, where they found narrow, elongate crystals of multicolored tourmaline (brown, grayish green, violet, and pink). The termination of some of the crystals contained abundant hollow tubes that created chatoyancy when cut into cabochons. Nearly all of the workings were subsequently destroyed during heavy rains in early 2007.

Fabrice Danet (fabdanet@wanadoo.mg)
Style Gems, Antsirabe, Madagascar

Pezzottaite from Myanmar. In late 2006, small pink beryl-like crystals (e.g., figure 38) were recovered from Khat-Chel, near Molo, in the Momeik area of Myanmar's Mogok District. They were brought to the attention of these contributors by Patrick de Koenigswarter of MinerK, St. Julia de Gras Capou, France, who suspected that they were pezzottaite. They reportedly came from a granitic pegmatite known to have produced near-colorless twinned phenakite crystals, fibrous pink "mushroom" tourmaline, and other minerals such as petalite and hambergite.

Six crystals and crystal groups were studied for this report. Individual crystals were slightly tabular and composed mainly of basal pinacoid faces combined with prismatic faces; no pyramidal faces were observed. Composite basal terminations were occasionally present; these appeared flower-like and were very slightly concave (again, see figure 38). There were no signs of corrosion on the crystal surfaces. Some of these crystals were of gem quality or had portions that were transparent enough to be faceted.

Strong pinkish orange ("salmon") to purplish pink dichroism was visible, even to the unaided eye. When viewed with magnification and polarizing filters, or a dichroscope, the pleochroism was very strong, shifting from orange to purple in all samples (e.g., figure 39).

The refractive indices were 1.594–1.609, with a birefringence of 0.015. The crystals were uniaxial negative, and specific gravity ranged from 2.92 to 2.95. These properties are very high for beryl, but within the lower range of those described for pezzottaite (B. M. Laurs et al., "Pezzottaite from Ambatovita, Madagascar: A new gem mineral," Winter 2003 *Gems & Gemology*, pp. 284–301; H. Hänni and M. S. Krzemnicki, "Caesium-rich morganite from Afghanistan and Madagascar," *Journal of Gemmology*, Vol. 28, No. 7, 2003, pp. 417–429). The very strong pleochroism is also distinctive for pezzottaite. Some samples showed weak greenish white fluorescence to short-wave UV radiation only, with no phosphorescence. We have often observed such short-wave-only UV fluorescence of various colors (orange to yellow to green) in near-colorless morganite.

A surface parallel to the c-axis was polished on two crystals, exposing inhomogeneous color distribution and an hourglass growth pattern, both of which are common in beryl-group minerals. Growth sectors under basal faces contained more inclusions than those under prism faces, and a darker pink color was seen in growth sectors parallel to the basal face.

To confirm the presence of pezzottaite, we performed X-ray diffraction, chemical analyses, and Raman spectroscopy. X-ray diffractograms obtained at Blaise Pascal University using a CRG Sigma 2080 powder diffractometer on several portions of a crystal clearly showed the splitting of peaks indicative of the presence of a trigonal phase (such as pezzottaite, compared to hexagonal beryl). Quantitative chemical analyses were obtained on the same crystal at Blaise Pascal University (on a Cameca SX100 electron microprobe), and on the crystal shown in figure 38 at the University of Nantes (with a PGT energy-dispersive detector attached to a Jeol 5800 scanning electron microscope); similar results were obtained from both samples. The crystals were strongly zoned in Cs content, ranging from 5.12 to 9.97 wt.% Cs_2O for the one studied in Nantes and 2.5 to 12 wt.% Cs_2O for the one analyzed in Clermont Ferrand (figure 40). The trace-element (Na, Rb, Ca) contents were also consistent with published analyses of pezzottaite (from Madagascar).

Using a Jobin Yvon T6400 dispersive Raman spectrometer, Raman spectra were obtained on several points of the crystal studied in Nantes, corresponding to locations of variable Cs content. All spectra were very similar to those published by Laurs et al. (2003), and all showed the peak at about 1103 cm^{-1}, reported as being indicative of the pezzottaite structure.

These analyses were sufficient to confirm that the crystals were dominantly pezzottaite (with the possible presence of a small amount of beryl). This is the third

Figure 38. This crystal of pezzottaite (8.2 × 6.2 mm) was recovered from the Momeik area near Mogok, Myanmar. The use of plane-polarized light shows the pleochroic colors of the material. Note the very slightly concave surface formed by the composite basal termination on the right side of the crystal. Courtesy of P. de Koenigswarter; photo by E. Fritsch.

Figure 39. This composite photo of two polished faces containing the c-axis (at about 90° to one another) of one crystal taken through a polarizing filter (ordinary ray, left; extraordinary ray, right) shows the very strong orange and purple pleochroism of the pezzottaite. An "hour-glass" growth pattern is also visible, as well as pink growth bands parallel to the c-axis. The dashed square (upper left photo) marks the area analyzed by SEM in figure 40. Photos by B. Devouard.

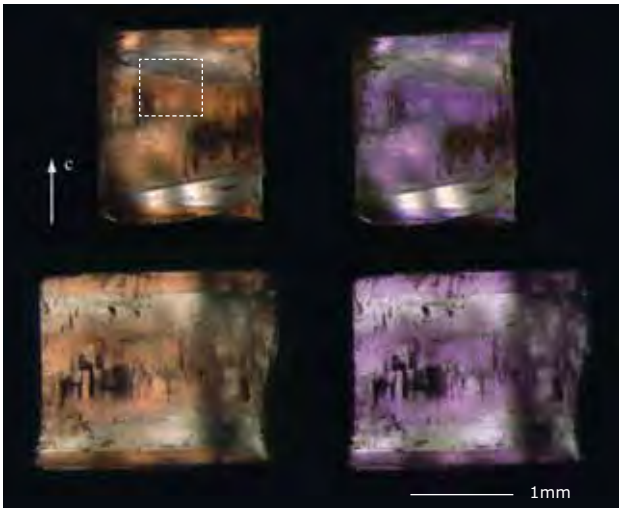

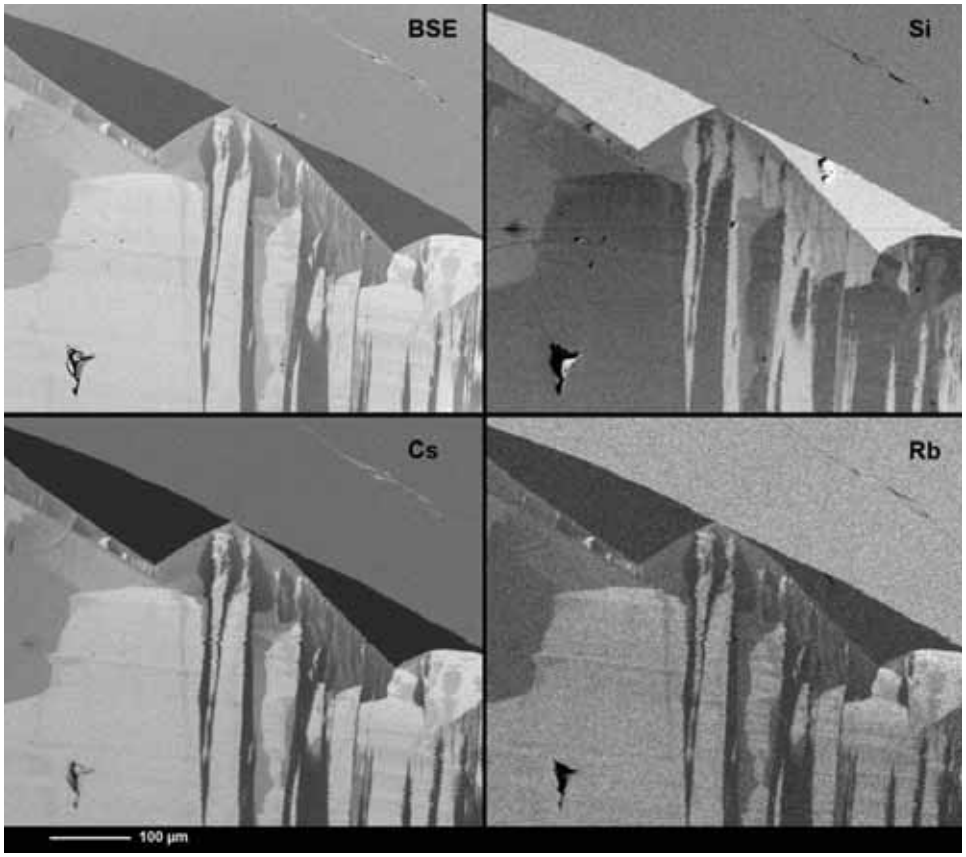

Figure 40. Strong chemical zoning is apparent in these SEM images of the Burmese pezzottaite. The image taken in backscattered electron (BSE) mode illustrates variations in overall atomic number, with lighter areas containing heavier elements (i.e., Cs). The distributions of Si, Cs, and Rb are also shown, with lighter areas corresponding to higher concentrations of those elements. The images reveal complex growth patterns. Images by B. Devouard.

reported occurrence for pezzottaite, after Madagascar and Afghanistan, and the first in Myanmar. The Burmese pezzottaite first debuted at the Munich gem show in early November 2006 (R. De Ascenção Guedes and L.-D. Bayle, "Munich 3–5 novembre 2006," *Le Règne Minéral*, No. 72, 2006, pp. 4–15), where it was represented as being from Kaha Chee in the Momeik area of the Mogok District.

Bertrand Devouard and Jean-Luc Devidal
(devouard@opgc.univ-bpclermont.fr)
Blaise Pascal University
Clermont Ferrand, France

Yves Lulzac
Nantes, France

EF

Cat's-eye prehnite. Recently, the Dubai Gemstone Laboratory received three translucent oval grayish yellowish green chatoyant cabochons for identification (4.95–5.40 ct; figure 41). At first glance, they resembled cat's-eye quartz in their chatoyancy and coloration. However, standard gemological testing proved that all three stones were cat's-eye prehnite.

All showed a spot R.I. of 1.62, with hydrostatic S.G. values ranging from 2.87 to 2.92. They were inert to both long- and short-wave UV radiation, and showed no pleochroism, no characteristic absorption spectrum, and no reaction to the Chelsea color filter. These properties are comparable to those reported for prehnite by R. Webster (*Gems*, 5th ed., revised by P. G. Read, Butterworth-Heinemann, Oxford, U.K., 1994, p. 361). Microscopic examination of the three samples revealed numerous extremely thin parallel channels or platelets as the cause of the chatoyancy, as well as small fissures (figure 42).

Reflectance IR spectroscopy and Raman analysis confirmed the identification as prehnite. EDXRF chemical analysis revealed the expected Ca, Si, and Al, as well as minor amounts of Fe.

Figure 41. These three chatoyant cabochons (5.40, 5.02, and 4.95 ct) were identified as cat's-eye prehnite. Photo by S. Singbamroong, © Dubai Gemstone Laboratory.

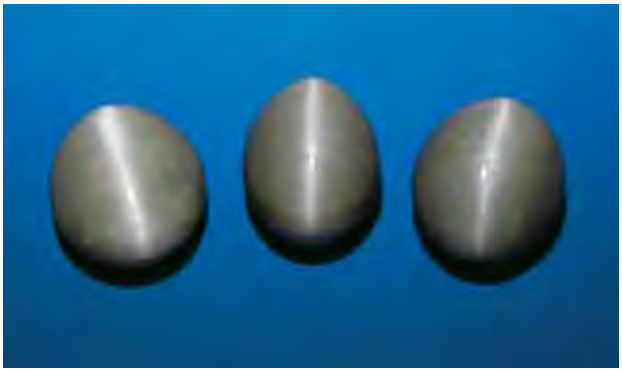

Figure 42. Numerous extremely thin parallel channels or platelets are the cause of the chatoyancy in the cat's-eye prehnite. Small fissures can also be seen near the right side of this view. Photomicrograph by S. Singbamroong, © Dubai Gemstone Laboratory; magnified 20×.

Cat's-eye prehnite is quite rare, and this is the first time we have seen it in our laboratory. The origin of these stones is unknown.

Sutas Singbamroong (sssutas@dm.gov.ae)
and Ayesha Rashid Ahmed
Dubai Gemstone Laboratory
Dubai, United Arab Emirates

Cat's-eye topaz from Sri Lanka. The Summer 1990 Gem News section (p. 164) reported on a 3.53 ct pale blue-green cat's-eye topaz with strong chatoyancy caused by a dense pattern of very fine, parallel etch ribbons. This was the first time that this rare gem material was reported in *Gems & Gemology*. We were therefore interested to examine another cat's-eye topaz, of significantly larger size (33.06 ct) and greater transparency, that was brought to our attention by Dudley Blauwet (Dudley Blauwet Gems, Louisville, Colorado). He obtained the cabochon (figure 43) while on a buying trip to Sri Lanka in late November 2006; the rough was reportedly recovered from the well-known gem mining area near Embilipitiya, in Uva Province, southern Sri Lanka.

Gemological testing clearly identified this gem as topaz. Microscopic examination revealed the cause of the chatoyancy to be numerous ultra-thin, parallel, acicular inclusions that appeared to be etch channels (figure 43, inset).

Mr. Blauwet's supplier indicated that a total of four pieces of the cat's-eye topaz were found, and that the other three samples were purchased by rare-stone dealers in Sri Lanka's capital city, Colombo.

BML and John I. Koivula

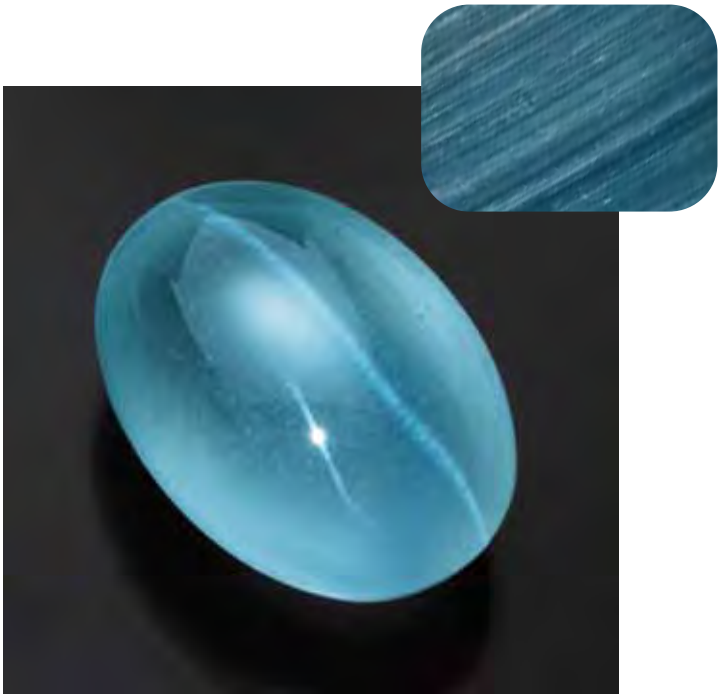

Figure 43. This 33.06 ct topaz from Sri Lanka is notable for its chatoyancy, transparency, and size. As shown in the inset, the chatoyancy is caused by numerous reflective, ultra-thin, parallel inclusions that appear to be etch channels. Courtesy of Dudley Blauwet, photo by Robert Weldon; photomicrograph by J. I. Koivula, magnified 30×.

Tourmaline (dravite and liddicoatite) from northeastern Mozambique. Gem tourmaline is well known from granitic pegmatites in the Nampula and Zambézia provinces of Mozambique (S. Lächelt, *Geology and Mineral Resources of Mozambique*, Direcção Nacional de Geologia Moçambique, Maputo, 2004, 515 pp.). Cabo Delgado Province in northeastern Mozambique was mentioned by Lächelt (2004) as a pegmatite locality, but to our knowledge no gem tourmaline has been reported from there. However, Farooq Hashmi (Intimate Gems, Jamaica, New York) recently showed us some rough and cut samples of tourmaline that reportedly came from Cabo Delgado. Mr. Hashmi obtained two parcels of this tourmaline in Dar es Salaam, Tanzania, in mid-2006. One parcel consisted of about 2 kg

Figure 44. This tourmaline, showing a range of color from orangy yellow to green to orangy brown, was reportedly mined in Cabo Delgado Province, Mozambique. Chemical analysis showed that all of this tourmaline is dravite. The yellow trilliant weighs 1.67 ct and was cut by Matt Dunkle, Aztec, New Mexico. Courtesy of Intimate Gems; photo by C. D. Mengason.

of broken fragments that ranged from green to yellow, orange, and brown. Most of the rough was of cabochon quality, with individual pieces averaging 1–2 g. The other parcel contained more-transparent pieces that were water-worn; they averaged 3 g each and ranged from greenish brown to brownish or grayish green. Mr. Hashmi saw several 2–3 kg parcels of the latter material while in Tanzania, and more recently he has seen the rough appear in the New York market. Although he purchased all of these tourmaline samples in Tanzania, he was informed by multiple sources that the material in both parcels came from Cabo Delgado. Mr. Hashmi loaned GIA several fragments and one faceted stone from the first parcel (e.g., figure 44), and one piece of rough and several faceted stones that were cut from the second parcel (e.g., figure 45).

Examination of the cut stone from the first parcel by one of us (EAF) showed the following properties: color—orangy yellow, with very weak colorless-to-yellow pleochroism; R.I.—n_o=1.632, n_e=1.612; birefringence—0.020; hydrostatic S.G.—3.02; Chelsea filter reaction—none; fluorescence—inert to long-wave UV radiation and weak yellow to short-wave UV; and a weak absorption band at 500 nm visible with the desk-model spectroscope. Microscopic examination revealed numerous negative crystals and lint-like aggregates of colorless inclusions. The several rough pieces from the first parcel (green, greenish yellow, orange, orangy brown, and brown) that were briefly tested showed moderate-to-strong pleochroism, were inert to long-wave UV radiation, and fluoresced very weak to moderate yellow to short-wave UV. The lighter colored samples had a stronger reaction to short-wave UV. Microscopic examination revealed planes of fluid inclusions and some negative crystals (figure 46), as well as rare colorless low-relief crystals, black disks, and a rounded brassy inclusion (figure 47). A colorless low-relief inclusion in one of the rough pieces was identified as an amphibole by Raman analysis.

The properties reported above are consistent with tourmaline, and the samples were identified as dravite by LA-ICP-MS chemical analysis performed by Dr. Mike Breeding of the GIA Laboratory in Carlsbad. All of the stones contained minor amounts of Fe and traces of Ti, Ga, and Sr. While the color of some of this Mozambique tourmaline is similar to dravite-uvite from Kenya, the refractive indices reported for the latter are considerably higher (n_o=1.643–1.646 and n_e=1.622–1.624; see H. A. Hänni et al., "Golden yellow tourmaline of gem quality from Kenya," *Journal of Gemmology*, Vol. 27, No. 7, 1981, pp. 437–442). However, the gemological properties of the Mozambique samples are comparable to those documented in samples with a similar hue range from Morogoro, Tanzania (Summer 2006 Gem News International, pp. 182–183).

LA-ICP-MS analysis of the cut stones and rough sample from the second parcel (again, see figure 45) showed that they consisted of either dravite or, surprisingly, liddicoatite. The three dravites were darker than most of the six liddicoatites that were tested.

Figure 45. Also reportedly from Cabo Delgado, this greenish brown to brownish/grayish green tourmaline was loaned for study from a separate parcel. The six stones in the top two rows proved to be liddicoatite (3.08–5.09 ct, including the piece of rough on the upper right), while the three on the bottom are dravite (2.43–4.37 ct). Courtesy of Intimate Gems; photo by C. D. Mengason.

The dravite samples from the second parcel showed the following properties: color—dark brownish green to dark grayish green, with moderate green-to-colorless pleochroism; R.I.—n_o=1.640, n_e=1.620; birefringence—0.020; hydrostatic S.G.—3.04–3.06; Chelsea filter reaction—none; fluorescence—inert to long- and short-wave UV radiation; and an absorption band at 500 nm visible with the desk-model spectroscope. Microscopic examination revealed only a very small "fingerprint" in one sample; no other inclusions or growth features were seen. LA-ICP-MS analysis showed that along with the elements normally associated with tourmaline, these dravite samples contained traces of Ti, Sr, and V.

The liddicoatite samples had the following properties: color—light brownish green to dark greenish brown, with

Figure 46. Negative crystals were common in some of the dravites shown in figure 44. Photomicrograph by Robert Weldon; magnified 15×.

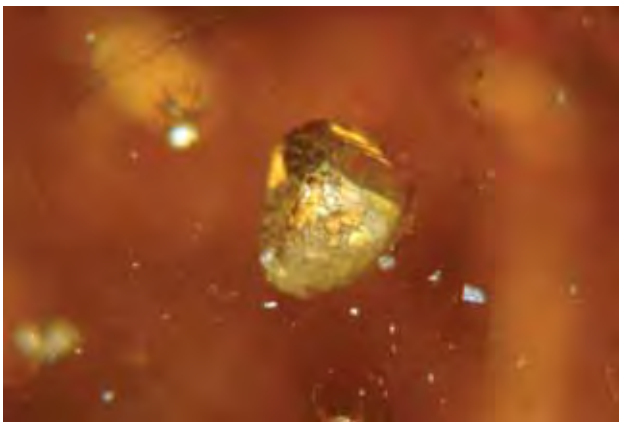

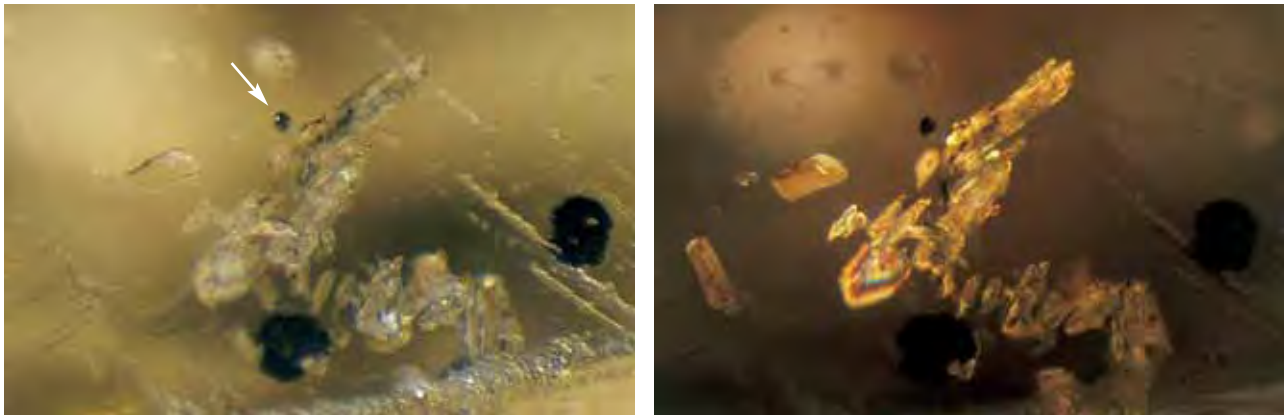

Figure 47. Also present in one of the dravite samples were colorless low-relief crystals (identified as an amphibole by Raman analysis), black disk-shaped crystals (probably graphite), and a minute rounded crystal with a brassy luster (probably pyrite; see arrow). The latter two inclusions were too deep in the stone for identification by Raman analysis. The birefringence of the amphibole inclusions is shown in the photo on the right, taken in cross-polarized light. Photomicrographs by J. I. Koivula; magnified 15×.

weak-to-moderate green-to-colorless pleochroism; R.I.—n_o=1.640, n_e=1.620; birefringence—0.020; hydrostatic S.G.—3.06; Chelsea filter reaction—none; fluorescence—inert to long- and short-wave UV radiation; and a weak absorption band at 500 nm visible with the desk-model spectroscope. In general, the stones were of high clarity; microscopic examination revealed angular color zoning, small transparent crystals, and growth tubes. Two of the stones contained a distinct dark green-to-brown triangular color zone (e.g., figure 48). The gemological properties are typical of liddicoatite (see D. M. Dirlam et al., "Liddicoatite tourmaline from Anjanabonoina, Madagascar," Spring 2002 *Gems & Gemology*, pp. 28–53), but the homogeneous brownish green to greenish brown coloration of most of the stones is rather unusual for gem-quality liddicoatite (see, e.g., Winter 2002 Gem News International, pp. 356–357).

We could find only one literature reference to liddicoatite from Mozambique: a chemical analysis of a sample from Muiane, Zambézia Province (T. G. Sahama et al., "On tourmaline," *Lithos*, Vol. 12, 1979, pp. 109–114). Gem dravite and liddicoatite are not geologically associated with one another in nature, so it is likely that the samples from that alluvial parcel originally came from different deposits in Mozambique. This is also suggested by the very different trace-element signature for the liddicoatite, as measured by LA-ICP-MS: Ti, Mn, Ga, Sr, Pb, and Bi.

Eric A. Fritz, BML, and John I. Koivula

Figure 48. A distinct triangular color zone is visible in this 3.08 ct liddicoatite when it is viewed at an angle to the table. Courtesy of Intimate Gems; photo by Robert Weldon.

Turquoise from Nacozari, Sonora, Mexico. In October 2006, we were informed by Jack Lowell (Colorado Gem & Mineral Co., Tempe, Arizona) about new production of turquoise from a large open-pit copper mine located about 110 km south of the U.S. border from Douglas, Arizona. Mr. Lowell reported that the Nacozari turquoise occurs in nodules that can weigh up to 1.4 kg, and that while much of the material is chalky, a significant portion is very hard with excellent color. He obtained about 30 kg of the turquoise, consisting of nodules (figure 49), samples that appear to be pseudomorphs after apatite (figure 50), and an unusual piece that contained abundant sulfide minerals (figure 51).

Mr. Lowell loaned GIA several rough and polished samples for examination, and the three polished stones (5.79–12.32 ct; figure 49) were characterized by one of us (EAF): color—greenish blue, with no pleochroism; spot R.I.—1.59 to 1.60, with no birefringence visible on the refractometer; hydrostatic S.G.—2.64 to 2.69; Chelsea filter reaction—none; fluorescence—uneven moderate chalky blue to long-wave UV radiation, and inert to short-wave UV; and an absorption band at 430 nm visible with the desk-model spectroscope. These properties are consistent with those reported for turquoise by M. O'Donoghue

Figure 49. Attractive turquoise has been produced recently from a copper mine at Nacozari, Sonora, Mexico, south of Douglas, Arizona. The cabochons shown here weigh 5.79–12.32 ct, and the nodule is 123 g. Intergrowths of quartz (white) and molybdenite (gray) are visible in the nodule. Courtesy of Jack Lowell; photo by Robert Weldon.

Figure 50. The crystal form shown by these turquoise specimens (2.5–10 cm long) suggests that they are pseudomorphs after apatite. Photo by Jack Lowell.

Figure 51. This 59.59 ct freeform turquoise cabochon contains numerous sulfide inclusions. The dark spots are Superglue-filled cavities. Courtesy of Jack Lowell; photo by Robert Weldon.

(*Gems*, 6th ed., Butterworth-Heinemann, Oxford, U.K., 2006, pp. 323–328), except that the R.I. values of the Mexican material are slightly higher. However, in the experience of the GIA Laboratory, the lower R.I. values reported for turquoise in the literature are typical for chalky, less dense turquoise. Microscopic examination of the cabochons revealed small inclusions of rounded quartz grains, mica "books," and anhedral pyrite grains (all of which were confirmed by Raman spectroscopy).

Three pieces of rough material (17–123 g) and one heavily included freeform cabochon (59.59 ct) were also examined. The morphology of two of the rough pieces was consistent with that of pseudomorphs after apatite; such pseudomorphs have also been documented from Anhui Province in China (see Q.-L. Chen and Y. Zhang, "Features of gem-mineralogy of apatite-pseudomorphic turquoise," *Journal of Gems & Gemmology*, Vol. 7, No. 4, 2005, pp. 13–16). All of the Nacozari rough material exhibited reactions to long- and short-wave UV radiation that were similar to those of the cabochons described above, as well as the 430 nm absorption band with the desk-model spectroscope. The larger piece of rough (figure 49) contained inclusions and intergrowths of pyrite, quartz, mica, and molybdenite (confirmed by Raman analysis). The inclusions in the freeform cabochon (figure 51) were identified with Raman microspectroscopy as pyrite and covellite, while marcasite, molybdenite, and epoxy were detected in minute cavities in the sample (figure 52). The presence of epoxy can be explained by the fact that Mr. Lowell used Superglue to stabilize the sample and ensure that the pyrite grains would be retained during the polishing process. FTIR spectroscopy showed no evidence of polymers (or waxes) in any of the other samples.

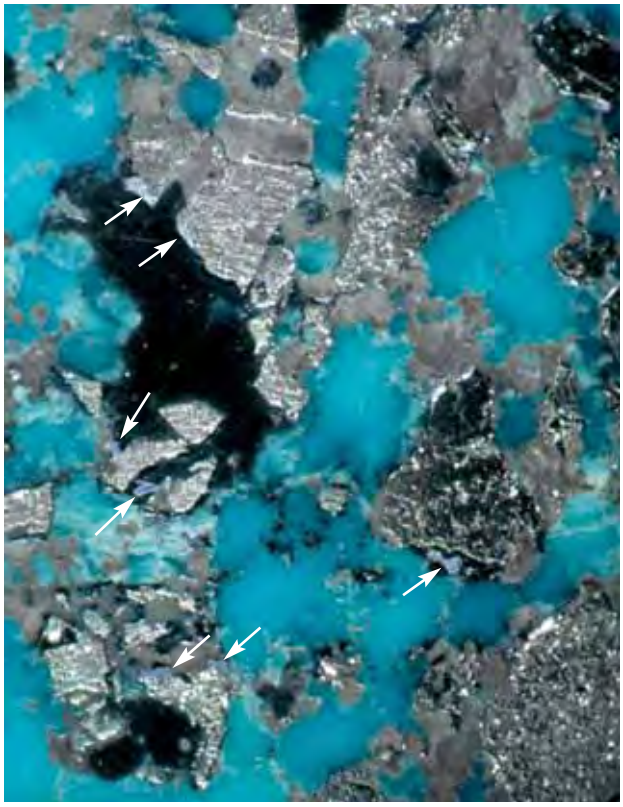

Figure 52. Raman analysis identified the inclusions in the turquoise cabochon in figure 51 as pyrite and covellite (silver metallic; see arrows). The dark areas are cavities that are filled with Superglue; Raman analysis of the cavity linings showed the presence of marcasite and molybdenite. The light brown areas consist of residue from the polishing wheel. Photomicrograph by J. I. Koivula; magnified 15×.

Future production of turquoise from the Nacozari deposit is uncertain, since the miners prefer to avoid the turquoise-bearing zones because the mineralogy of those areas is unfavorable for the ore treatment processes used to obtain copper.

Eric A. Fritz, John I. Koivula, BML

TREATMENTS

Lead glass–filled rubies with hollow backs set in a closed-back mounting. Recently, the SSEF Swiss Gemmological Institute received the ear pendant in figure 53 for analysis. It was set with what appeared to be three rubies and two diamonds. The ear pendant was purchased in the United States, and the client had been informed that it contained valuable Burmese rubies.

The red stones, which appeared to be rose cut, were set in a closed-back mounting, so it was necessary to unset them for analysis. This revealed the first of several surprises: Their bases had been carefully hollowed out, creating thin (~1 mm) concave ruby slices (figure 53, right). As the stones were heavily included, this deception was not apparent when they were mounted. An estimation of their weight based on measurable dimensions would have been overly high.

The red stones were easily identified as rubies based on standard gemological testing (R.I.—1.762–1.770; birefringence—0.008; hydrostatic S.G.—3.96; UV fluorescence—dull red to long-wave and inert to short-wave; and a Cr spectrum in a handheld spectroscope). A close look with the microscope revealed a narrow set of intersecting fissures along rhombohedral twinning planes; these fissures contained many gas bubbles and glassy swirls.

Figure 53. Although sold as a valuable jewel set with Burmese rubies, the ear pendant on the left turned out to be a clever fraud. When unmounted and observed from the back (right), the stones proved to be concave slices of lead glass–filled ruby. Photos by M. S. Krzemnicki, © SSEF.

Occasionally, blue flashes were observed. These features are well-known evidence of lead-glass filling in rubies (see, e.g., GAAJ Research Laboratory, "Lead glass impregnated ruby," www.gaaj-zenhokyo.co.jp/researchroom/kanbetu/2004/gaaj_alert-040315en.html, March 15, 2004; V. Pardieu, "Lead glass filled/repaired rubies," www.aigslaboratory.com/Filearticle/55.pdf, January 17, 2005; S. F. McClure et al., "Identification and durability of lead glass–filled rubies," Spring 2006 *Gems & Gemology*, pp. 22–34). Also noted were a hexagonal zoning pattern and linear particle trails with some rutile needles, indicating that the rubies probably had not been subjected to high-temperature heat treatment.

Chemical analysis of all three stones with EDXRF spectroscopy revealed chromium and iron as the main trace elements. Traces of gallium, very little titanium, and (with high excitation) very distinct lead peaks were also detected. Based on the microscopic observations and chemical analyses, the stones were identified as lead glass–filled rubies. Any filling of fissures with a glass involves heating. When the chemical composition of the stones was compared to those in the SSEF reference database, it matched that of material from Africa, such as from Madagascar or Tanzania. A Burmese origin could be excluded.

The degree of care and effort expended to produce this item was astonishing. Although ultimately the stones were easily identified, they proved unequivocally that the only way to evaluate gems presented in a closed-back setting is to unmount them. The risk of fraud is too great otherwise.

Michael S. Krzemnicki (gemlab@ssef.ch)
SSEF Swiss Gemmological Institute
Basel, Switzerland

MISCELLANEOUS

October 2006 Myanmar Gem Emporium, and other gem news from Myanmar. Attended by 1,495 gem merchants from 10 countries, the second session of this twice-yearly government sale of Myanmar gem materials took place October 19–29 in the Myanmar Convention Center, Yangon. Colored gemstones and pearls were sold in both tender and competitive bidding. The stones sold in tender consisted of ruby (45%), blue sapphire (41%), and other gems (14%; e.g., purple, yellow, and colorless sapphire; spinel; zircon; moonstone; peridot; danburite; topaz; garnet; and aquamarine). Gems sold in competitive bidding included ruby, sapphire, spinel, peridot, and quartz.

Jadeite sales took place in a separate venue. Over the first eight months of the 2006–2007 budget year, Myanma Gem Enterprise (under the Ministry of Mines) reported sales of US$300 million.

The Myanmar Pearl Enterprise (also under the Ministry of Mines) in February 2006 held the first cultured pearl sale for local merchants; the entire stock was sold for 2 million kyat (~US$323,500). During a second sale in December 2006 (a tender system), most of the cultured pearls offered were "gold" colored, and 90% of the lots sold. Myanmar is now producing cultured pearls from eight farms, of which three are government-run, two are managed by domestic private companies, and three are run by foreign firms. Total yearly production is estimated at 750 kg.

Petrified wood from Natogyi township, central Myanmar, has been selling well along the China-Myanmar border in Muse; it is used as a decorative stone. Some of the petrified wood is opalized, and pieces showing green color are the most highly prized.

The small gem shops in Yangon continue to sell synthetic material alongside natural gems. Those noted by this contributor included gadolinium gallium garnet (all colors), blue synthetic corundum (offered as irradiated blue topaz), and glass imitations of peridot. In addition, various small cultured pearls from India were available.

U Tin Hlaing
Dept. of Geology (retired)
Panglong University, Myanmar

ANNOUNCEMENTS

***G&G* online calendar.** A regularly updated list of conferences and museum exhibits pertaining to gems is now available on the *G&G* web site at www.gia.edu/gemsandgemology.

Conferences

Gem-A Scottish Branch Annual Conference. A variety of topics will be covered at this conference, hosted by the Scottish Branch of the Gemmological Association and Gem Testing Laboratory of Great Britain, to be held May 4–7, 2007, in Perth, Scotland. Visit www.scotgem.demon.co.uk/conf2007.html.

2007 ICA Congress. The International Colored Gemstone Association Congress will be held May 5–9 in Dubai, United Arab Emirates. The theme is "Embracing Global Trends from Mine to Market." Presentations will be given by industry leaders on gem sources, manufacturing centers, marketing, branding, laboratory services, and education/ethics/economics. Visit www.gemstone.org/congress.

Granitic Pegmatites: The State of the Art. Held May 6–12, 2007, at the Universidade do Porto, Portugal, this workshop will focus on the study of granitic pegmatites, and will include a field trip to rare-element pegmatites in northeastern Portugal and central-western Spain. Visit www.fc.up.pt/peg2007.

2007 GAA-NSW Conference. This year's conference of the New South Wales division of the Gemmological Association of Australia will be held May 18–20 in Hobart, Tasmania. Subjects will include the history of gems and lapidary, rare ivories, and Art Deco/Art Nouveau jewelry. Visit www.gem.org.au/conference.htm.

Santa Fe Symposium 2007. The 21st annual Santa Fe Symposium on jewelry manufacturing technology will be held in Albuquerque, New Mexico, May 20–23. Visit www.santafesymposium.org.

GAC-MAC 2007. This year's joint meeting of the Geological Association of Canada and the Mineralogical Association of Canada will take place May 23–25, in Yellowknife, Northwest Territories. The conference will include a session on Canadian diamonds. A "Geology of Gem Deposits" short course will take place May 21–22, and a post-conference fieldtrip to the Ekati and Diavik diamond mines is scheduled for May 26–27. Visit www.nwtgeoscience.ca/yellowknife2007.

Maine Pegmatite Workshop. The 5th Maine Pegmatite Workshop will be held May 26–June 3, in Poland, Maine. In addition to the in-depth curriculum, field trips to gem-bearing pegmatites in New England are planned. Visit homepage.mac.com/rasprague/PegShop.

New Diamond and Nanocarbons. Held May 28–31, in Osaka, Japan, this conference will address recent developments in the growth and characterization of synthetic diamond. NDNC is a merger of the International Conference of New Diamond Science and Technology (ICNDST) and the Applied Diamond Conference (ADC). Visit www2.convention.co.jp/NDNC2007.

JCK Show–Las Vegas 2007. Held June 1–5, this gem and jewelry trade show will also host a comprehensive educational program May 30–31. Seminars will cover industry trends, diamond cut, sales and marketing strategies, legal issues for retailers and manufacturers, and new developments in gemology. To register, call 203-840-5684 or visit jckvegas2007.expoplanner.com.

PegCamp 2007—West. This one-week course, held June 3–10 in Mesa Grande, California, will cover the mineralogy, internal structure, and evolution of granitic pegmatites through the field examination of pegmatites and related granites. Visit www.pegmatology.com/pegcamp.htm.

Essentials of Color Science. Munsell Color Science Laboratory's *Summer Short Course 2007* will take place June 5–8 at the Rochester Institute of Technology, Rochester, New York. The session will include lectures on color perception and appearance, digital color imaging systems, colorimetry, spectrophotometry, and color appearance models. Visit www.cis.rit.edu/mcsl/outreach/courses.php.

First European Gemmological Symposium: "Presence and Future of Gemmology." Honoring the 75th Anniversary of the German Gemmological Association, this international symposium will take place June 22–24, in Idar-Oberstein, Germany, and will offer presentations by gemological researchers and business leaders from the gem and jewelry industry. Visit www.dgemg.de/gemmologen_75.

PegCamp 2007—Rockies. This one-week course, held July 8–15 in Canon City, Colorado, will cover the mineralogy, internal structure, and evolution of granitic pegmatites through the field examination of pegmatites and related granites. Visit www.pegmatology.com/pegcamp.htm.

30th International Gemmological Conference. Held July 15–19 in Moscow, Russia, this conference will cover new gem deposits, synthetics, treatments, gem identification methods, and markets. Only IGC delegates may give presentations, but the conference is open to observers and students. E-mail balvlad@iem.ac.ru.

ECROFI-XIX: European Research on Fluid Inclusions. This conference will be held on July 17–20 at the University of Bern in Bern, Switzerland. The program will include a session titled "LA-ICP-MS Workshop: Analysis and data interpretation of inclusions in minerals." A pre-conference field trip on July 16 will take participants to the Bernese Alps and will include a visit to a large Alpine cleft lined with quartz crystals and other minerals. Visit illite.unibe.ch/ecrofi/index.htm

AOGS2007. The Asia Oceania Geosciences Society's 4th Annual Meeting will take place July 30–August 4 in Bangkok, Thailand. The conference will include a session titled "Gem Materials in Bio- and Geosphere." Visit www.asiaoceania.org/aogs2007.

PegCamp 2007—East. This one-week course, held August 6–13 in Poland, Maine, will cover the mineralogy, internal structure, and evolution of granitic pegmatites through the field examination of pegmatites and related granites. Visit www.pegmatology.com/pegcamp.htm.

NAJA 28th Annual Mid-Year Education Conference. The National Association of Jewelry Appraisers will hold this conference August 11–14 at the Cobb Galleria Convention Center in Atlanta, Georgia. Visit www.NAJAappraisers.com.

Goldschmidt 2007. The 17th Annual V. M. Goldschmidt Conference will take place August 19–24 in Cologne, Germany, and will feature a session titled "Applied geochemistry—from brines and rare-earth elements to diamonds" in honor of long-time *G&G* contributor Dr. Alfred A. Levinson. The session will consist of two parts: "Exploration Geochemistry" and "Gem Mineralogy, Diamonds and Gemstones." Visit www.goldschmidt2007.org.

24th European Crystallographic Meeting. Held August 22–27 in Marrakech, Morocco, this conference will include a session titled "Crystallography in Art and Archeology." Visit www.ecm24.org.

Diamond Symposium in Kimberley. The Geological Society of South Africa's Directorate of Professional Programmes will host this colloquium August 30–September 2 in Kimberley, South Africa. The conference program will include field trips to diamond deposits. Visit www.gssa.org.za.

IV International Conference on the Application of Raman Spectroscopy in Art and Archaeology. This meeting, held September 5–8 in Modena, Italy, will explore current trends and advanced techniques in the application of Raman spectroscopy to art and cultural heritage research. Visit www.chimica.unimore.it/RAA2007/raa2007.htm.

Diamond 2007. The 18th European Conference on Diamond, Diamond-like Materials, Carbon Nanotubes, and Nitrides will be held in Berlin, Germany, on September 9–14. Presentations on the growth, processing, and characterization of diamond will be given. Visit www.diamond-conference.elsevier.com or e-mail diamond-conference@elsevier.com.

II International Conference "Crystallogenesis and Mineralogy." Held October 1–5 in St. Petersburg, Russia, this conference will explore mineral formation, crystal growth in nature and the laboratory, and crystal morphology. Visit www.minsoc.ru/KM2007.

CGA Gem Conference 2007. The Canadian Gemmological Association's annual gemological conference will take place October 19–21 in Vancouver, British Colombia. Visit www.gemconference2007.com.

Mineralientage München. The 44th Munich mineral show in Germany will take place November 2–4 and feature a special exhibit on gem crystals from Pakistan. Visit www.mineralientage.com.

Art2008. Scheduled for May 25–30, 2008, in Jerusalem, Israel, the 9th International Art Conference on Nondestructive Investigation and Analysis will focus on items of cultural heritage, but will have implications for gem testing. Visit www.isas.co.il/art2008.

ICAM 2008. Gems will be one of the subjects covered at the 9th International Congress for Applied Mineralogy on September 8–10, 2008, in Brisbane, Australia. Visit www.icam2008.com.

Exhibits

Colored diamonds at the London Natural History Museum. On loan from Alan Bronstein and Harry Rodman, the Aurora Collection of 296 naturally colored diamonds is now on display at the Natural History Museum in London. Visit www.nhm.ac.uk/about-us/news/2006/november/news_9996.html.

Bernd Munsteiner carvings at the GIA Museum. From mid-May 2007 to March 2008, "Reflections in Stone" will showcase gem carver Bernd Munsteiner's work during the period 1966–2003. The exhibit will include carved quartz, tourmaline, and beryl, ranging from pieces set in jewelry to large table-top sculptures. Advance reservations are required; to schedule a tour, call 760-603-4116 or e-mail museum@gia.edu.

Symbols of Identity—Jewelry of Five Continents. On display through May 31, 2007, at the Mingei International Museum in San Diego, this exhibit features examples of personal adornment from native cultures in North and South America, Africa, Asia, and Europe. Visit www.mingei.org/curex.html.

French Jewelry at the Legion of Honor. "Masterpieces of French Jewelry," an exhibition of notable French jewelry pieces from American collectors, will be on display at the Legion of Honor art museum in San Francisco through June 7, 2007. Among the pieces included are the Taj Mahal diamond necklace by Cartier, given to actress Elizabeth Taylor by Richard Burton in the 1970s, and an Art Nouveau brooch owned by former first lady Jacqueline Kennedy Onassis. Visit www.thinker.org/legion/exhibitions.

Native American Jewelry. "Shared Images: The Jewelry of Yazzie Johnson and Gail Bird" will be on display through June 2007 at the Heard Museum in Phoenix, Arizona. The exhibit includes examples of their belts, earrings, bracelets, rings, and necklaces. Visit www.heard.org.

Gold at AMNH. "Gold," an exhibition exploring the historical fascination with this precious metal, is on display at the American Museum of Natural History in New York through August 19, 2007. The exhibit includes both rare natural specimens and significant cultural artifacts. Visit www.amnh.org/exhibitions/gold.

Jewelry of Ben Nighthorse. Ben Nighthorse Campbell, who represented Colorado in the U.S. Senate from 1992 to 2004, has enjoyed a successful second career as an innovative jewelry designer. This collection of his work, which debuted at the Smithsonian Institution's National Museum of the American Indian in 2004, is on display at the Colorado History Museum in Denver through December 31, 2007. Visit www.coloradohistory.org.

ERRATUM

The Summer 2006 issue contained a GNI entry on triploidite from China (pp. 183–184). Subsequent chemical analyses of this material showed that it is triplite, rather than triploidite. The chemical formula has been revised as follows: $(Mn^{2+}_{1.60}Fe^{2+}_{0.21}Mg_{0.15}Ca_{0.04})(P_{1.00}O_4)(F_{0.80}(OH)_{0.20})$. The authors regret this error in the identification of the material.

Take the Challenge

THE FOLLOWING 25 QUESTIONS are based on information from the Spring, Summer, and Winter 2006 issues of GEMS & GEMOLOGY (the Fall 2006 Symposium/GRC proceedings issue is not covered because it is principally an abstract volume). Refer to the feature articles and "Notes and New Techniques" in those issues to find the single best answer for each question. All answers can be found in the 2006 issues—no further research is necessary. Mark your choice on the response card provided in this issue. (Sorry, no photocopies, scans, or facsimiles will be accepted; go to www.gia.edu/gemsandgemology to purchase additional copies of this issue.) Mail the card so that we receive it no later than Monday, August 6, 2007. All entries will be acknowledged with a letter and an answer key after the due date, so please remember to include your name and address (and write clearly!).

Score 75% or better, and you will receive a GIA CONTINUING EDUCATION CERTIFICATE, and if you are a member of the GIA Alumni Association, you will earn 10 Carat Points. (Be sure to include your GIA Alumni membership number on your answer card and submit your Carat card for credit.) Earn a perfect score, and your name also will be listed in the Fall 2007 issue of GEMS & GEMOLOGY. Good luck!

1. In Ballerina "chocolate pearls," the coloration is apparently a result of
   - A. a new silver nitrate dyeing process.
   - B. modification of organic components in the nacre.
   - C. modification of aragonite components in the nacre.
   - D. modification of organic components in the bead nucleus.

2. Testing by the GIA Laboratory showed that the lead-glass material used to fill fractures and cavities in rubies could be damaged by
   - A. steam and/or ultrasonic cleaning.
   - B. immersion in pickling solution.
   - C. exposure to household oven cleaner.
   - D. both B and C.

3. One possible indicator that a cultured pearl is silver dyed is its
   - A. reaction to rubbing with acetone.
   - B. inert reaction to long- and short-wave UV radiation.
   - C. distinctive FTIR spectrum.
   - D. Raman spectrum that indicates the presence of organic components.

4. The gemological properties that make transparent rhodonite so difficult to facet include
   - A. multiple perfect, brittle cleavages.
   - B. Mohs hardness of 2.5–3.5.
   - C. large inclusions of galena and spessartine.
   - D. both A and C.

5. The Cullinan I is the largest _____ currently in existence.
   - A. rough diamond
   - B. faceted diamond
   - C. faceted colorless diamond
   - D. flawless diamond

6. Tortoise shell used as a gem material was most commonly taken from the shell of the
   - A. green turtle.
   - B. loggerhead turtle.
   - C. Kemp's Ridley turtle.
   - D. hawksbill turtle.

7. One useful indication of treatment in Ballerina "chocolate pearls" is
   - A. their reddish orange fluorescence to long-wave UV radiation.
   - B. an increase in general absorption toward the high-wavelength (low-energy) side of their UV-Vis-NIR spectra.
   - C. a strong band around 1514 cm^{-1} in their FTIR spectra.
   - D. both A and B.

8. Which of the following is/are believed necessary for the formation of Leopard opal?
   - A. Availability of silica
   - B. Permeability and porosity of the host vesicular basalt
   - C. Environmental factors favoring the formation of play-of-color opal
   - D. All of the above

9. Reflective graining in diamonds is believed to be caused by
   A. micro-inclusions of water and carbonates.
   B. damage during polishing.
   C. plastic deformation.
   D. compressive strain caused by multiple growth centers.

10. The colorful appearance of Rainbow andradite from Japan is a result of the combination of what two optical effects?
   A. Thin-film interference and some diffraction
   B. Dispersion and some diffraction
   C. Refraction and thin-film interference
   D. X-ray diffraction and dispersion

11. The presence of a lead-glass filler in rubies is most easily detected by
   A. X-ray diffraction analysis.
   B. observation with magnification.
   C. LA-ICP-MS.
   D. heating to temperatures sufficient to melt the filler.

12. The most reliable nondestructive method for separating tortoise shell from its imitations is
   A. reaction to short-wave ultra-violet radiation.
   B. specular reflectance infrared spectroscopy.
   C. visible absorption spectroscopy.
   D. hot-point testing.

13. What standard gemological measurement(s) is/are not meaningful for the characterization of Leopard opal?
   A. Refractive index
   B. Specific gravity
   C. UV fluorescence
   D. Both A and B

14. Cu-bearing elbaite tourmaline has been reported from Brazil, Mozambique, and
   A. Madagascar.
   B. Afghanistan.
   C. Nigeria.
   D. Namibia.

15. Internal graining in a diamond that is noticeable from a narrow viewing angle but fades with very subtle movement
   A. would lower the clarity one grade.
   B. would mandate a clarity grade no better than VS.
   C. would prevent a clarity grade of Internally Flawless.
   D. would likely not affect the clarity grade.

16. Lead glass–filled rubies tested by the GIA Laboratory began to show sweating and beading of the glass filler when heated to
   A. 500°C.
   B. 600°C.
   C. 700°C.
   D. 1000°C.

17. The large variation in the reactions shown by zircon inclusions in Madagascar sapphires heated to 1400–1550°C was likely due to
   A. sample contamination.
   B. beryllium diffusion treatment of some of the tested sapphires.
   C. natural radiation damage.
   D. hafnium oxide (HfO_2) substitution.

18. Chemical analysis of Rainbow garnet from Japan established that it was composed of alternating layers of
   A. andradite and grossular.
   B. andradite and andradite with a grossular component.
   C. andradite and spessartine.
   D. andradite and grossular with an andradite component.

19. For trace-element analysis using a well-characterized standard, LA-ICP-MS can accurately quantify
   A. more elements than both LIBS and SIMS.
   B. more elements than LIBS but fewer than SIMS.
   C. more elements than SIMS but fewer than LIBS.
   D. fewer elements than both LIBS and SIMS.

20. Beryllium diffusion–treated corundum commonly has a Be concentration of
   A. <1 ppm.
   B. a few hundred ppb.
   C. a few to several hundred ppm.
   D. >1,000 ppm.

21. Infrared spectroscopy established that the Cullinan I and II diamonds are
   A. type Ia.
   B. type Ib.
   C. type IIa.
   D. type IIb.

22. Formation of discoid fractures was observed around zircon inclusions in corundum that had been heated to
   A. 1550°C.
   B. 1620°C.
   C. 1680°C.
   D. 1730°C.

23. The "greasy lap" technique for faceting transparent rhodonite uses a mixture of diamond grit and
   A. axle grease.
   B. petroleum jelly.
   C. olive oil.
   D. mineral oil.

24. CIBJO and LMHC use the term *Paraíba tourmaline* to describe elbaite of moderate to strong color saturation that contains Cu and is
   A. blue.
   B. bluish green to greenish blue.
   C. green.
   D. any of the above.

25. After graining features have been identified, GIA graders make the final determination of their impact on a diamond's clarity grade using
   A. a 10× loupe and fiber-optic light.
   B. a microscope and darkfield illumination.
   C. a 10× loupe and fluorescent light.
   D. both A and B.

BOOK REVIEWS

Pearls

*By Elisabeth Strack, 678 pp., illus., publ. by Rühle-Diebener-Verlag, Stuttgart, Germany, 2006. €106.10 (US$115.00)**

Broad in scope and deep in detail, this is the most comprehensive book ever written about pearls. It is a rich and valuable resource for industry professionals, students, and anyone with a personal interest in the subject. *Pearls* is the expanded, updated, English-language edition of *Perlen*, which was published in German in 2001. Like the original, the new edition is just under 8 × 10 inches (20.3 × 25.4 cm), hardcover, and printed on high-quality coated stock with excellent color reproduction.

The book is divided into two sections: "Natural Pearls" and "Cultured Pearls." Chapters then thoroughly cover the history, biology, types, geography, formation, structure, farming, properties, grading, marketing, testing, treating, imitating, care, and uses of pearls. *Pearls* is well-illustrated with color photos, maps, charts, and explanatory diagrams. An extensive bibliography follows each chapter, and there are eight indices, arranged by various topics.

That one person gathered the information, wrote the text, shot many of the photos, and assisted with the translation of this book is astounding and commendable. *Pearls* is broad and deep, so it necessarily took years to research and write. That led to one of its few flaws: Some of the information is unavoidably outdated. A second minor drawback is that the English is a little awkward in places.

Pearls is an excellent choice for anyone seeking a wealth of information about natural and cultured pearls.

DOUG FISKE
Gemological Institute of America
Carlsbad, California

Not Your Mama's Beading: The Cool and Creative Way to String 'Em Along

By Kate Shoup Welsh, 224 pp., illus., publ. by Wiley Publishing [www.wiley.com], Hoboken, NJ, 2006. US$14.99

As a longtime beader, I have read my share of books on the subject. They are usually quite informative, and I often learn new techniques from them. However, I wouldn't go so far as to say that I actually had fun reading them. That was until I found *Not Your Mama's Beading*. With project titles such as "Swinging by the Chandeliers," "The Short and Winding Rope," and "Girls Gone Bridaled," the table of contents (not to mention the book title) makes it clear that Kate Shoup Welsh has a great sense of humor. Imagine having a conversation with your funniest friend, and you'll get a sense of this book's voice.

The book is divided into three sections, with several chapters in each. The first section looks at beads throughout history, including their use in trade and fashion. It also has an informative overview on materials and tools. The section closes with a chapter that teaches basic beading and stringing techniques for the beginner.

The second section consists of specific projects that range from very easy to somewhat complicated, grouped by type. There are chapters on necklaces, rings, bracelets, miscellaneous personal adornments, and gift items. Some of the more interesting (yet simple) projects include bookmarks, zipper pulls, and even bulletin board tacks. Each includes the estimated cost, a materials list, and a rating of the level of commitment needed to complete the project. The diagrams included for the more complicated projects are clear and easy to follow. There is truly something for everyone here.

The beader will find a wealth of helpful information in the third section. Included here are patterns, illustrations of different types of tools and findings, and charts of bead and wire sizes. There are also some nicely prepared lists of absolute essentials for bead stringing, bead stitching, and wireworking kits.

I highly recommend *Not Your Mama's Beading*. The creative beader will find some great projects to try and will enjoy some laughs along the way.

JANA E. MIYAHIRA-SMITH
Gemological Institute of America
Carlsbad, California

**This book is available for purchase through the GIA Bookstore, 1949 Kellogg Ave., Carlsbad, CA 92008. Telephone: 800-421-8161, ext. 4200; outside the U.S. 760-603-4200. Fax: 760-603-4266. E-mail: myorder@gia.edu or visit www.gia.edu*

Special Exhibition Jadeite: Treasure of Orient

By the National Science Museum [www.kahaku.go.jp/english], 202 pp., illus., publ. by the Mainichi Newspapers Co., Tokyo, 2004 [in Japanese; no price information available].

In Japan, most people believe that jadeite jade comes from China due to its strong association with Chinese culture. In fact, other than Myanmar (Burma), Japan is the only Asian country where jadeite has been found. The Japanese National Science Museum and the Mainichi Newspapers Co. (one of the largest newspaper companies in Japan) organized a special jadeite exhibition, held from November 2004 to February 2005, and this book was published as a companion to that exhibit.

The first part of the book reviews the history of jadeite and nephrite jade in Chinese culture, with photos showing typical jewelry and art objects from the Qing Dynasty (1644–1911). The second part introduces the mineralogy and geology of jadeite. This is the first work known to this reviewer that systematically describes Japanese jadeite localities and their exploration, as well as their petrology and mineralogy. Included are maps of the localities and photos of rough jadeite. As an example, the use of jadeite from Itoigawa River, in Niigata Prefecture, can be traced back about 5,000 years, although an accurate mineralogical identification was first reported only in 1939, in the *Journal of Mineralogical and Petrological Sciences*. Several new silicate minerals characteristically associated with Itoigawa jadeite, such as blue itoigawite, have been discovered in this region.

The third part of the book covers most of the known ancient jadeite-using cultures in Japan and Korea. Manufacturing techniques such as hole-drilling, shaping, and polishing, as well as early distribution networks, are described and summarized.

The book concludes with a brief introduction to the basic gemology of jadeite. Well-known gem identification techniques, such as FTIR and Raman spectroscopy, are reviewed, as are common jadeite treatments. This section also includes some attractive photos of jadeite jewelry, carvings, and other products belonging to Japanese collectors.

This is an educational book covering a number of elements that may be unfamiliar to Western readers.

TAIJIN LU
Vista, California

Hope Diamond: The Legendary History of a Cursed Gem

By Richard Kurin, 388 pp., illus., publ. by Smithsonian Books [www.smithsonianstore.com], Washington, DC, 2006. $24.95

What other jewel has captured the imagination and adoration of so many people as the Hope diamond? Many books have been written about the Hope, ranging from scholarly treatises to folkloric musings. This version is more of a historical journey, covering more than 300 years and three continents, featuring major and minor royal players as well as famous jewelers.

The book begins by recounting the history of what came before the Hope diamond, with rich details of 15th-century trade routes, products, customs, and systems of commerce along the thousands of miles between India and Europe. Exactly where and when the original diamond was purchased by French gem merchant Jean-Baptiste Tavernier is still unclear. Research reveals that it might have come from the former mine of Kollur in the Golconda region, which the author was successful in locating (though no mining currently takes place, as the area is a wilderness reserve). It might have been purchased from a corrupt mine supervisor (who should have turned such a stone over to the Sultan of Golconda), not from one of the merchants who acted as middlemen. It is delicious that even these facts remain in question today. What is more of a puzzle is why Tavernier held on to the diamond for 15 years, through hard times—having his ship sunk, being imprisoned, finding himself in the middle of an armed conflict—and never sold it until he returned to France.

Tavernier eventually did sell the diamond, along with more than a thousand others, to King Louis XIV on December 6, 1668. It was entered into the royal accounts as 112¾ ct. This is the point in time where the account of the blue diamond as we know it becomes available, as it is whittled down through its journey from one hand to another. All the historical highlights as well as the years of disappearance are there—the looting of the Crown Jewels during the French Revolution, the extravagance of England's King George IV, and the Gilded Age in America. Also fascinating is the transition of Tavernier's "*beau violet*" to the "French Blue of the Crown," the "George IV Diamond," and, finally, Henry Philip Hope's modest designation of "No. 1." Yet even Mr. Hope's acquisition of the diamond, like Tavernier's, is shrouded in mystery—though the author theorizes that it was discreetly sold to pay George IV's enormous debts after his death in 1830. However, we do know that the diamond that is now ensconced with high honor at the Smithsonian Institution has been slimmed down to 45.52 ct.

This book is armchair traveling at its best. It is also one of the best-researched books on the subject, with more than 50 pages of credits and sources for photographs, illustrations, text excerpts, and lyrics, with substantial endnotes and references. Should you put the book down for a while, you can bring yourself up to date with the timeline. One of the more fascinating features is the two-page appendix on the diamond's value from 1668 to 1958. This poses a real appraiser's challenge—assessing a 2007 value!

Finally, Dr. Kurin notes in the epilogue that there are 21 missing documents that could complete the historical picture of the Hope. "In all then," he says, "there are still discoveries to be made."

GAIL BRETT LEVINE
National Association of Jewelry Appraisers
Rego Park, New York

OTHER BOOKS RECEIVED

Precious Minerals (Gemology). *By Ruslan I. Kostov, 453 pp., illus., publ. by PENSOFT [www.pensoft.net], Sofia, Bulgaria, 2003 [in Bulgarian; no price information available].* This is a very detailed monograph intended for mineralogists, gemologists, jewelry designers, and art critics. The first section, "Principles of Gemology," recounts the history of gemology and jewelry in the Middle East, Egypt, Greece, Rome, India, China, and the Americas. It also provides a detailed description of gems described in the Bible. The second section is devoted to the principles of crystallography and mineralogy. The third (and largest) section describes virtually all precious, semiprecious, and decorative stones, as well as metals and alloys. The last section covers methods of identification, study, faceting, and evaluation.

Also included are six appendices with lists of about 750 of the world's largest diamonds and about 150 of the largest brilliant-cut diamonds (with weight, name, color, date of discovery, and deposit), a glossary of mineral names in four languages (Bulgarian, Russian, English, and German), a dictionary of gemological materials and terminology (in Bulgarian), and two lists of stones with hardness and colors indicated.

BORIS SHMAKIN
Institute of Geochemistry
Siberian Branch
Russian Academy of Sciences
Irkutsk, Russia

Faceting History: Cutting Diamonds and Colored Stones. *By Glenn Klein, 242 pp., illus., publ. by the author [www.glennklein.com], Lake Forest, CA, 2005, US$21.99.* Award-winning faceter Glenn Klein chronicles the development of gem-faceting procedures and equipment over the centuries. *Faceting History* begins with background on the early appreciation of gems and the evolution of cut designs before delving into the advances made over the past hundred years. The scholarly text is well supplemented by facet diagrams and historical photos and illustrations.

STUART OVERLIN
Chicago, Illinois

Symposium on Agate and Cryptocrystalline Quartz. *Daniel Kile, Thomas Michalski, and Peter Modreski, Eds., 144 pp., illus., publ. by Friends of Mineralogy (Colorado Chapter), Colorado School of Mines Geology Museum, and U.S. Geological Survey, 2005, US$20.00.* The Symposium on Agate and Cryptocrystalline Quartz, held September 10–13, 2005, in Golden, Colorado, examined the mineralogy, origin, and worldwide occurrence of agate and other forms of cryptocrystalline quartz. This booklet contains summaries of 33 presentations delivered by speakers from the United States and five other countries. Accompanying the text are tables and illustrations, plus a series of color plates.

STUART OVERLIN

The Art of Diamond Cutting, 2nd ed. *By Sofus S. Michelsen and Basil Watermeyer, 147 pp., illus., publ. by Sofus S. Michelsen [sofus_sidney@direcway.com], Port Angeles, WA, 2005, US$49.95.* Intended to help the experienced colored stone faceter move into diamond cutting, this work provides basic instruction in the five steps of polishing diamonds: analyzing the rough, cleaving/sawing, bruting, blocking, and brillianteering. Also included are a brief description of the modern diamond industry and suggestions on how independent cutters can gain work and sell finished stones, a guide to grading and pricing rough diamonds, and a glossary of diamond terminology.

THOMAS W. OVERTON
Gemological Institute of America
Carlsbad, California

Alexandrite. *By Yury S. Kozlov, 143 pp., illus., publ. by Nauka Publishers [www.maik.rssi.ru], Moscow, 2005, €33.00.* This mineralogical monograph, a translation of the 2003 Russian-language edition, reviews the current scientific knowledge of the titular gem. Chapters cover chemical and gemological properties, the Ural mines, crystallography, X-ray spectral analysis, and cathodoluminescence studies of alexandrite color characteristics. Also included are 60 pages of color plates of alexandrite mineral specimens as well as appendices providing information on alexandrite dealers and pricing.

THOMAS W. OVERTON

MEDIA REVIEW

Aphrodite's Drop: The Power of Pearls. *A Faction Films production [www.factionfilms.co.uk], London, 75 min., 2005, available in DVD format, £30.00.* In this documentary, director Sylvia Stevens offers an engaging glimpse at the world of pearls, from their colorful past to the emergence of cultured pearls in the 20th century and today's elegant jewelry creations. *Aphrodite's Drop* takes the viewer behind the scenes of modern pearl production to reveal the difficult labor and painstaking quality control behind each of these treasures. Historic footage and exotic location shots from the South Seas cut away to interviews with industry insiders such as Ward Landrigan (Verdura), Martin Coeroli (Perles de Tahiti), Andy Muller (formerly of Golay Buchel), and Joanna Hardy (Sotheby's London).

STUART OVERLIN

GEMOLOGICAL ABSTRACTS

COLORED STONES AND ORGANIC MATERIALS

Characterization of vaterite in low quality freshwater-cultured pearls. H. Y. Ma [mhyyy@126.com] and I.-S. Lee, *Materials Science and Engineering C*, Vol. 26, 2006, pp. 721–723.

Vaterite is a relatively unstable phase of calcium carbonate that is rarely seen in nature. However, low-quality freshwater cultured pearls from Leidian, southern China, were found to contain vaterite. These formed part of a sample suite consisting of 4–8 mm cultured pearls that ranged from high quality (good luster and white or very light yellow color) to low quality ("lusterless" and yellowish brown color).

The cultured pearls were sliced in half, and their internal concentric structure was observed with an optical microscope. In the low-quality samples, a layer near the center was filled with irregular crystals (3 µm in longest dimension); this was overlain by a layer of needle-shaped crystals (45 µm long). The outermost layer consisted of irregular granular crystals (3–45 µm) that were mixed with organic materials. The optical properties of the crystals in the outer layer were consistent with vaterite; this was confirmed by X-ray diffraction analysis, which also documented aragonite and calcite in the samples. Micro-region infrared spectra further confirmed the presence of vaterite, with absorption bands at 1087 and 1050 cm^{-1} (ν_1); 830 cm^{-1} (ν_2); 1489, 1450, and 1420 cm^{-1} (ν_3); and 762 and 743 cm^{-1} (ν_4).

Vaterite was not detected in any of the high-quality cultured pearls; instead, aragonite was the main component. The authors suggest that the presence of vaterite may influence the quality of freshwater cultured pearls—the more vaterite,

This section is designed to provide as complete a record as practical of the recent literature on gems and gemology. Articles are selected for abstracting solely at the discretion of the section editors and their reviewers, and space limitations may require that we include only those articles that we feel will be of greatest interest to our readership.

Requests for reprints of articles abstracted must be addressed to the author or publisher of the original material.

The reviewer of each article is identified by his or her initials at the end of each abstract. Guest reviewers are identified by their full names. Opinions expressed in an abstract belong to the reviewer and in no way reflect the position of Gems & Gemology

the lower the quality. A high content of organic materials may contribute to the stability of vaterite in such cultured pearls. *KSM*

Development of pearl aquaculture and expertise in Micronesia. M. Ito [hiroito@mail.fm], *World Aquaculture*, Vol. 37, No. 3, 2006, pp. 36–42.

The article details a six-year project to develop pearling operations in the eastern-central Pacific islands of Micronesia (specifically, the Marshall Islands, Palau, and the Federated States of Micronesia). Working with U.S. government agencies, the College of Micronesia began a project to culture black pearls. One difficulty was a lack of wild oyster stock from which to collect spat (embryonic oysters). A low-cost hatchery was constructed to develop the stocks and serve as a training facility for pearling workers.

The article also recounts difficulties faced by the established black cultured pearl industry in French Polynesia, which were caused by overproduction coupled with economic difficulties in a number of key Asian markets. *RS*

OH in naturally occurring corundum. A. Beran [anton.beran@univie.ac.at] and G. R. Rossman, *European Journal of Mineralogy*, Vol. 18, No. 4, 2006, pp. 441–447.

Corundum is nominally anhydrous, but it may contain traces of OH. This impurity is useful for providing a possible indication of geologic origin, and it also can be affected by heat treatment. Using FTIR spectroscopy, the authors detected OH defects in ~20% of 159 natural sapphire and ruby samples tested, as shown by the presence of an absorption peak at 3310 cm^{-1}, sometimes with weaker peaks at 3233 and 3185 cm^{-1}. Strong OH absorptions were correlated to saturated blue color and to blue sapphires from basaltic sources.

The absorption coefficient of the 3310 cm^{-1} peak was less than 0.5 cm^{-1} for all samples. Given the total absorption of OH peaks in the IR spectra, the authors describe techniques for estimating the actual concentration of OH in a corundum sample. Using certain approximations, they report that the absolute concentration of OH in corundum generally corresponds to less than 0.5 ppm H_2O, though it ranged up to 10 ppm H_2O. *DMK*

DIAMONDS

Characteristics of diamondiferous Plio-Pleistocene littoral deposits within the palaeo–Orange River mouth, Namibia. R. I. Spaggiari [spaggiari.renato@debeersgroup.com], B. J. Bluck, and J. D. Ward, *Ore Geology Reviews*, Vol. 28, 2006, pp. 475–492.

Over 75 million carats of diamonds, of which 95% are gem quality, have been produced from Namibian gravel deposits within the past 100 years. The Orange River system, both modern and ancestral, transported diamonds from various sources in southern Africa to the Namibian coast. The diamonds were then swept northward by the prevailing currents and deposited in a variety of sedimentary environments. Although somewhat of an oversimplification, diamond size and grade both decrease in a northerly direction from the mouth of the Orange River.

Using mine records dating from 1947 and eight years of geologic observations of various open-pit mines and trenches, the authors provide valuable insights into the details of the diamond deposits. They focused on barrier beaches and spits proximal to the mouth of the Orange River that formed during Late Pliocene and Early Pleistocene times, when diamond output from the Orange River was lower than usual. The authors theorized that the large quantity of diamonds in these deposits must have been partially sourced by reworking pre-existing beach sediments. Within both the barrier beaches and spits, diamond size and grade varied considerably and was correlated to the energy of ocean waves in each depositional environment (e.g., subtidal, intertidal, and back barrier). Intertidal settings (high wave energy) in both barrier beaches and spits had average stone sizes of 1–2 ct and grades of 1.5–6 carats per hundred tons; these deposits were most economic. The authors suggest that relating sediments to their depositional environment should lead to more accurate sampling and mining programs. *KAM*

Electron energy loss spectroscopic studies of brown diamonds. U. Bangert, R. Barnes, L. S. Hounsome [hounsome@excc.ex.ac.uk], R. Jones, A. T. Blumenau, P. R. Briddon, M. J. Shaw, and S. Öberg, *Philosophical Magazine*, Vol. 86, No. 29–31, 2006, pp. 4757–4779.

The origin of brown coloration in type IIa diamonds is of particular interest to the gem trade due to the widespread use of high-pressure, high-temperature (HPHT) treatments to decolorize natural and synthetic diamonds. The mechanisms responsible for their brown coloration, however, are widely disputed. Electron energy loss spectroscopy (EELS) and theoretical modeling were performed on natural and CVD synthetic type IIa brown diamonds, before and after HPHT annealing. In addition, a natural type IIa colorless diamond was included for reference purposes.

EELS examines the local electronic structure of extended defects in diamond by measuring the energy loss of an electron beam, which is caused by inelastic scattering when electrons in the beam come in contact with electrons in the sample. EELS has a spatial resolution of ~10 nm and energy resolution down to 0.3 eV. Transmission electron microscopy (TEM) has revealed that there are large differences between the dislocation densities observed in CVD synthetic (10^5 cm^{-2}) and natural (10^9 cm^{-2}) diamonds, even though both have similar brown colors and absorption spectra. Furthermore, it has shown

that the number of dislocations does not change significantly with HPHT treatment.

EELS analysis confirmed that dislocations do not lead to additional energy losses in brown or HPHT-treated colorless diamonds, indicating that dislocations cannot be a major source of brown color. EELS also revealed the presence of graphitic inclusions in some natural brown diamonds that disappear with HPHT treatment, and therefore may have contributed to their color. Most importantly, EELS analysis of a striated brown/colorless natural type IIa diamond revealed an increase in energy loss in the brown portions due to sp^2 and π-bonded defects. Positron annihilation studies, TEM, and modeling suggest these defects are {111} disks of vacancy clusters that are likely responsible for the brown color and produce an absorption spectrum similar to that seen in type IIa natural and CVD synthetic brown diamonds. The concentration of vacancy clusters decreased with HPHT treatment and the loss of brown color. The authors suggest that these defects form by climb-and-collapse processes in natural diamonds and during the growth of CVD synthetic diamonds. HPHT annealing at ~2200°C likely results in dissolution of the collapsed defects and the removal of brown color in natural diamonds; whereas in CVD synthetic diamonds, the decoloration probably occurs by a mechanism known as hydrogen passivation of the vacancy disks at ~1900°C.

CMB

Origin of brown coloration in diamond. L. S. Hounsome [hounsome@excc.ex.ac.uk], R. Jones, P. M. Martineau, D. Fisher, M. J. Shaw, P. R. Briddon, and S. Öberg, *Physical Review B*, Vol. 73, 2006, pp. 125203-1–125203-8.

The brown color in synthetic diamonds produced by chemical vapor deposition (CVD) is typically ascribed to nitrogen and/or hydrogen defects created during growth, while brown coloration in natural type IIa diamonds is thought to relate to defects caused by plastic deformation. The authors deviate from these theories and speculate that brown coloration in both natural and CVD synthetic diamonds is caused by other types of defects. In the absorption spectra of both types, the authors observed the same underlying continuum, which suggests that the brown color is due to a single type of defect.

The authors believe that vacancies are involved with brown coloration because nitrogen-vacancy defects have been formed in experiments that transformed natural brown diamonds into colorless stones. To test this hypothesis, they performed calculations utilizing quantum mechanics of a hypothetical diamond containing a "disk" of vacancies within the structure. The resulting theoretical absorption spectra compared well against experimental spectra. In their modeling, disks containing <200 vacancies remained stable due to surface reconstruction. The authors proposed two mechanisms to help explain the reduction of brown color during annealing. First, dangling bonds are created by the interruption of the crystal structure at the surface where the carbon atoms are not fully bonded, and these open bonds introduce surface defect states that are similar to those created by the presence of impurities. The researchers modeled the effects of using hydrogen to eliminate these dangling bonds and found that the surface states were no longer optically active. Second, modeling of large vacancy disks (i.e., >200 vacancies) showed that they will likely collapse into optically inactive dislocation loops. *SE-M*

Morphology of diamonds with the surface graphitized at the high *P-T* conditions. V. M. Sonin, E. I. Zhimulev, and A. A. Chepurov, *Proceedings of the Russian Mineralogical Society*, Vol. 135, No. 1, 2006, pp. 112–117 [in Russian].

Natural and synthetic octahedral diamond crystals weighing 20–50 mg were packed in MgO powder and subjected to a pressure of 7.0 GPa and a temperature range of 2300–2400°C for 1–10 minutes. Their surfaces were examined after the resulting graphite films were removed using a mixture of 10% solution of $K_2Cr_2O_7$ and concentrated H_2SO_4.

All of the crystal faces became dull from corrosion. After short periods of treatment, small dimples with flat bottoms and mostly irregular contours formed, sometimes with triangular shapes oriented along edges. Longer periods of treatment produced thicker graphite films, and all crystal surfaces—including defects and cracks—were evenly covered with irregularly contoured dimples that did not follow the crystal symmetry. This corrosion morphology differs significantly from etch features generated by solution or oxidation processes. However, similar corrosion morphology was seen in the authors' experiments with diamond crystals in silicate melts, but at lower pressures and temperatures. The authors propose that the corrosion morphology seen on natural diamond crystals, even when graphite films are not present, is evidence of surface graphitization through post-formation transformation processes. *BMS*

Study of the transformation of hydrogen-containing centers in diamond at high PT parameters. I. N. Kupriyanov, Yu. N. Pal'yanov [palyanov@uiggm.nsc.ru], V. S. Shatsky, A. A. Kalinin, V. A. Nadolinnyi, and O. P. Yur'eva, *Doklady Earth Sciences*, Vol. 406, No. 1, 2006, pp. 69–73.

Hydrogen is second only to nitrogen in abundance as an impurity in diamond. However, little has been published about the interactions of H defects (most notably IR absorptions at 3107 and 1405 cm^{-1}) in the diamond lattice at elevated pressures and temperatures. A better knowledge of H defect behavior may increase understanding of the influence of fluids deep within the earth's mantle where diamonds form.

To evaluate changes in the 3107 cm^{-1} H absorption and the concentration and degree of aggregation of nitro-

gen defects at elevated pressure and temperature, seven diamond crystals from the Udachnaya, Mir, and Aikhal kimberlite pipes in Russia and a few HPHT-grown synthetic diamonds were annealed at 7 GPa and 1800, 1900, and 2000°C, using a multi-anvil split-sphere apparatus. The samples were analyzed before and after annealing using FTIR and photoluminescence spectroscopy and electron paramagnetic resonance (EPR; X-band frequency).

The synthetic diamonds contained high concentrations of N (2000–3000 ppm) and a strong 3107 cm^{-1} line before annealing. The natural samples consisted of type IaB, IIa, and IaAB diamonds with hydrogen centers. Some of the IaAB samples had a brown color that is typical of plastically deformed diamonds. After annealing, the IR spectra of all the samples (except those that were plastically deformed) showed no change in the 3107 cm^{-1} line or in nitrogen aggregation. Only the platelet-related B′ defects showed a reduction. This suggests that the 3107 cm^{-1} H defect is relatively stable. However, the plastically deformed type IaAB brown diamonds showed a gradual decrease in the intensity of both the B′ defect and the 3107 cm^{-1} absorption line. The natural diamonds showed similar, yet variable, results in their photoluminescence and EPR spectra. After annealing, N3 and H3 defects generally increased and the 490.7 nm system decreased dramatically; these effects were most prominent in the plastically deformed brown diamonds. The combined results indicate a clear relationship between the reduced intensity of the 3107 cm^{-1} H defect absorption line during annealing and the high concentration of plastic deformation defects in the brown diamonds. This correlation is most likely due to interactions between hydrogen-containing defects and migrating dislocations/vacancies within the deformed diamond lattice. *CMB*

TEM imaging and analysis of microinclusions in diamonds: A close look at diamond-growing fluids. O. Klein-BenDavid [ofrak@vms.huji.ac.il], R. Wirth, and O. Navon, *American Mineralogist*, Vol. 91, 2006, pp. 353–365.

Most natural diamonds grow from highly concentrated, high-density fluids, some of which can be trapped inside the crystal. During cooling, micro-inclusions (<1 μm) may form, and the fluids remain inside the inclusions as residual, low-density fluids. Therefore, fluid-bearing micro-inclusions are a key source of information about diamond-forming fluids and the crystallization environment in the earth's mantle.

Transmission electron microscopy (TEM) can be used to determine the size, crystallography, and mineralogy of micro-inclusions. The authors examined three fibrous coated diamonds (two gray and one green) from the Diavik mine in Canada and one from the Jubileynaya mine in Siberia. Tiny slices of the diamonds ($10 \times 15 \times 0.2$ μm) were extracted from different zones by milling with a focused ion beam.

A variety of micro-inclusions (diameters 30–700 nm) were found by TEM imaging, including carbonates (dolomite and magnesite), apatite, high-silica mica, halides, and pyroxene. Vacant spaces adjacent to the mineral phases in the micro-inclusions were most likely occupied by low-density fluids prior to milling by the ion beam. The presence of halides along with carbonates confirmed that diamonds can grow from chlorine-carbonate–rich fluids. Cavities of a few micrometers in size in two diamonds were filled with Al- and Si-rich minerals.

FTIR spectroscopy showed that the diamonds were type IaA and contained water. The chemical composition of the micro-inclusions (analyzed by electron microprobe) suggested that the trapped fluids consisted of carbonatitic + hydrous-silicic fluids, carbonatitic + hydrous-saline fluids, hydrous-saline fluids, and carbonatitic + S-Fe-Ni–rich fluids. *KSM*

GEM LOCALITIES

Gemmology, geology and origin of the Sandawana emerald deposits, Zimbabwe. J. C. Zwaan [zwaan@naturalis.nnm.nl], *Scripta Geologica*, No. 131, 2006, pp. 1–212.

Emeralds from the Sandawana deposits, Zimbabwe, have relatively high refractive indices (n_o=1.590–1.594, n_e=1.584–1.587) and specific gravity values (2.74–2.77), with evenly distributed color ranging from medium-to-dark green, and dichroism of yellowish green to bluish green. They contain inclusions of actinolite and cummingtonite needles and long prismatic laths of albite and apatite, as well as phlogopite, calcite, dolomite, quartz, and ilmenorutile; partially healed fissures were also seen. Electron-microprobe analyses were performed on four gem-quality medium-to-dark green emeralds, and one light green emerald extracted from a pegmatite, all from the Zeus mine. Microprobe analyses are reported for numerous inclusions, and the trace-element contents of 22 emeralds were also measured.

The emeralds had relatively high concentrations of Cr, Na, Mg, Li, and Cs, and are readily distinguished from emeralds from most other localities by traditional gemological techniques. The Sandawana emeralds formed at the contacts between the Mweza greenstones and granitic pegmatites emplaced during the main deformation event at the southern end of the Zimbabwe craton. A late-stage Na-rich "solution-melt" containing F, P, Li, Be, and Cr caused albitization of the pegmatite and phlogopitization in the greenstone host rock. Synkinematic growth of phlogopite was accompanied by emerald, fluorapatite, holmquistite, and chromian ilmenorutile, indicating Na-K metasomatism in the emerald-bearing shear zone. *RAH*

The Silver Bow sapphire occurrence, Montana: Evidence for a volcanic bedrock source for Montana's alluvial

sapphire deposits. A. L. Berger [alberger@vt.edu] and R. B. Berg, *Economic Geology*, Vol. 101, No. 3, 2006, pp. 679–684.

The first confirmed bedrock source of the alluvial sapphire deposits in southwest Montana has been found 9 km west of Butte. The source rock of the Silver Bow occurrence is a sapphire-bearing felsic lapilli tuff of the Eocene-age Lowland Creek volcanic field. A felsic composition is atypical of known primary sapphire deposits and may represent a previously unrecognized deposit type. Mass wasting of this volcanic unit during the Quaternary Period resulted in the deposition of several debris flows, which constitute the majority of the sapphire deposit. Two distinct corundum populations were recovered from the debris flows: over 5,500 pale-colored predominantly green, blue-green, and yellow-green sapphires; and 54 dark blue sapphires. The pale-colored sapphires had surface features indicative of resorption—and in some cases, spinel reaction rims—suggesting their origin as refractory magmatic xenocrysts of originally metamorphic origin. In contrast, the dark blue sapphires showed little if any evidence of reaction rims and had no adhering reaction minerals; this is consistent with a magmatic phenocryst origin.

RAH

Smaragd aus Dayakou, China [Emerald from Dayakou, China]. B. Ottens, *Lapis*, Vol. 31, No. 4, 2006, pp. 13–20, 50 [in German].

A considerable number of emerald specimens from Dayakou, China, have appeared on the market. The author visited the deposit, which is in a remote area of Yunnan Province just north of the border with Vietnam. The emeralds are a byproduct of scheelite mining, and are typically hosted by massive quartz; freely grown crystals with pinacoid terminations are rare. Typically the emeralds form prismatic, sometimes extremely long crystals (allegedly, up to 1.5 m). They can show good color and contain 0.2–0.3% Cr and 0.9–1.3% V. Only a small percentage of the crystals are transparent, and the material is cut almost exclusively into cabochons. The article is illustrated with many photographs of landscapes, mines, and emerald specimens.

RT

Smaragde selbstgesammelt: Die Fundstelle von Minnesund in Norwegen [Collecting emeralds: The deposit at Minnesund in Norway]. P. Imfeld and S. Weiss, *Lapis*, Vol. 31, No. 5, 2006, pp. 32–35, 54 [in German].

Minnesund, better known as Eidsvoll or Byrud, is a small but historically interesting emerald deposit in Norway near Lake Mjösa. It was first described in 1876 and exploited by underground mining from 1899 to 1909, producing deep-green prismatic crystals up to 5 cm long. Together with chromium (0.1–0.3%), the Minnesund emeralds contain relatively high amounts of vanadium (0.9–1.5%) and iron (0.2–1.8%). Today, collectors can search the mine dumps and placers along the lake shore for a fee of approximately US$10. With some patience, it is still possible to find small emerald-bearing specimens as well as (sometimes fine) single crystals. The article shows pictures of old and new material. *RT*

Study of melt inclusions in the Nezametnoye corundum deposit, Primorsky region of the Russian Far East: Petrogenetic consequences. V. A. Pakhomova [pakhomova@nm.ru], B. L. Zalishchak, E. G. Odarichenko, M. I. Lapina, and N. S. Karmanov, *Journal of Geochemical Exploration*, Vol. 89, 2006, pp. 302–305.

The Nezametnoye placer deposit is known for corundum, zircon, gold, and ores of tungsten and tin. The igneous intrusive complex is mainly composed of granitoid rocks; these are cut by thin dikes of Neogene basalt. Metasomatism is observed in all rocks except basalt. The corundum crystals are barrel or tabular shaped and may show growth zones, silkiness due to rutile needles, and asterism.

The corundum contains inclusions of rutile, zircon, albite, hercynite, columbite, monazite, and fluorite. Silicate melt inclusions are also present; analysis by scanning electron microscopy revealed that the glasses are composed of 59–62 wt.% SiO_2 with Al, Na, K, Fe, Ca, P, V, and Cl. Raman spectroscopy showed that primary fluid inclusions are dominated by CO_2. Analysis of the melt and fluid inclusions showed the corundum probably formed at 780–820°C and 1.7–3 kbar in a granosyenite magma. The authors did not find any genetic relationship between the basalt and corundum mineralization, as was postulated in previous studies of the deposit. *KSM*

INSTRUMENTS AND TECHNIQUES

Applications of large size spectroscopic instrument in identification of jadeite. Y. Liu, Q. Deng, and L. Wang, *Spectroscopy and Spectral Analysis*, Vol. 26, No. 3, 2006, pp. 577–582 [in Chinese].

Due to high demand for genuine jadeite, a wide variety of jadeite-like materials and simulants exist in the Chinese market, such as "Australia jade" (dyed quartzite), dyed quartz, glass, and various mineral and rock look-alikes. These simulants can be accurately identified through methods such as FTIR and Raman spectroscopy, X-ray diffractometry, and electron-microprobe analysis, as well as standard gemological testing. In this article, the authors investigated several jadeite simulants (dolomite-tremolite, plagioclase-actinolite, plagioclase, marble, plagioclase-serpentine-quartz, and anorthite) from the Chinese market and compared their gemological and spectroscopic properties.

Each material showed characteristic features. Dolomite-tremolite displayed clear cleavages within individual grains (0.3–2 cm grain size), as well as carbonate IR

absorption bands at 1432 and 883 cm^{-1} and five tremolite-related IR bands from 1204 to 926 cm^{-1}. Plagioclase-actinolite commonly contained dark spots (0.5–4.0 cm); five tremolite peaks at 1095, 1047, 993, 957, and 921 cm^{-1} were found in the IR spectrum when the beam was focused on the dark spots. The plagioclase sample resembled jadeite in its surface and structural features; however, its X-ray diffraction pattern matched plagioclase, with diffraction peaks at 3.198 and 3.225 Å. "Marble jade" could be distinguished by grain sizes of 0.05–0.1 cm, its fracture pattern, and relatively low hardness; the X-ray diffraction pattern showed that the major components were dolomite, mica, quartz, and calcite. Plagioclase-serpentine-quartz showed the closest appearance to jadeite, but had a specific gravity of 2.93 (well below that of jadeite at ~3.30). The authors' identification of anorthite was mainly based on its Raman spectrum. *TL*

Neoteric optical media for refractive index determination of gems and minerals. M. Deetlefs [quill@qub.ac.uk], K. R. Seddon, and M. Shara, *New Journal of Chemistry*, Vol. 30, 2006, pp. 317–326.

Ionic liquids may offer a substitute for a gemologist's immersion liquids. Ionic liquids are composed entirely of anions and cations (i.e., negatively and positively charged molecules), are stable, and can be tailor-made to specific refractive indices. This article describes how several similar high-R.I. ionic liquids based on polyhalide anions and 1-alkyl-3-methylimidazolium cations were prepared, characterized, and assessed for mineralogical and gemological use.

Following the synthesis of the ionic liquids, their purity and physical properties were characterized. The synthesized liquids had R.I.'s ranging from 1.410 to 2.080. The authors demonstrated how immersion of four sample materials (colorless quartz, orange beryl, brown corundum, and cubic zirconia) aided observation of inclusions. The effects of time, impurities, and different cation functional groups on physical properties and stability were also addressed.

The authors concluded that ionic liquids offer tunable properties and are less hazardous than the heavy liquids currently used for gemology, which are hard to work with, unpleasant, and somewhat toxic. Although the liquids investigated in this paper with an R.I.>1.8 were opaque to the unaided eye, these materials offer some promise as a gemological tool. *Editor's note:* Although ionic liquids have been referred to as "green solvents," very little is known about their toxicity to humans and their impact on the environment. *DMK*

JEWELRY HISTORY

The emerald and gold necklace from Oplontis, Vesuvian area, Naples, Italy. C. Aurisicchio [carlo.aurisichio@uniroma1.it], A. Corami, S. Ehrman, G. Graziani, and S. N. Cesaro, *Journal of Archeological Science*, Vol. 33, No. 5, 2006, pp. 725–734.

The authors performed gemological and chemical analysis of 19 emerald crystals believed to be part of a gold necklace found in an excavated Roman villa in Oplontis (Naples), with the intention of determining the possible commercial exchange routes that brought gems to ancient Rome. This villa was buried during the eruption of Mount Vesuvius in 79 AD.

The crystals appeared greasy, were semitransparent to opaque, and ranged from bluish to deep green. They were all drilled and exhibited etching, scratches, and other damage. The emeralds had relatively high refractive indices (n_o=1.588, n_e=1.581), suggesting an extensive amount of aluminum substitution. Microscopic analysis revealed characteristic fine tubules, two-phase liquid/gas inclusions, mica flakes, and limonite, all oriented parallel to the optic axis.

Analysis of the emeralds by electron microprobe, proton-induced X- and gamma-ray emission (PIXE/PIGE), and FTIR spectroscopy indicated that they all likely originated from the same source. Comparing their chemical compositions to those of known historic emeralds suggested two possible sources: the El Sikait (Egypt) and Habachtal (Austria) deposits. Statistical analysis of the data led the authors to strongly favor an Egyptian origin for the Oplontis emeralds. *PJ*

JEWELRY RETAILING

All that glitters. A. Gengler, *Money*, Vol. 35, No. 10, 2006, pp. 163–165.

The rising values of diamonds and precious metals are causing jewelry prices to increase at the retail counter. However, shoppers may be able to circumvent higher-cost items by seeking jewelry that has been in stock for a long time. The article also provides tips on how to beat higher prices on some specific types of jewelry: opting for palladium in place of more costly platinum, considering 14K gold instead of 18K, and seeking treated or "light-sized" diamonds (e.g., 0.90 ct instead of a full carat). *RS*

Net worth. S. O'Laughlin, *Brandweek*, Sept. 18, 2006, pp. 22–26.

Online sales of jewelry and luxury goods are expected to double to $6.1 billion between 2005 and 2010. The diamond jewelry company Blue Nile sells 5–10 items priced at $10,000 each day. The advent of online sales has changed how luxury firms are marketing their goods by creating customizable product options and highly sophisticated web sites. According to a 2006 survey, 93% of individuals with a net worth >$10 million made an Internet purchase in the previous 12 months. Several trends have helped. After the ostentation of the 1990s, the wealthy have become lower-key in their lifestyles, and the Internet can allow customers

to buy very expensive items inconspicuously. Additionally, many wealthy people are time-starved and respond to the convenience of online purchases. Finally, they have established a level of comfort with buying luxury goods and services online. The article also describes how traditional luxury retailers have established an online presence and how new Internet-only marketers have arisen during the past several years, allowing the wealthy in areas outside traditional centers of affluence to purchase luxury goods without having to travel. *RS*

PRECIOUS METALS

Pt and Pd vie for market share. C. Hewitt, *Metal Bulletin Monthly*, No. 431, November 2006, pp. 34–39.

The use of platinum in jewelry manufacturing has decreased over the past three years, in part due to the steeply rising price of the metal. Consumer demand for platinum remains robust, but the high cost of maintaining stocks of this jewelry has led wholesalers and retailers to cut inventories and send dated pieces back to the manufacturers. Manufacturers have in turn switched a larger proportion of their output to more profitable white gold and palladium.

The Chinese market accounts for 45% of the platinum used in jewelry, and in 2005 demand was down to its lowest in seven years. This record drop occurred in part because 2005 was considered an inauspicious year for marriage and in part because of rising per-ounce prices. At the same time, Chinese demand for palladium rose 71% after consumers were introduced to new 99% palladium (Pd990) and 95% palladium (Pd950) alloys and were encouraged by retailers to consider palladium as a good investment.

Palladium, although rising in value at a similar rate to platinum (but still much lower priced in absolute terms), is gaining in popularity as manufacturers search for a cheaper but viable substitute for platinum. Additionally, the lower density of palladium means that almost twice the number of products of identical volume can be produced from a given weight of palladium compared to platinum.

North American interest in palladium grew last year as more manufacturers were exposed to it through the efforts of the Palladium Alliance International (PAI). This organization has also initiated marketing in the profitable Chinese markets of Beijing and Shanghai. Global demand for palladium is forecast to rise approximately 8% in 2007. *JEC*

SYNTHETICS AND SIMULANTS

Gemological characteristics of GE synthetic jadeite jade. S. Cao, L. Qi, Q. Guo, and Y. Lu, *Journal of Gems and Gemmology*, Vol. 8, No. 1, 2006, pp. 1–4 [in Chinese with English abstract].

General Electric has been developing a proprietary process for producing synthetic jadeite since the 1980s. The authors studied two cabochons of this material using electron-microprobe analysis, cathodoluminescence, and visible-range, FTIR, and Raman spectroscopy.

It was difficult to visually distinguish the synthetic jadeite from its natural counterpart, and the materials had similar gemological properties. The major chemical components of the synthetic jadeite were SiO_2 (59.74–61.72 wt.%), Al_2O_3 (23.90–24.97 wt.%), and Na_2O (13.65–14.85 wt.%); the trace elements were Cr_2O_3 (0.05–0.07 wt.%), K_2O (0.02–0.04 wt.%), and CaO (0.02–0.06 wt.%). IR absorption spectra displayed characteristic peaks at 3614, 3471, and 3373 cm^{-1}, which differed from natural jadeite; however, Raman peaks located at 1039, 989, 700, and 376 cm^{-1} were similar to those of the natural counterpart. The visible absorption spectra of the synthetic jadeites were dominated by two strong and broad bands centered at 630 and 445 nm (due to Cr^{3+}); in contrast, natural jadeite sometimes shows a weak band at 437 nm due to Fe^{3+} substitution for Al^{3+}. The synthetic jadeite also showed strong red cathodoluminescence. *TL*

High-rate growth of large diamonds by microwave plasma chemical vapor deposition with newly designed substrate holders. Y. Horino [y-horino@aist.go.jp], A. Chayahara, Y. Mokuno, H. Yamada, and N. Fujimori, *New Diamond and Frontier Carbon Technology*, Vol. 16, No. 2, 2006, pp. 63–69.

To meet the demands of electronic semiconductor device applications, the achievable diameters of synthetic diamond wafers will need to increase. High-pressure, high-temperature (HPHT) growth is not practical for producing synthetic diamonds with large diameters. Chemical vapor deposition (CVD) is presently the most promising technique. This article describes two developments that increased the growth rate of microwave plasma–grown CVD synthetic diamond films: the design of custom substrate holders and the addition of nitrogen to the growth chamber. The sample holders have a stepped structure composed of two layers, with the radius of the upper layer varying between experiments. The emission from the microwave plasma increased in intensity as the radius of the upper layer decreased, which resulted in a faster growth rate. Adding nitrogen to the chamber further doubled the growth rates and also resulted in a macroscopically smooth (100) face. Growth rates greater than 100 µm/hour were achieved for (100) synthetic diamond when the new substrate holders were coupled with the addition of nitrogen. The largest crystal grown by this method was 4.65 ct, with a maximum thickness of 10 mm. The synthetic diamond films were evaluated by optical and atomic force microscopy, micro-Raman and cathodoluminescence spectroscopy, and X-ray diffraction analysis to assess crystal quality and impurity levels. *JSS*

Spotting a fake. S. Lawson [simon.lawson@dtc.com], *Physics World*, Vol. 19, No. 6, 2006, pp. 23–27.

This article describes the formation and properties of natural and synthetic diamond, and describes how spectroscopy and fluorescence imaging using two different instruments developed by the Diamond Trading Company can confidently and rapidly distinguish most synthetics from their natural counterparts. The DiamondSure is a compact testing device built around a microspectrometer: It compares the diamond's spectrum to a reference database, thereby giving the sample a "pass" or "refer" evaluation within a few seconds. The vast majority of natural diamonds (98%) are "passed," while all synthetics, simulants, and 2% of natural stones get a "refer" message, indicating they should be sent to a lab for further testing. The other instrument, the DiamondView, is used to generate ultra short-wave UV fluorescence patterns that image the growth history of the sample. Since the growth patterns of HPHT-grown synthetic diamonds are distinctive, this device is very useful for separating them from natural stones. *DMK*

MISCELLANEOUS

Accepting jewelry as collateral. H. Hoff [hhoff@markspaneth.com], *The Secured Lender*, Vol. 62, No. 6, 2006, pp. 94–95.

Most lenders shy away from accepting diamond jewelry as collateral for commercial loans. One reason is the popular belief that jewelry inventory is more vulnerable to theft or fraud than, for example, apparel. However, the author notes that jewelry is less theft-prone than people realize. In addition, diamond jewelry has a close-out value of around 35%–40%—and possibly more than 50%—as compared to 15%–20% for garments. The author also points out that, in the event goods cannot be sold, the diamond and gold components can be converted to funds. However, the author recommends that lenders who work with jewelry engage an expert to properly evaluate the inventory. *RS*

Continuity and change in the international diamond market. D. L. Spar, *Journal of Economic Perspectives*, Vol. 20, No. 3, 2006, pp. 195–208.

The author describes changes in the diamond market over the last decade and how De Beers, the dominant player, has responded to them. Through its marketing arm, the Diamond Trading Company, De Beers still controls most of the (large) production from Botswana and South Africa. Before 1990, however, it controlled a much greater share of the diamond market through contracts with governments of producing nations. Beginning in the 1990s, changes to the industry resulted from political developments (such as the fall of the Soviet Union and the end of apartheid in South Africa), new discoveries in Canada, and the emergence of the anti–conflict diamond movement.

The author offers a lengthy history of De Beers's operations since 1888, then discusses recent challenges, particularly noting that the conflict diamond issue has worked to the company's benefit by driving consumer demand to producers, such as De Beers, who can guarantee the "integrity" of their diamonds. Moreover, although De Beers has lost market share in recent years, its sight system has proved extremely successful judging by how new entrants into the market have adopted it. *RS*

Diamond aren't forever. V. Walt, *Fortune*, Vol. 154, No. 11, 2006, pp. 50–56.

The article discusses the issues depicted in the movie *Blood Diamond*, noting that the vast majority of diamonds come from well-run mining operations in non-conflict countries, as well as from the former conflict area of Koidu in Sierra Leone. However, a minority of diamonds are still traded outside of official networks in violation of the Kimberley Process. The article also highlights the existence of several "fair trade" diamond operations in Sierra Leone that attempt to insure equitable returns to miners and villagers. *RS*

Visual problems among electronic and jewelry workers in Thailand. O. Unitmanon, W. Pacharatrakul, K. Boonmeepong, L. Thammagurun, N. Laemun, S. Taptagaporn, and V. Chongsuvivatwong [cvirasak@medicine.psu.ac.th], *Journal of Occupational Health*, Vol. 48, No. 5, 2006, pp. 407–412.

The authors examined a group of Thai jewelry and electronics workers in Samutprakan Province, southeast of Bangkok, to determine the prevalence of visual disorders and visual strain, and to identify possible corrective measures. Although 18 factories were contacted, only seven agreed to participate in the study. Among the sampled workers, 91.5% were female and the average age was 26.2. Fifty-two percent of the workers had at least one kind of vision problem that might have affected their performance, and 48.3% of the work sites had substandard illumination levels.

The corrective measures included improvement of lighting conditions, the introduction of short breaks, and correction of visual performance problems (e.g., by prescription glasses). Six months after implementation, improvements were noted among the electronics workers but not the jewelry workers. The authors theorize that because the jewelry workers were already required to move about the factory as part of their jobs (taking a completed jewel to the next station for finish work), the additional break times would not have had a significant effect on the visual strain they experienced. *TWO*

The Last Page

Take the *G&G* Challenge

To celebrate the 20th anniversary of the *G&G* Challenge, we're hoping to get **every** *Gems & Gemology* reader to participate (see pp. 81–82 of this issue). The multiple-choice quiz, prepared by the journal's editors, is designed to reinforce key concepts from the past year's articles. But there's no need to cram or memorize facts for this test: Just have the Spring, Summer, and Winter 2006 issues of *G&G* on hand so you can review each article and carefully select the best answer. (The Fall 2006 Symposium/GRC proceedings issue is not covered because it consists primarily of abstracts, with no peer-reviewed articles.)

As gemology confronted rapid technological changes in the 1980s, the Challenge was created to encourage readers to keep up with developments by reading *G&G* carefully. Since its debut in the Spring 1987 issue, the Challenge has consistently drawn an enthusiastic response from around the world. Those who successfully complete it can receive a GIA Continuing Education Certificate, 10 Carat Points in the GIA Alumni Association recognition program, and (for all those scoring 100%) special acknowledgment in the journal. But in addition to these tangible rewards, many participants simply enjoy the stimulation of continually learning and testing their gemological knowledge.

No one better exemplifies the spirit of lifelong learning than loyal Challenge participant Alice Christianson of St. Catherine's, Ontario, Canada. Ms. Christianson came to gemology in the 1970s as a photographer, after a local jeweler hired her to shoot pictures of gems. She enrolled at GIA, graduating in 1981, and began building a library of gemological books and journals, including *Gems & Gemology*. Now at age 83, Ms. Christianson has taken part in the Challenge every year except 1998, when she was recovering from a stroke. She has earned a perfect score nearly every time.

"It covers so much, and you get so much more out of the issues," she says of the Challenge. "You don't just stick them on the shelf. Every time I look at one, I find something I missed the first time."

If you've never participated in the Challenge before, why not make this year's your first try? Whatever your gemological background may be, the *G&G* Challenge offers a unique resource that will enhance your professional knowledge. We don't need your answer card until Monday, August 6, but why wait? Sharpen your pencil and take the Challenge today!

Stuart Overlin
Associate Editor

What are the benefits of participating in the *G&G* Challenge?

A. Receiving a GIA Continuing Education Certificate

B. Recognition in the Fall 2007 issue of *G&G*

C. Earning 10 Carat Points as a GIA Alumni Association member

D. The satisfaction of improving your gemological expertise

Answer: All of the above!

GEMS & GEMOLOGY SPRING 2007 PAGES 1–94 VOLUME 43 NO. 1